

**XV International Conference on
Gravitational Microlensing
Conference Book**

January 20–22, 2011

University of Salerno, Italy

Editors

V. Bozza, S. Calchi Novati, L. Mancini, G. Scarpetta
(Local Organizing Committee)

Organized by the Astrophysics Group of the
Physics Department of the University of Salerno

Sponsored by IIASS (International Institute for Advanced Scientific Studies),
INFN (Istituto Nazionale di Fisica Nucleare), International Ph.D. in Astrophysics,
and University of Salerno

<http://smc2011.physics.unisa.it>

Foreword

This volume collects the abstracts in extended format of the 15th Microlensing Conference held in the University of Salerno on January 20-22, 2011. The Conference has gathered 68 scientists from 17 countries confirming microlensing as a mature and established tool of research over a broad range of astrophysical issues, from dark matter searches to the detection of new extrasolar planets of very low mass, down to Earth-size or below. The 3-days Conference has been preceded by a 2-days school on “Modelling Planetary Microlensing Events” focused on this last issue. The abstracts collected here offer an updated snapshot of the current researches in this field. The topics include: the status of current surveys, planetary events, dark matter searches, cosmological microlensing, theoretical investigations and an outlook towards the future, with in particular a discussion on the possible role to be played by microlensing searches for exoplanets in the forecoming space missions, WFIRST and EUCLID. Finally, the conference has been enriched by a series of topical speeches on related issues from a non-microlensing point of view: the physics of giant planet accretion and evolution, “new physics” and dark matter in the LHC era and an update on the GAIA mission and its potential to characterize planetary systems with high-precision astrometry.

Scientific Rationale

25 years after the seminal intuition by Bohdan Paczynski, microlensing has rapidly evolved into a new promise for modern astrophysics. Indeed, the detection of celestial bodies by their gravitational effects on the light of background sources has proved to be a very powerful tool for the study of many aspects of our Galaxy and beyond.

The original proposal of using microlensing to estimate the amount of baryonic dark matter in the form of compact substellar bodies is still topical. The observation of microlensing events toward nearby galaxies still represents a hard challenge for present observational facilities. Very strong efforts are under way for upgrading the current strategies in particular toward the galaxy M31.

Hundreds of microlensing events are discovered toward the Galactic Bulge every year. This considerable amount of statistics can be used to characterize the stellar populations of the bulge and the disc of our Galaxy. After several years of observations, the significance of the microlensing sample in the characterization of our Galaxy is growing more and more.

Yet, the most intriguing perspective offered by microlensing is represented by its power to discover new extrasolar planets of very low mass, down to Earth-size or below. Several planetary events have already been detected and studied, while many more are expected as soon as future dedicated telescopes become operational. Interestingly, microlensing is already being used to estimate the abundance of planets around stars in the disc of our Galaxy and to characterize their distributions in distance and mass. As the planetary anomalies typically last only a few hours, the cooperation among all observing groups is mandatory, in order to characterize the events properly and maximize the scientific achievements. Even amateur astronomers are now giving their fundamental contribution. In this respect, microlensing stands as a perfect example of how science can unite the whole mankind in a common path toward pure knowledge.

Salerno Microlensing Conference 2011 will gather all people active in this field, providing the state of the art of microlensing searches and the perspectives opened by new methodologies and new observational and computational facilities. Colloquia on dark matter searches and planet formation theories are also foreseen as a central part of the conference. The three-days conference will be preceded by a school dedicated to the delicate issue of efficient modelling of planetary microlensing events, which requires major efforts and new ideas from new talents in order to get access to the precious physical information hidden in microlensing light curves. For one week in January 2011, Salerno will thus be the place in which the present and the future of microlensing will be unveiled.

Valerio Bozza
Local Organizing Committee

Welcome address

On behalf of the Rector of Salerno University, professor Raimondo Pasquino, the Dean of the Science Faculty, professor Mariella Transirico, the Decan of the Department of Physics, professor Ferdinando Mancini and the Organizing Committee, I welcome all the participants to this exciting Conference.

This University has the peculiar status to be at the same time one of the youngest Universities in Italy and the oldest one.

The re-establishment of Salerno University in the Modern Era dates back to about forty years ago, and as you can see, in a very short time it has grown in the Irno valley as a university campus, with about forty thousand students, more than one thousand professors and researchers, distributed in ten faculties.

Five years ago the Campus was completed with the Medical Science Faculty, realizing the ideal link with one of the oldest Medical Schools of the West, the so called “Scuola Medica Salernitana”.

Salerno was not the seat of the first Medieval University, but the Medical School was the first to organize studies and diffuse culture on international scale during the medieval period.

According to the legend, the “Scuola Medica Salernitana” traces its origins to four erudite: the Greek Pontus, the Jew Helinus, the Arab Abdela, and the Latin Salernus. Thanks to the encounter of these four cultures the Medical School established its knowledge divulgating the Greek, Jewish, Arab and Latin medical knowledge. The divulgation in the West of the Islamic and Greek Medical Science is certainly due to Constantino the African (XI century), thanks to his translations into Latin of the most important Arabic and Greek medical treatises.

I like to read some words extracted from the nobel lecture of Abdus Salam (1979)

“Scientific thought and its creation is the common and shared heritage of mankind. In this respect, the history of science, like the history of all civilization, has gone through cycles. Perhaps I can illustrate this with an actual example.

Seven hundred and sixty years ago, a young Scotsman left his native glens to travel south to Toledo in Spain. His name was Michael, [...] Michael reached Toledo in 1217 AD. [...] From Toledo, Michael travelled to Sicily, to the Court of Emperor Frederick II. Visiting the medical school at Salerno, chartered by Frederick in 1231, Michael met the Danish physician, Henrik Harpestraeng [...] Henrik had come to Salerno to compose his treatise on blood-letting and surgery. Henrik’s sources were the medical canons of the great clinicians of Islam, Al-Razi and Avicenna, which only Michael the Scot could translate for him. Toledo’s and Salerno’s schools, representing as they did the finest synthesis of Arabic, Greek, Latin and Hebrew scholarship, were some of the most memorable of international assays in scientific collaboration”.

The “Scuola Medica Salernitana” was at the height of its fame in the XIV century and carried on its teaching for nine centuries, until Giocchino Murat’s decree, dated the 25th of January 1812, prescribed the closure.

After two centuries, we all, coming here in the Salerno University from east and west countries, renew in some sense the old tradition, establishing an ideal link with the cultural heritage of the “Scuola Medica Salernitana” .

I hope you will enjoy your stay in Salerno and I wish you good and useful work.

Gaetano Scarpetta
Chair of the Local Organizing Committee

Local Organizing Committee

V. Bozza
S. Calchi Novati
L. Mancini
G. Scarpetta (Chair)

Scientific Organizing Committee

J.-P. Beaulieu	France
D. Bennett	USA
I. Bond	New Zealand
S. Calchi Novati (Chair)	Italy
M. Dominik	UK
A. Gould	USA
C. Han	South Korea
Ph. Jetzer	Switzerland
E. Kerins	UK
M. Moniez	France
T. Sumi	Japan
Y. Tsapras	UK
A. Udalski	Poland
L. Wyrzykowski	UK

Scientific Secretary

O. De Pasquale
V. Di Marino
T. Nappi
S. Russo

CONTENTS

Foreword	iii
Scientific Rationale	v
welcome	vi
Organization	ix
Participants	xvi
School Program	xix
Conference Program	xx
School on Modelling Planetary Microlensing Events	1
Introduction to microlensing	2
<i>Philippe Jetzer</i>	
From microlensing observations to science	3
<i>Martin Dominik</i>	
The theory and phenomenology of planetary microlensing	4
<i>Scott Gaudi</i>	
From raw images to lightcurves: how to make sense of your data	5
<i>Yiannis Tsapras</i>	
The efficient modeling of planetary microlensing events	6
<i>David Bennett</i>	
Contour integration and downhill fitting	7
<i>Valerio Bozza</i>	
Microlensing modelling and high performance computing	8
<i>Ian Bond</i>	

Conference topical speeches	9
Giant planet accretion and dynamical evolution: considerations on systems around small-mass stars <i>Alessandro Morbidelli</i>	10
The dark matter - LHC endeavour to unveil TeV new physics <i>Antonio Masiero</i>	14
Characterization of planetary systems with high-precision astrometry: the Gaia potential <i>Alessandro Sozzetti</i>	15
Status of current surveys	18
Status of the OGLE-IV survey <i>Andrzej Udalski</i>	19
MOA-II observation in 2010 season <i>Takahiro Sumi</i>	20
The RoboNet 2010 season <i>Yiannis Tsapras</i>	22
Cosmological Microlensing	25
Dark matter determinations from Chandra observations of quadruply lensed quasars <i>David Pooley</i>	26
Cosmic equation of state from strong gravitational lensing systems <i>Marek Biesiada & Beata Malec</i>	27

Galactic Microlensing: the dark matter search	31
PAndromeda - the Pan-STARRS M31 survey for dark matter	32
<i>Arno Riffeser, Stella Seitz, Ralf Bender, C.-H. Lee, Johannes Koppenhoefer</i>	
Final OGLE-II and OGLE-III results on microlensing towards the LMC and SMC	34
<i>Lukasz Wyrzykowski</i>	
Analysis of microlensing events towards the LMC	37
<i>Luigi Mancini & Sebastiano Calchi Novati</i>	
Simulation of short time scale pixel lensing towards the Virgo cluster	39
<i>Sedighe Sajadian & Sohrab Rahvar</i>	
M31 pixel lensing and the PLAN project	40
<i>Sebastiano Calchi Novati</i>	
 Planetary events	 44
MOA-2009-BLG-266LB: the first cold Neptune with a measured mass	45
<i>David Bennett</i>	
Increasing the detection rate of low-mass planets in high-magnification events and MOA-2006-BLG-130	46
<i>Julie Baudry & Philip Yock</i>	
The complete orbital solution for OGLE-2008-BLG-513	49
<i>Jennifer Yee</i>	
Planetary microlensing event MOA-2010-BLG-328	51
<i>Kei Furusawa</i>	
Binary microlensing event OGLE-2009-BLG-020 gives orbit predictions verifiable by follow-up observations	53
<i>Jan Skowron</i>	

Theoretical investigations	59
Microlensing and planet populations - What do we know, and how could we learn more	60
<i>Martin Dominik</i>	
The Frequency of extrasolar planet detections with microlensing simulations	65
<i>Rieul Gendron & Shude Mao</i>	
A semi-analytical model for gravitational microlensing events	66
<i>Denis Sullivan, Paul Chote, Michael Miller</i>	
GPU-assisted contouring for modeling binary microlensing events	70
<i>Markus Hundertmark, Frederic V. Hessman, Stefan Dreizler</i>	
Red noise effect in space-based microlensing observations	74
<i>Achille Nucita, Daniele Vetrugno, Francesco De Paolis, Gabriele Ingrosso, Berlinda M. T. Maiolo, Stefania Carpano</i>	
Light curve errors introduced by limb-darkening models	76
<i>David Heyrovsky</i>	
Isolated, stellar-mass black holes through microlensing	77
<i>Kailash Sahu, Howard E. Bond, Jay Anderson, Martin Dominik, Andrzej Udalski, Philip Yock</i>	
The observability of isolated compact remnants with microlensing	80
<i>Nicola Sartore & Aldo Treves</i>	
Gravitational microlensing by the Ellis wormhole	82
<i>Fumio Abe</i>	
The deflection of light ray in strong field: a material medium approach	100
<i>Asoke Kumar Sen</i>	
Rapidly rotating lenses - repeating orbital motion features in close binary microlensing	104
<i>Matthew Penny, Eamonn Kerins, Shude Mao</i>	

Towards the future: new facilities/instrumentation/procedures	107
Microlensing with the SONG global network	108
<i>Uffe G. Jørgensen, Kennet B. W. Harpsøe, Per K. Rasmussen, Michael I. Andersen, Anton N. Sørensen, Jørgen Christensen-Dalsgaard, Søren Frandsen, Frank Grundahl, Hans Kjeldsen</i>	
Next-generation microlensing pilot planet search and the frequency of planetary systems	112
<i>Dan Maoz & Yossi Shvartzvald</i>	
Kohyama Astronomical Observatory: current status	116
<i>Atsunori Yonehara, Mizuki Isogai, Akira Arai, Hiroki Tohyama</i>	
Optimal imaging for gravitational microlensing	118
<i>Kennet B.W. Harpsøe, Uffe G. Jørgensen, Per K. Rasmussen, Michael I. Andersen, Anton N. Sørensen, Jørgen Christensen-Dalsgaard, Søren Frandsen, Frank Grundahl, Hans Kjeldsen</i>	
IPACs role as the science center for NASAs WFIRST mission	121
<i>Kaspar von Braun</i>	
EUCLID microlensing planet hunt	122
<i>Jean-Philippe Beaulieu & Matthew Penny</i>	
Space-based microlensing exoplanet survey: WFIRST and/or Euclid	124
<i>David Bennett</i>	
Microlensing with Gaia satellite	125
<i>Lukasz Wyrzykowski</i>	
Poster session	127
Critical curve topology in special triple lens configurations	128
<i>Kamil Danek</i>	
PAndromeda - a dedicated deep survey of M31 with Pan-STARRS 1	129
<i>Chien-Hsiu Lee, Arno Riffeser, Stella Seitz, Ralf Bender, Johannes Koppenhoefer</i>	

SMC2011 Participants

Abe, Fumio	Nagoya University, Japan
Baudry, Julie	University of Orsay, France
Bachelet, Etienne	University of Toulouse, France
Beaulieu, Jean-Philippe	Institut d'Astrophysique de Paris, France
Bennett, David	University of Notre Dame, USA
Bond, Ian	Massey University, New Zealand
Bonino, Donata	INAF - Turin Astronomical Observatory, Italy
Bozza, Valerio	University of Salerno, Italy
Browne, Paul	University of St Andrews, UK
Calchi Novati, Sebastiano	University of Salerno, Italy
Danek, Kamil	Charles University, Czech Republic
De Paolis, Francesco	University of Salento, Italy
Dominik, Martin	University of St Andrews, UK
Dominis Prester, Dijana	University of Rijeka, Croatia
Fouqué, Pascal	University of Toulouse, France
Furusawa, Kei	Nagoya University, Japan
Gardioli, Daniele	INAF - Turin Astronomical Observatory, Italy
Gaudi, Scott	Ohio State University, USA
Gendron, Riel	University of Manchester, UK
Gould, Andrew	Ohio State University, USA
Harpsøe, Kennet	Niels Bohr Institute, Denmark
Harris, Pauline	Victoria University of Wellington, New Zealand
Henderson, Calen	Ohio State University, USA
Heyrovsky, David	Charles University, Czech Republic
Horne, Keith	University of St Andrews, UK
Hundertmark, Markus	University of Göttingen, Germany
Jetzer, Philippe	University of Zurich, Switzerland
Jørgensen, Uffe G.	Niels Bohr Institute, Denmark
Lambiase, Gaetano	University of Salerno, Italy
Lee, Chien-Hsiu	University Observatory Munich
Liebig, Christine	University of St Andrews
Lubini, Mario	University of Zurich, Switzerland
Malec, Beata	Copernicus Center for Interdisciplinary Studies, Poland
Mancini, Luigi	University of Salerno, Italy
Maoz, Dan	Tel-Aviv University, Israel
Masiero, Antonio	University of Padova, Italy
Mirzoyan, Sergey	University of Salerno, Italy
Miyake, Noriyuki	Nagoya University, Japan

Morbidelli, Alessandro	Observatoire de la Cote d’Azur, France
Muraki, Yasushi	Konan University, Japan
Nucita, Achille	University of Salento, Italy
Orio, Marina	INAF - Padova Astronomical Observatory, Italy
Paulin-Henriksson, Stéphane	CEA - Paris, France
Payandeh, Farrin	Payame Noor University Tabriz, Iran
Penny, Matthew	University of Manchester, UK
Pooley, David	Eureka Scientific, USA
Retana Montenegro, Edwin F.	Universidad de Costa Rica, Costa Rica
Riffeser, Arno	Max Planck Institute for Extraterrestrial Physics, Germany
Sahu, Kailash	Space Telescope Science Institute, USA
Sajadian, Sedighe	Sharif University of Technology, Iran
Sartore, Nicola	INAF - IASF Milano, Italy
Scarpetta, Gaetano	University of Salerno, Italy
Sen, Asoke Kumar	Sen Assam University, India
Shvartzvald, Yossi	Tel-Aviv University, Israel
Skowron, Jan	Ohio State University, USA
Sozzetti, Alessandro	INAF - Turin Astronomical Observatory, Italy
Sullivan, Denis	Victoria University of Wellington, New Zealand
Sumi, Takahiro	Nagoya University, Japan
Tortora, Crescenzo	University of Zurich, Switzerland
Tsapras, Yiannis	Queen Mary University, UK
Udalski, Andrzej	Warsaw University Observatory, Poland
Vetrugno, Daniele	University of Salento, Italy
Vilasi, Gaetano	University of Salerno, Italy
von Braun, Kaspar	California Institute of Technology, USA
Yee, Jennifer	Ohio State University, USA
Yock, Philip	University of Auckland, New Zealand
Yonehara, Atsunori	Kyoto Sangyo University, Japan
Wyrzykowski, Łukasz	University of Cambridge, UK

School on Modelling Planetary Microlensing Events

Program

Tuesday, January 18, 2011

- | | | |
|-------|--|-----------------|
| 09:00 | Introduction to microlensing | Philippe Jetzer |
| 10:50 | <i>Coffee Break</i> | |
| 11:15 | From microlensing observations to science | Martin Dominik |
| 13:00 | <i>Lunch Break</i> | |
| 14:45 | The theory and phenomenology of planetary microlensing | Scott Gaudi |
| 16:45 | <i>Coffee Break</i> | |
| 17:15 | From raw images to lightcurves: how to make sense of your data | Yiannis Tsapras |

Wednesday, January 19, 2011

- | | | |
|-------|---|---------------|
| 09:00 | The efficient modeling of planetary microlensing events | David Bennett |
| 10:50 | <i>Coffee Break</i> | |
| 11:15 | Contour integration and downhill fitting | Valerio Bozza |
| 13:00 | <i>Lunch Break</i> | |
| 14:45 | Microlensing modelling and high performance computing | Ian Bond |
| 16:45 | <i>Coffee Break</i> | |

SMC2011 Program

Thursday, January 20, 2011

09:00 Registration
09:30 *Greetings*
09:40 Communications

Chair: Gaetano Scarpetta

Status of current Surveys I

09:50 Status of the OGLE-IV survey	Andrzej Udalski
10:20 MOA-II observation in 2010 season	Takahiro Sumi

10:50 *Coffee Break*

Topical Speech I

11:20 Formation and evolution of our solar system	Alessandro Morbidelli
--	-----------------------

Theoretical investigations I

12:10 Microlensing and planet populations: what do we know, and how could we learn more?	Martin Dominik
12:40 The frequency of extrasolar planet detections with microlensing simulations	Rieul Gendron

13:00 *Lunch Break*

Chair: Philippe Jetzer

Dark Matter Search

14:40 PAndromeda - the Pan-STARRS M31 survey for dark matter	Arno Riffeser
15:10 Final OGLE-II and OGLE-III results on microlensing towards the LMC and SMC	Lukasz Wyrzykowski
15:30 Analysis of microlensing events towards the LMC	Luigi Mancini
15:50 Simulation of short time scale pixel lensing towards the Virgo cluster	Sedighe Sajadian
16:10 M31 pixel lensing and the PLAN project	Sebastiano Calchi Novati

16:30 *Coffee Break*

Towards the future I

17:00	Microlensing with the SONG global network	Uffe G. Jørgensen
17:20	Next-generation microlensing pilot planet search and the frequency of planetary systems	Dan Maoz
17:40	Kohyama Astronomical Observatory: current status	Atsunori Yonehara
18:00	The lucky imaging technique for microlensing observations	Kennet Harpsøe

Friday, January 21, 2011

Chair: P. Yock

Status of current Surveys II

09:00	The 2010 MicroFUN season	Jennifer Yee
09:30	The RoboNet 2010 season	Yiannis Tsapras

Theoretical investigations II

10:00	A semi-analytical model for gravitational microlensing events	Denis Sullivan
10:20	GPU-assisted contouring for modeling binary microlensing events	Markus Hundertmark
10:40	Rapidly rotating lenses - repeating orbital motion features in close binary microlensing	Matthew Penny

11:00 *Coffee Break*

Topical Speech II

11:30	The dark matter - LHC endeavour to unveil TeV new physics	Antonio Masiero
-------	--	-----------------

Cosmological microlensing

12:20	Dark matter determinations from Chandra observations of quadruply lensed quasars	David Pooley
12:40	Cosmic equation of state from strong gravitational lensing systems	Beata Malec

13:00 *Lunch Break*

Chair: Pascal Fouqué

Planetary events

- | | | |
|-------|--|---------------|
| 14:30 | MOA-2009-BLG-266LB: the first cold Neptune with a measured mass | David Bennett |
| 14:50 | Increasing the detection rate of low-mass planets in high-magnification events and MOA-2006-BLG-130 | Julie Baudry |
| 15:10 | The complete orbital solution for OGLE-2008-BLG-513 | Jennifer Yee |
| 15:30 | Planetary microlensing event MOA-2010-BLG-328 | Kei Furusawa |
| 15:50 | Binary microlensing event OGLE-2009-BLG-020 gives orbit predictions verifiable by follow-up observations | Jan Skowron |
| 16:10 | <i>Coffee Break</i> | |
| 17:30 | <i>Tour of the old town of Salerno</i> | |
| 20:00 | <i>Social dinner</i> | |

Saturday, January 22, 2011

Chair: Francesco De Paolis

Towards the future II

- | | | |
|-------|---|------------------------|
| 09:00 | IPACs role as the science center for NASAs WFIRST mission | Kaspar von Braun |
| 09:30 | EUCLID microlensing planet hunt | Jean-Philippe Beaulieu |
| 09:50 | Simulating the planet hunting capability of Euclid | Matthew Penny |
| 10:10 | Space-based microlensing exoplanet survey: WFIRST and/or Euclid | David Bennett |
| 10:40 | <i>Coffee Break</i> | |

Topical Speech III

- | | | |
|-------|--|---------------------|
| 11:10 | Characterization of planetary systems with high-precision astrometry: the Gaia Potential | Alessandro Sozzetti |
|-------|--|---------------------|

12:00 Microlensing with Gaia satellite Łukasz Wyrzykowski

Theoretical investigations III

12:20 Red noise effect in space-based microlensing observations Achille Nucita

12:40 Light curve errors introduced by limb-darkening models David Heyrovsky

13:00 *Lunch Break*

Chair: Scott Gaudi

14:40 Isolated, stellar-mass black holes through microlensing Kailash Sahu

15:00 The observability of isolated compact remnants with microlensing Nicola Sartore

15:20 Gravitational microlensing by the Ellis wormhole Fumio Abe

15:40 The deflection of light ray in strong field: a material medium approach Asoke Kumar Sen

16:00 How to stop a runaway (Monte Carlo Markov) Keith Horne

16:20 *Coffee Break*

16:50 Open session

Poster Session

Critical curve topology in special triple lens configurations Kamil Danek

PAndromeda - a dedicated deep survey of M31 with Pan-STARRS 1 Chien-Hsiu Lee

School on Modelling Planetary Microlensing Events

Introduction to microlensing

Philippe Jetzer

From microlensing observations to science

Martin Dominik

The theory and phenomenology of planetary microlensing

Scott Gaudi

From raw images to lightcurves: how to make sense of your data

Yiannis Tsapras

The efficient modeling of planetary microlensing events

David Bennett

Contour integration and downhill fitting

Valerio Bozza

Microlensing modelling and high performance computing

Ian Bond

Introduction to microlensing

Philippe Jetzer

*Institute of Theoretical Physics, University of Zurich
Switzerland*

In the lecture I will present the basic formalism of gravitational lensing such as the lens equation and the special case of the Schwarzschild lens with its application in microlensing. I will discuss the microlensing probability for different targets such as the galactic bulge, LMC, SMC and the Andromeda galaxy as well as give a short review of the present status of microlensing searches conducted by the various collaborations in particular with respect to the problem of the galactic dark matter content in form of MACHOs.

From microlensing observations to science

Martin Dominik

*SUPA, University of St Andrews, School of Physics & Astronomy
United Kingdom*

An elaborate integrated strategy incorporating target selection and scheduling, data flow, assessment, and final analysis is required to ensure that the scientific goals that we aim for are achieved. Specific issues that need to be taken care of are dealing with uncertainties, ambiguities, and degeneracies, as well as having the capacity to keep track with data being acquired at ever increasing rate. I will present you with some challenges.

The theory and Phenomenology of Planetary Microlensing

Scott Gaudi

*Department of Astronomy, Ohio State University
USA*

I discuss the theory and phenomenology of planetary microlensing. I begin with a review of the basic theoretical formalism: starting with the time delay surface, and continuing with the lens equation, I describe how critical curves, caustics, and magnifications can be computed. I then explore the properties of the caustic curves of planetary microlenses. I illustrate the topology of caustic curves and how these change with the parameters of the planetary system. In addition, I review the generic, universal behavior of images near caustics. I then delve into the rich phenomenology and salient observable properties of planetary microlensing light curves, and discuss how these can be intuitively understood based on consideration of the microlensed images and shape of and magnification near the caustics. Finally, I demonstrate how all of these considerations can be used to roughly estimate the properties of a planetary system giving rise to an observed light curve based purely on visual inspection.

From raw images to lightcurves: how to make sense of your data

Yiannis Tsapras
Queen Mary University
UK

I will present an overview of astronomical image processing with special focus on the difference imaging technique in the context of microlensing observations towards the galactic bulge. Starting from how to calibrate the raw data, I will discuss the various steps involved in the analysis, possible pitfalls, and how to extract the photometric information from the images in order to construct a clean lightcurve. Examples using the RoboNet DIA software will be given.

The Efficient Modeling of Planetary Microlensing Events

David P. Bennett
University of Notre Dame, Notre Dame, IN
USA

I present a general method for the modeling of planetary microlensing events, with an emphasis on the most difficult events which involve more than two lens masses, microlensing parallax and/or orbital motion. Finite source calculations are done with the image centered ray-shooting method, which can be made both highly efficient and flexible enough to model any events.

Contour integration and downhill fitting

Valerio Bozza

*Department of Physics, University of Salerno
Italy*

By Green's theorem, the two-dimensional integration on the microlensed images is written as a line integral on the image boundaries. We will discuss the advantages and the shortcomings of this method, presenting several improvements of the basic idea: parabolic correction, error control, optimal sampling, limb darkening. We will also review some basic downhill fitting methods, which rapidly provide preliminary models for microlensing events starting from suitable initial conditions.

Microlensing Modelling and High Performance Computing

*Ian Bond
Massey University
New Zealand*

I will go over the practical aspects of the modelling and analysis of microlensing events. I will discuss two programming environments for high performance computing: cluster computers and GPU (graphical processor units) platforms. I will describe, with examples, how to design and implement software to run on these platforms. In particular, GPUs are emerging as a powerful tool for scientific computation and their potential in microlensing modelling is promising. The use of GPUs will be particularly emphasized in this seminar.

Conference topical speeches

Giant planet accretion and dynamical evolution: considerations on systems around small-mass stars

Alessandro Morbidelli

The dark matter - LHC endeavour to unveil TeV new physics

Antonio Masiero

Characterization of planetary systems with high-precision astrometry: the Gaia potential

Alessandro Sozzetti

Giant planet accretion and dynamical evolution: considerations on systems around small-mass stars

Alessandro Morbidelli

*Observatoire de la Cote d’Azur, Nice
France*

1 Introduction

The classical model of giant planet formation envisions that multi-Earth mass solid cores formed from the accretion of planetesimals and that these cores then captured by gravity a massive atmosphere from the gas in the proto-planetary disk [1]. A problem in this scenario is that the solid cores have to grow on a timescale shorter than the gas-dissipation timescale, which observations set to be a few My only [2]. This is not easy, particularly in disks with small densities, such as those around low-mass stars. For this reason it is expected that giant planets cannot form around low-mass stars [3] or they form very rarely [4]. However, micro-lensing and radial velocity detections show that giant planets do exist around stars down to at least $0.2M_{\oplus}$. This conflict between models and observations suggests that the process of giant planet accretion needs to be revisited

2 The problem of core accretion

It has been recently pointed out that our ideas on the accretion of the cores of the giant planets were simplistic even in the case of disks around solar-mass stars.

In fact, N-body simulations show that, once the cores become sufficiently massive (about $1M_{\oplus}$), they tend to scatter the planetesimals away, rather than accrete them. In doing this, they clear their neighboring region, which in turn limits their own growth, even if initially there are a lot of solids available in the system. If damping effects are included in the simulation, in the hope of limiting the ability of the cores to scatter the planetesimals away, the result is that the planetesimals end up in stable circular orbits that are dynamically separated from the cores (i.e. no close encounters with the cores are possible). Effectively, the cores open radial gaps in the planetesimal distribution [5]. One could think that core migration or planetesimal radial drift due to gas drag can help to break the isolation of the cores from the planetesimals. However the simulations show that, in these cases, most planetesimals

end up locked in resonances with the cores; resonances prevent collisions, so radial migration is unlikely to boost accretion in a significant way [5].

3 Hints for a new model of formation of giant planets cores

New results on the migration of proto-planets in gas-disks show that the concept of inward migration of Earth-mass objects (the so-called Type I migration [6]) is valid only in idealized isothermal disks. In more realistic radiative disks, the migration of the proto-planets is outward in the inner part of the disk and inward in the outer part [7][8][9]. There are therefore one (or sometimes two) orbital radii where migration is cancelled. All proto-planets formed in the disk tend to migrate towards these equilibrium radii [10]. This can concentrate the proto-planets in a narrow region of space and favor further mutual accretion, thus leading to the formation of giant planets cores. A proof-of-concept simulation will be presented at the conference, leading to the formation of a $12M_{\oplus}$ body from a system of $1M_{\oplus}$ planetary embryos.

If this idea is correct, the formation of the cores of the giant planets is not due to the local runaway accretion of small planetesimals, but to the concentration of all planetary embryos that formed throughout the disk and their subsequent mutual collisions. This is a big change of emphasis. The concept of the *local* surface density is not relevant any more because the material is migrated to the site of growth of the core from a large range of distances. This gives hope that the formation of the cores is less sensitive to the surface density of the disk than previously expected, and that therefore giant planet formation is more likely also around low-mass stars.

4 Dynamical evolution of giant planets

Once giant planets are formed, they open gaps in the gas distribution in the proto-planetary disk. Once this happens, giant planets are expected to undergo Type II migration towards the central star [11].

Also Type-II migration, though, is an idealized concept. It is valid in the case where planets are much less massive than disks and they open extremely deep gaps that gas cannot pass through. In the other cases, the planets do not migrate at the Type-II rate; they can even move outward and, instead of gaps, they can open cavities in the inner part of the disk, removing most the gas between the star and the orbit of the planet [12].

In case of two (or more) planets, the migration pattern is even more complex. For two planets in resonance, migration is inward if the outer planet has a mass comparable to the inner one, or larger. If the outer planet has a mass that is a sizeable

fraction of the inner one (as in the Jupiter-Saturn case), migration is outward. If the outer planet has a negligible mass (say Jupiter and Neptune), migration is inward again [13]. Thus, for our solar system we can envision that Jupiter migrated inwards while Saturn was growing and then, once Saturn reached a mass close to its current one, they migrated outward. This kind of evolution may be relevant for the system around the star OGLE-06-109L, discovered by microlensing, which looks like a Sun-Jupiter-Saturn system slightly scaled down in mass.

References

- [1] Pollack, J. B., Hubickyj, O., Bodenheimer, P., Lissauer, J. J., Podolak, M., Greenzweig, Y. 1996. Formation of the Giant Planets by Concurrent Accretion of Solids and Gas. *Icarus* 124, 62-85
- [2] Haisch, K. E., Jr., Lada, E. A., Lada, C. J. 2001. Disk Frequencies and Lifetimes in Young Clusters. *The Astrophysical Journal* 553, L153-L156
- [3] Laughlin, G., Bodenheimer, P., Adams, F. C. 2004. The Core Accretion Model Predicts Few Jovian-Mass Planets Orbiting Red Dwarfs. *The Astrophysical Journal* 612, L73-L76
- [4] Alibert, Y., Mordasini, C., Benz, W. 2011. Extrasolar planet population synthesis. III. Formation of planets around stars of different masses. *Astronomy and Astrophysics* 526, A63
- [5] Levison, H. F., Thommes, E., Duncan, M. J. 2010. Modeling the Formation of Giant Planet Cores. I. Evaluating Key Processes. *The Astronomical Journal* 139, 1297-1314
- [6] Goldreich, P., Tremaine, S. 1980. Disk-satellite interactions. *The Astrophysical Journal* 241, 425-441
- [7] Paardekooper, S.-J., Mellema, G. 2006. Halting type I planet migration in non-isothermal disks. *Astronomy and Astrophysics* 459, L17-L20
- [8] Baruteau, C., Masset, F. 2008. On the Corotation Torque in a Radiatively Inefficient Disk. *The Astrophysical Journal* 672, 1054-1067
- [9] Kley, W., Crida, A. 2008. Migration of protoplanets in radiative discs. *Astronomy and Astrophysics* 487, L9-L12
- [10] Lyra, W., Paardekooper, S.-J., Mac Low, M.-M. 2010. Orbital Migration of Low-mass Planets in Evolutionary Radiative Models: Avoiding Catastrophic Infall. *The Astrophysical Journal* 715, L68-L73

- [11] Lin, D. N. C., Papaloizou, J. 1986. On the tidal interaction between protoplanets and the protoplanetary disk. III - Orbital migration of protoplanets. *The Astrophysical Journal* 309, 846-857
- [12] Crida, A., Morbidelli, A. 2007. Cavity opening by a giant planet in a protoplanetary disc and effects on planetary migration. *Monthly Notices of the Royal Astronomical Society* 377, 1324-1336
- [13] Morbidelli, A., Crida, A. 2007. The dynamics of Jupiter and Saturn in the gaseous protoplanetary disk. *Icarus* 191, 158-171

The Dark Matter - LHC Endeavour to Unveil TeV New Physics

*Antonio Masiero
INFN - University of Padova
Italy*

After more than four decades of relentless tests of the Standard Model (SM) of particle physics, one can safely state that it correctly describes the fundamental interactions all the way up to the energy scale of 100 GeV. Yet, the observational evidences that neutrinos are massive and that a large amount of non-baryonic dark matter exists corroborate the theoretical demand for the presence of new non-SM physics at the TeV scale. Interestingly enough, the main theoretical motivation for new physics (NP) at the electroweak scale (i.e., the presence of an ultraviolet SM completion to enforce the stability of the electroweak breaking scale) nicely joins the need for some form of cold matter: indeed, most theoretically dictated extensions of the SM (low-energy supersymmetry, extra-dimensions, etc.) entail the existence of some new stable particle which can play the role of dark matter candidate. I'll discuss the interplay between the searches for TeV NP which are going on at the LHC and the searches for dark matter related to TeV NP both in direct and indirect DM probes. It is exciting that the coming decade has the potentiality to witness the simultaneous success of the high-energy (LHC) and astroparticle (DM) roads in our endeavour to unveil the presence of NP at the electroweak scale.

Characterization of Planetary Systems with High-Precision Astrometry: The Gaia Potential

Alessandro Sozzetti

INAF - Osservatorio Astronomico di Torino

Italy

1 Introduction

In its all-sky survey, the ESA global astrometry mission Gaia, due to launch in late 2012, will perform high-precision astrometry and photometry for 1 billion stars down to $V = 20$ mag. The data collected in the Gaia catalogue, to be published by the end of the decade, will likely revolutionize our understanding of many aspects of stellar and Galactic astrophysics. One of the relevant areas in which the Gaia observations will have great impact is the astrophysics of planetary systems. There are many complex technical problems related to and challenges inherent in correctly modelling the signals of planetary systems present in measurements collected with an observatory poised to carry out precision astrometry at the micro-arcsecond (μas) level. Provided these are well understood, Gaia μas astrometry has great potential for important contributions to the astrophysics of planetary systems, particularly when seen in synergy with other indirect and direct methods for the detection and characterization of planetary systems.

2 Astrometric Modeling of Planetary Systems

The problem of the correct determination of the astrometric orbits of planetary systems using Gaia data (highly non-linear orbital fitting procedures, large numbers of model parameters) will present many difficulties. For example, it will be necessary to assess the relative robustness and reliability of different procedures for orbital fits, with a detailed understanding of the statistical properties of the uncertainties associated with the model parameters. For multiple systems, a trade-off will have to be found between accuracy in the determination of the mutual inclination angles between pairs of planetary orbits, single-measurement precision and redundancy in the number of observations with respect to the number of estimated model parameters. It will be challenging to correctly identify signals with amplitude close to the measurement uncertainties, particularly in the presence of larger signals induced by other

companions and/or sources of astrophysical noise of comparable magnitude. Finally, for systems where dynamical interactions are important (a situation experienced already by Doppler surveys), fully dynamical fits involving an n-body code might have to be used to properly model the Gaia astrometric data and to ensure the dynamical stability of the solution (see Sozzetti 2005). All the above issues could significantly impact Gaia's planet detection and characterization capabilities. For these reasons, a Development Unit (DU), within the pipeline of Coordination Unit 4 (object processing) of the Gaia Data Processing and Analysis Consortium, has been specifically devoted to the modelling of the astrometric signals produced by planetary systems. The DU is composed of several tasks, which implement multiple robust procedures for (single and multiple) astrometric orbit fitting (such as Markov Chain Monte Carlo algorithms) and the determination of the degree of dynamical stability of multi-planet systems.

Δd (pc)	N_\star	Δa (AU)	ΔM_p (M_J)	N_d	N_m
0-50	1×10^4	1.0 - 4.0	1.0 - 13.0	1400	700
50-100	5×10^4	1.0 - 4.0	1.5 - 13.0	2500	1750
100-150	1×10^5	1.5 - 3.8	2.0 - 13.0	2600	1300
150-200	3×10^5	1.4 - 3.4	3.0 - 13.0	2150	1050

(a)

Case	N. of systems
Detection	~ 1000
Orbits and masses to < 15 - 20% accuracy	$\sim 400 - 500$
Successful coplanarity tests	~ 150

(b)

Table 1: Left: Number of giant planets of given ranges of mass (ΔM_p) and orbital separation (Δa) that could be detected (N_d) and measured (N_m) by Gaia, as a function of increasing distance (Δd) and stellar sample (N_\star). Right: Number of planetary systems that Gaia could potentially detect, measure, and for which coplanarity tests could be carried out successfully. See Casertano et al. (2008) for details.

2.1 The Gaia Legacy

Gaia's main contribution to exoplanet science will be its unbiased census of thousands of planetary systems (see Table 1) orbiting hundreds of thousands nearby ($d < 200$ pc), relatively bright ($V \leq 13$) stars across all spectral types, screened with constant astrometric sensitivity. As a result, the actual impact of Gaia measurements in exoplanets science is broad, and rather structured. The Gaia data have the potential to: a) significantly refine our understanding of the statistical properties of extrasolar planets; b) help crucially test theoretical models of gas giant planet formation and migration; c) achieve key improvements in our comprehension of important aspects of the formation and dynamical evolution of multiple-planet systems; d) aid in the understanding of direct detections of giant extrasolar planets; e) provide important supplementary data for the optimization of the target selection for future observatories

aiming at the direct detection and spectral characterization of habitable terrestrial planets. Finally, ongoing studies are now focusing on the detailed understanding of the planet discovery potential of Gaia as far as low-mass stars (Sozzetti et al., in preparation) and post-main-sequence objects (Silvotti, Sozzetti, & Lattanzi 2011) and are concerned.

In conclusion, the Gaia mission is now set to establish the European leadership in high-precision astrometry for the next decade. The largest compilation of high-accuracy astrometric orbits of giant planets, unbiased across all spectral types up to $d \simeq 200$ pc, will allow Gaia to crucially contribute to several aspects of planetary systems astrophysics (formation theories, dynamical evolution), in combination with present-day and future extrasolar planet search programs.

References

- [1] S. Casertano S., M.G. Lattanzi, A. Sozzetti A., S. Jancart, R. Morbidelli, R. Pannunzio, D. Pourbaix, D. Queloz, & A. Spagna, *Astron. & Astrop.*, **482**, 699, 729 (2008)
- [2] R. Silvotti, A. Sozzetti, & M.G. Lattanzi, *AIP Conf. Ser.*, in press (2011)
- [3] A. Sozzetti, *Pub. Astr. Soc. Pac.*, **117**, 1021, 1048 (2005)

Status of current surveys

Status of the OGLE-IV Survey *Andrzej Udalski*

MOA-II observation in 2010 season *Takahiro Sumi*

Session Chair: Martin Perl

The deflection of light ray *Asoke Kumar Sen*
in strong field: a material medium approach

Status of the OGLE-IV Survey

*Andrzej Udalski
Warsaw University Observatory
Poland*

On the night of March 4/5, 2010, after ten months long break, the OGLE survey resumed regular observations entering the OGLE-IV phase. With the new 32 chip mosaic camera covering 1.4 square degrees on the sky with the resolution of 0.26 arcsec/pixel and fast reading time of the entire array of 20 seconds the observing capabilities of the OGLE survey increased by an order of magnitude compared to the previous OGLE-III phase. With this observing set-up the OGLE project continues its 18 years long tradition of being one of the largest sky surveys worldwide with the current outcome of about 40 Terabytes of raw data per year.

During the 2010 Galactic bulge observing season OGLE-IV regularly monitored large fraction of the Galactic bulge conducting pilot observations for the second generation microlensing survey. About 4.5 square degrees of the Galactic bulge regions with the highest microlensing rate were observed with the cadence of 20 minutes while additional 8.5 square degrees with the cadence of 1 hour. Moreover, large area of the Galactic bulge was observed once or twice a day.

The automatic data pipeline of OGLE-IV images reductions has been recently finished. Its full implementation at the telescope, expected in early 2011, will allow to restart on-line (real time) reductions of the huge data-stream coming from the OGLE telescope and restart the data analysis systems like the OGLE Early Warning System.

MOA-II observation in 2010 season

*Takahiro Sumi
Solar-Terrestrial Environment Laboratory
Nagoya University
Japan*

1 Introduction

Since the first discovery of exoplanets orbiting main-sequence stars in 1995 [1], more than 500 exoplanets have been discovered via the radial velocity method and more than 50 have been detected via their transits. Several planetary candidates have also been detected via direct imaging, and astrometry.

The gravitational microlensing was proposed as a unique method to search exoplanets [2, 3]. The planet's gravity induces small caustics, which can generate small deviations in standard [4] single-lens microlensing light curves. Compared to other techniques, microlensing is sensitive to smaller planets, down to an Earth mass [5], and in wider orbits of 1-6 AU. Because microlensing observability does not depend on the light from the lens host star, it is sensitive to planets orbiting faint host stars like M-dwarfs and even brown dwarfs. Furthermore, it is sensitive to distant host stars at several kpc from the Sun, which allows the Galactic distribution of planetary systems to be studied.

In 2003, the gravitational microlensing method yielded its first definitive exoplanet discovery [8]. So far ten planetary systems with eleven planets have been found by this technique [7], which have very distinct properties from those detected by other techniques.

Although the radial velocity and transit discoveries are more numerous, microlensing is uniquely sensitive to the cold Neptunes outside of the snow-line, and the microlensing results to date indicate that this class of planets may be the most common type of exoplanet yet discovered [8].

2 Observations

The MOA-II carries out survey observations toward the Galactic Bulge (GB) to find exoplanets and toward the large and small Magellanic clouds (LMC and SMC) for searching MACHOs via the gravitational microlensing using a 1.8m telescope,

equipped with a mosaic camera with 10 chips of 2kx4k-pixel CCD[9], at Mt. John Observatory in New Zealand. We observe our target fields very frequently (every 15-90 min) and analyze data in real-time to issue alerts. This high cadence is specifically designed to find the short timescale planetary signature. Our real-time anomaly alert system searches for planetary signatures in ongoing microlensing events in which new data points are available on the light curves within 5 min after exposure. In 2010 season, we continued this observational strategy.

3 Results

In 2010 season, we detected 607 microlensing events and issued the alerts toward the GB. Among these, 5 events show planetary or brown dwarf signatures in their light curves thanks to the data by OGLE-IV survey and intensive follow-up observations by μ FUN, PLANET, RoboNet, MiNDSTEp.

In 2010, we found one event toward the LMC that shows a clear asymmetry due to the parallax. This indicates that the lens object is likely a foreground disk star.

We are grateful to OGLE, μ FUN, PLANET, RoboNet, MiNDSTEP collaborations for close cooperation.

References

- [1] Mayor, M., & Queloz, D. 1995, *Nature*, 378, 355
- [2] Liebes, S. 1964, *Phys. Rev.*, 133, 835
- [3] Mao, S., & Paczyński, B. 1991, *ApJ*, 374, L37
- [4] Paczyński, B. 1986, *ApJ*, 304,1
- [5] Bennett, D. P., & Rhie, S. H. 1996, *ApJ*, 472, 660
- [6] Bond, I. A., et al. 2004, *ApJ*, 606, L155
- [7] Miyake, N., et al. 2011, *ApJ* in press, arXiv:1010.1809
- [8] Sumi, T., et al. 2010, *ApJ*, 710, 1641
- [9] Sako, T., et al. 2008, *Experimental Astronomy*, 22, 51

The RoboNet 2010 season

Yiannis Tsapras
Queen Mary University
UK

1 The Las Cumbres Observatory Global Telescope Network

The Las Cumbres Observatory (LCOGT) [1] is a privately funded institute which owns and operates the 2m Faulkes Telescopes in Hawaii and Australia. LCOGT is in the process of developing a global network of 1m and 0.4m telescopes capable of robotic around-the-clock observations. These will be used for science as well as education. The 0.4m and 1m prototypes are currently being tested and deployment around the world will begin in 2011. The first ones will be deployed in Chile and South Africa, followed by Tenerife, Australia and China. The complete network will comprise of twelve to fifteen 1m and twenty-four 0.4m telescopes and is expected to be complete by the end of 2014. The final numbers depend on the relative costs. The SUPA-II Planet Hunter bid from the University of St Andrews will finance the construction of an extra three 1m telescopes with exactly the same specifications.

The 0.4m telescopes will be primarily used for educational purposes. Schools from around the world will have access to these telescopes through web interfaces and will be able to make observations during daylight hours in Europe by using the telescopes in Chile, Hawaii and Australia. Furthermore, they will have the option to get involved in certain science projects, like microlensing or transits, and contribute observations. The LCOGT education pages provide descriptions of possible projects available to the students. The 1m telescopes will be used for science observations. Each site will eventually host two to four telescopes which can be operated individually or in parallel, allowing simultaneous observations of targets in different pass-bands. Each telescope will be fitted with a fast readout CCD camera that has a field of view of about half a degree and filters in the UBVRI and Pan-STARRS Z and Y bands. Each cluster of telescopes will have an optical fiber-feed to a shared medium-resolution spectrograph.

The observation requests sent out to the telescopes will be scheduled by a highly dynamic scheduling algorithm that will constantly farm the database of TAC-approved science projects for the most appropriate observations to perform at any given time given the current conditions and the scientific priority.

2 RoboNet: A microlensing search for cold planets

In order to draw conclusions about planetary populations, it is not enough to just detect planets, it is necessary to understand the selection bias of the surveys. This requires the adoption of an observing strategy that is not based on human intervention, since this cannot be simulated. RoboNet’s unique advantage is that our entire system is completely automated, which makes it easier to understand the selection biases of our strategy. As the system is designed for a network with continuous Bulge coverage, we expect to address this question with the help of the full LCOGT network in future seasons.

The methodology used by the RoboNet team is described in [2]. Our pilot campaign (RoboNet-I) contributed to 5 of the first 6 microlensing planet discoveries and provided the impetus to develop our system further. We are continuing this development in preparation for the deployment of the LCOGT network of 1m and 0.4m telescopes.

RoboNet has pioneered the technique of adaptive scheduling of microlensing targets through the use of a prioritisation algorithm that continuously shuffles the observable microlensing targets, giving higher priority to the ones that are more likely to reveal a planetary signal [3]. It calculates the optimal frequency at which each ongoing microlensing event needs to be sampled at in order to maximize the planet detection probability. Once an observation is obtained for a specific event, it’s priority is adjusted upwards in the case that it deviates from the expected single-lens case, or downwards if it doesn’t. The relative priorities are reassessed every few minutes and active events that have not been observed recently will start to appear higher and higher in the list until an observation is obtained. At that point their relative priority will be readjusted according to the previous scheme. In order to be sensitive to ”cold Earths”, a sampling interval of 15-45 mins is required, which the extended robotic network will be able to deliver.

RoboNet makes use of difference image analysis software [4] to extract accurate brightness measurements from the incoming images which are used to construct the event lightcurves. One image is selected as a template and all other images are geometrically and photometrically aligned to and subtracted from it. Any stars that show variability are immediately obvious on the resulting subtracted images, while stars of constant brightness leave no residuals.

The resulting lightcurves are immediately shared with the extended microlensing community via automated rsync transfers but are also available on the project website for downloading. The lightcurves are continuously assessed by our SIGNALMEN software, which uses robust methods to automatically detect the onset of anomalous features. If such a feature is detected, an override request is sent to the network to obtain prompt observations that will confirm or disprove the anomaly. While most observations are performed in queued observing mode, we sometimes use our override

capability in order to respond to anomaly alerts. Once more telescopes are included in our network, we will be able to operate in a fully automated mode throughout the microlensing season.

References

- [1] www.lcogt.net
- [2] Tsapras, Y. et al., 2009, AN, 330, 4
- [3] Horne, K., Snodgrass, C., Tsapras, Y., 2009, MNRAS, 396, 2087
- [4] Bramich, D., 2008, MNRAS, 386, L77-81

Cosmological Microlensing

Dark matter determinations from Chandra observations of quadruply lensed quasars

David Pooley

Cosmic equation of state from strong gravitational lensing systems

Marek Biesiada & Beata Malec

Dark Matter Determinations from *Chandra* Observations of Quadruply Lensed Quasars

David Pooley
Eureka Scientific
USA

I present all publicly available *Chandra* observations of 14 X-ray bright quadruply lensed quasars. The X-ray data reveal flux ratio anomalies which are more extreme than those seen at optical wavelengths, confirming the microlensing origin of the anomalies originally seen in the optical data. The X-ray emitting regions are essentially point sources and therefore give a microlensing signal unencumbered by source size considerations. Building on our previous work, we have completed a thorough investigation of the best way to analyze the X-ray data, resulting in improved determinations of the X-ray flux ratios. We have constructed custom microlensing magnification maps for a range of stellar fractions for the four images of each quasar, and we have implemented a more sophisticated Bayesian analysis of the data to determine the most likely dark matter fraction in the lensing galaxies.

Cosmic Equation of state from Strong Gravitational Lensing Systems

Marek Biesiada

*Department of Astrophysics and Cosmology, Institute of Physics
University of Silesia Poland*

Beata Malec

*Copernicus Center for Interdisciplinary Studies
Cracow Poland*

1 Introduction

Accelerating expansion of the Universe is a great challenge for both physics and cosmology. In light of lacking the convincing theoretical explanation, an effective description of this phenomenon in terms of cosmic equation of state turns out useful.

The strength of modern cosmology lies in consistency across independent, often unrelated pieces of evidence. Therefore, every alternative method of restricting cosmic equation of state is important. Strongly gravitationally lensed quasar-galaxy systems create such new opportunity by combining stellar kinematics (central velocity dispersion measurements) with lensing geometry (Einstein radius determination from position of images).

2 Idea and methods

Strong gravitationally lensed systems create opportunity to test cosmological models of dark energy in a way alternative to Hubble diagrams (from SNIa or GRBs), CMBR or LSS. The idea is that formula for the Einstein radius in a SIS lens (or its SIE equivalent)

$$\theta_E = 4\pi \frac{\sigma_{SIS}^2}{c^2} \frac{D_{ls}}{D_s}$$

depends on the cosmological model through the ratio: (angular-diameter) distance between lens and source to the distance between observer and lens. Provided one has reliable knowledge about lensing system: the Einstein radius θ_E (from image astrometry) and stellar velocity dispersion σ_{SIS} (central velocity dispersion inferred from

spectroscopy) one can use such well studied systems to test background cosmology. This method is independent on the Hubble constant value (H_0 gets cancelled in the distance ratio) and is not affected by dust absorption or source evolutionary effects. It depends, however, on the reliability of lens modelling (e.g. SIS or SIE assumption). The method was proposed by Biesiada [1] and also discussed in details by Grillo et al. (2008) [2].

Here we apply such method to a combined data sets from SLACS and LSD surveys of gravitational lenses [2]. In result we obtain the cosmic equation of state parameters, which generally agree with results already known in the literature. This demonstrates that the method can be further used on larger samples obtained in the future [3]. We have also performed joint analysis taking into account standard rulers (combining lensing system data with CMB acoustic peak location and BAO data) and standard candles (SNIa data - we used Union08 compilation by Kowalski et al. (2008) [4]). The observables we used had different parameter degeneracies and so different restrictive power in the parameter spaces of cosmological models. It can be best seen in figures.

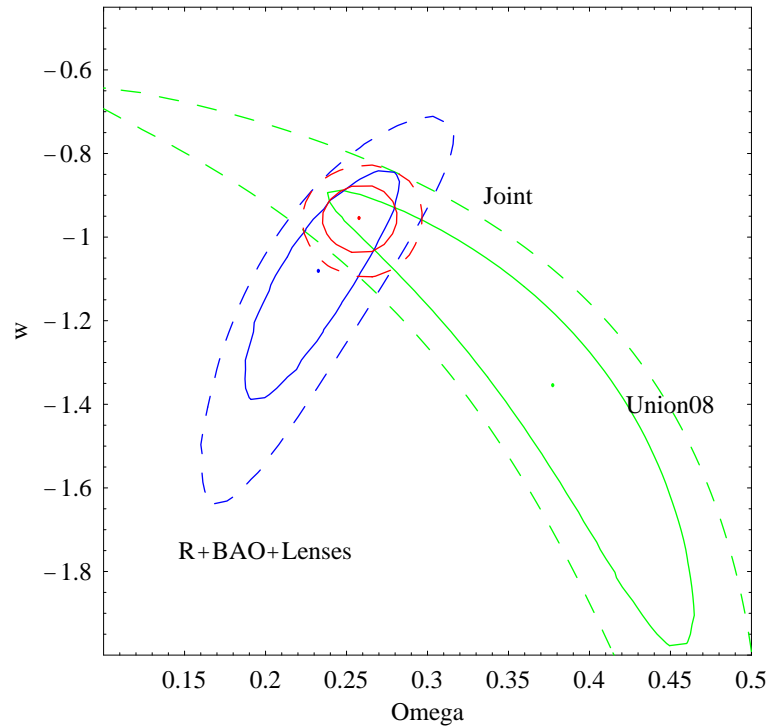


Figure 1: Best fits (dots) and (68 %, 95%) confidence regions in (Ω, w) plane for quintessence model. Confidence regions displayed separately for standard rulers, standard candles and joint analysis.

We considered five cosmological scenarios of dark energy, widely discussed in current literature. These are Λ CDM, Quintessence, Chevalier-Polarski-Linder model, Chaplygin gas and Braneworld scenario. Then we performed χ^2 fits to different cosmological scenarios on described samples. The probes were combined by calculating joint likelihoods.

Because standard rulers and standard candles probe distance measures based on different concepts (angular diameter distance and luminosity distance), one step before making a full joint fit we performed fits based on rulers and candles separately.

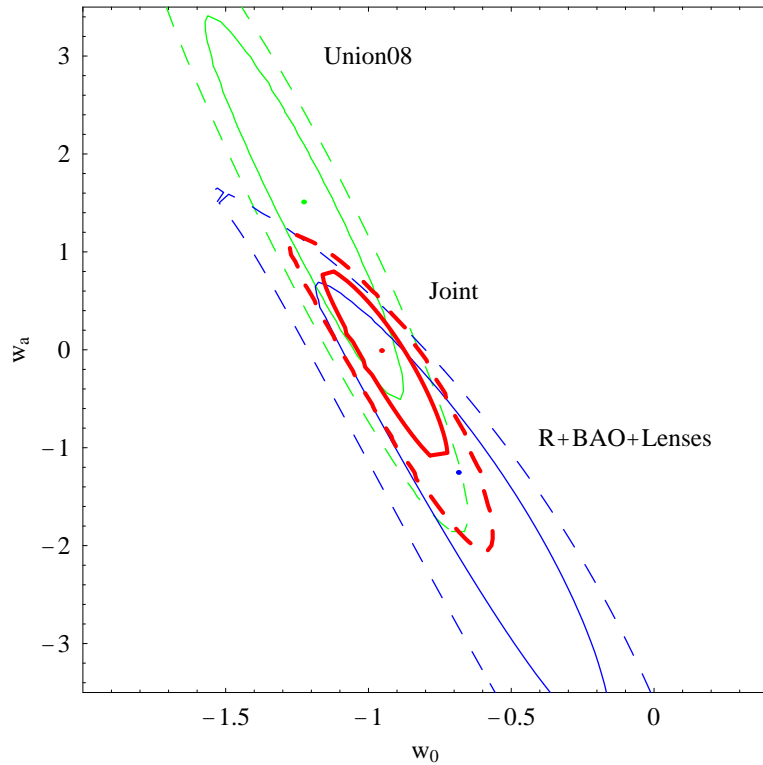


Figure 2: Best fits (dots) and (68 %, 95%) confidence regions in (w_0, w_a) plane for Chevalier-Linder-Polarski model. Confidence regions displayed separately for standard rulers, standard candles and joint analysis.

3 Conclusions

The best fits we obtained for the model parameters in joint analysis turned out to prefer cases effectively equivalent to Λ CDM model. They are also in agreement with other combined studies performed by other authors on different sets of diagnostic

probes. As comparison between models in terms of chi-square values does not account for the relative structural complexity of the models we also made use of information theoretic methods. According to Akaike criterion (AIC) Λ CDM it is only slightly preferred over the quintessence and both models with a dynamical equation of state $w(z)$ (CPL parametrization) and Chaplygin gas scenario get considerably less support from the data. Odds against the brane-world scenario are so high that it can be considered as ruled out by the data. According to the Schwartz Bayesian Information criterion (BIC) Λ CDM wins, the quintessence model is considerably less supported by data, and the other ones are ruled out.

This work was supported by the Polish Ministry of Science Grant no. N N203 390034.

References

- [1] M. Biesiada, Phys. Rev. D **73**, 023006 (2006).
- [2] C. Grillo, M. Lombardi and G. Bertin, A&A **477** 397-406, (2008).
- [3] M. Biesiada, A. Pirkowska, B. Malec, MNRAS **406**, 1055B (2010)
- [4] M. Kowalski, et al., ApJ **686**, 749-778, (2008).

Galactic Microlensing: the dark matter search

PAndromeda - the Pan-STARRS M31 survey for dark matter

Arno Riffeser, Stella Seitz, Ralf Bender, C.-H. Lee, Johannes Koppenhoefer

Final OGLE-II and OGLE-III results on microlensing towards the LMC and SMC

Lukasz Wyrzykowski

Analysis of microlensing events towards the LMC

Luigi Mancini & Sebastiano Calchi Novati

Simulation of short time scale pixel lensing towards the Virgo cluster

Sedighe Sajadian & Sohrab Rahvar

M31 pixel lensing and the PLAN project

Sebastiano Calchi Novati

PAndromeda - A Dedicated Deep Survey of M31 with Pan-STARRS 1

*Arno Riffeser, Stella Seitz, Ralf Bender, Chien-Hsiu Lee, Johannes Koppenhoefer
Max Planck Institute for Extraterrestrial Physics, Garching
Germany*

Pan-STARRS 1 Science Consortium University of Hawaii, Pan-STARRS Project Office, Max Planck Institute for Astronomy, Max Planck Institute for Extraterrestrial Physics, Johns Hopkins University, University of Durham, University of Edinburgh, Queens University of Belfast, Harvard-Smithsonian Center for Astrophysics, Los Cumbres Observatory Global Telescope Network, National Central University of Taiwan

The 1.8 m Panoramic Survey Telescope and Rapid Response System (Pan-STARRS) on Haleakala, Maui, began its regular survey in spring 2010. With its ~ 7 deg² field of view and the use of orthogonal transfer array CCDs [1] it represents the system with the highest data-flow today. In addition to the large area 3Pi Survey some fields are exposed deeper, and visited more frequently. One of these so called medium deep fields (MD) targets the Andromeda galaxy. PAndromeda monitors M31 for 2% of the overall PS1 time. This means that M31 is observed for 0.5 h per night during a period of 5 months per year. PAndromeda is designed to identify gravitational microlensing events, caused by bulge and disk stars (self-lensing) and by compact matter in the halos of M31 and the MW (halo lensing, or lensing by MACHOs). The main science goals of PAndromeda are measuring the masses and mass-fraction of compact objects in the M31 and MW halos, and constraining the M31 bulge mass function at the low mass end. As a side product PAndromeda is also able to search for microlensing events towards M32 and NGC 205.

The interpretation of the microlensing events (see [2]) requires i) understanding the mix of stellar ages and metallicities in the bulge, disk, and halo of M31 as obtained from resolved stellar populations (census of supergiants, OB-associations, analysis of CMD diagrams as a function of location) variability studies (from Cepheids to LPVs), and color gradients in the light profiles, ii) deriving improved 3 dimensional models for the density and velocity distributions of the bulge and disk, iii) including improved constraints on the extinction in M31 [3]. All these informations can directly extracted from the PAndromeda data itself.

The continuous monitoring in the r' and i' bands with PAndromeda allows to confirm the achromaticity of events; the main filter (detection filter) is the r' -band to optimize the number of source stars accessible for measurable lensing events, which

depends on the brightness of the stars, the photon noise (mostly by M31), and the sensitivity of filters in each band. During the first season we focussed on the integration depth in the filters r' and i' . We split the r' -band imaging into two integrations (separated by 4-6 hours) per night, for the whole season. This allows to measure light curves with shorter time scales than 1 day more accurately, since a large fraction of events is predicted (and found in previous surveys) with short time scales. PAndromeda monitored M31 from 07/23/2010 till 12/27/2010 on 91 nights (58%). In total 1782 images were exposed, 1179 in r' (90 nights, 70740 sec) and 603 in i' band (66 nights, 36180 sec). The total amount of reduced data is 14 TB. Depending on our observing strategy in 2011 the remaining filters and integration times for PAndromeda will be chosen such, that in turn these observations can be used to study many other aspects of M31 with the aim to improve the predictions of the microlensing event rates. These microlensing predictions depend on the mass function of stars, their luminosities and sizes as determined by their ages and metallicities, on their density and velocities distributions, and on the extinction.

The PS1 Gigapixel Camera (GPC1) produces images consisting of 3840 CCDs ($60 \times 8 \times 8$) with roughly 580×590 pixels each. This results in 1.3×10^9 pixels which are exposed and read-out. The GPC1 data are de-biased, flat-fielded, and astrometrically registered with the Pan-STARRS Image Processing Pipeline (by Magnier E.). A reduced GPC1 exposure requires a disk storage of 8.0 GB consisting of frame, weight and mask. After this basic reduction the data are further processed by our own image processing software (MUPIPE, [4]). For the PAndromeda difference imaging analysis we adapted the MUPIPE pipeline to the specifications of PS1 data and data flow and implemented it into the Astro-WISE system.

From the 2010 season we analyzed the central field of M31 ($21' \times 21'$). This is to test the detection process in the field where we expect the highest lensing rate because of self lensing. So far we detected 3 high quality microlensing light-curves. The third one is very bright with 19 mag in r' . Note that high flux excess events are more difficult to reconcile with self-lensing than with halo-lensing [5]. The full data set is currently analyzed.

References

- [1] Burke *et al.* (2007), (SPIE) Conference, 6501, ed. M. M. Blouke, 07
- [2] Riffeser *et al.* (2006), ApJS, 163, 225
- [3] Montalto *et al.* (2009), A&A, 507, 283
- [4] Gössl & Riffeser (2002), A&A, 381, 1095
- [5] Riffeser *et al.* (2008), ApJ, 684, 1093

Final OGLE-II and OGLE-III results on microlensing towards the LMC and SMC

Lukasz Wyrzykowski
Institute of Astronomy, University of Cambridge
UK

1 Introduction

For almost two decades compact halo objects (MACHOs) have been one of the best candidate for Dark Matter (DM). The main channel of detecting them is through the microlensing phenomenon, however the results from two microlensing surveys, MACHO and EROS, are in contradiction as to the abundance of MACHOs in the Galaxy.

We present an independent and the most comprehensive result so far from the OGLE microlensing survey of the Large and Small Magellanic Clouds running continuously for over 13 years. In both Clouds, we report the detection of the total of 8 events with 2 more plausible candidates. All but one of them are consistent with the expected signal from lensing by Clouds own stars (self-lensing), therefore there is no need of introducing dark microlenses.

2 LMC: 2+2 events and 2 candidates

There were 4 events found in the OGLE-II and OGLE-III data. Another 2 more were flagged as potential candidates in OGLE-III data. The optical depth derived for these events was $\tau_{\text{LMC-O2}} = 0.43 \pm 0.33 \times 10^{-7}$ and $\tau_{\text{LMC-O3}} = 0.16 \pm 0.12 \times 10^{-7}$ for OGLE-II and OGLE-III, respectively ([2], [4]).

Time-scales, locations and positions of these events on the colour-magnitude diagram indicate all of them are very likely to be solely caused by self-lensing. Source stars in all events seem to belong to the LMC and events occurred in the areas where the self-lensing contributes the most to the overall microlensing optical depth.

Small number of events seen by OGLE indicates the excess of events seen by MACHO group is probably not caused by microlensing. OGLE data ruled out as microlensing one of the MACHO events (#7), which showed another bump after many years.

3 SMC: 1+3 events

Previously there were 2 events found in the SMC by MACHO and EROS groups and both were confirmed to be due self-lensing.

In the OGLE data there were 4 events detected giving $\tau_{\text{SMC-O2}} = 1.55 \pm 1.55 \times 10^{-7}$ [3] and $\tau_{\text{SMC-O3}} = 1.27 \pm 0.96 \times 10^{-7}$. Events 03 and 04 are good candidates for self-lensing due to their time-scales and locations. Event 01 is a rather weak candidate and could be also due to a variable star.

In the most likely microlensing model for the event OGLE-SMC-02 the lens is a $10 M_{\odot}$ binary black hole from the Galactic halo [1]. Such events, however, are not seen towards the LMC, which calls for further observations and theoretical studies.

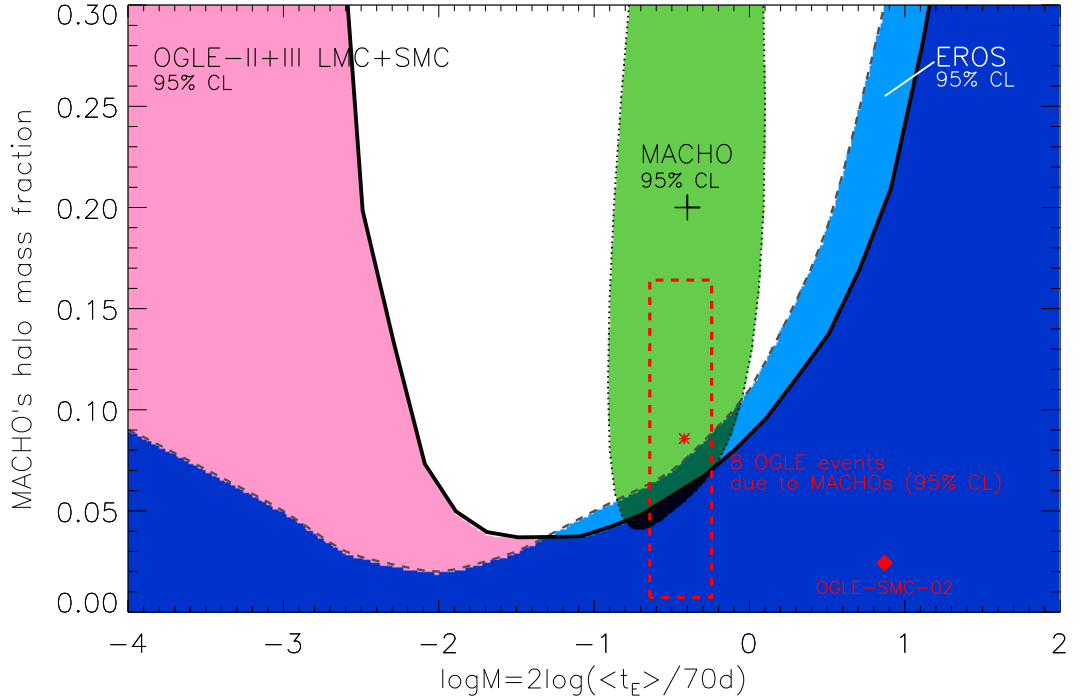


Figure 1: MACHOs contribution to the total halo mass as measured by MACHO group and upper limits from EROS and OGLE data.

4 Conclusions

Based on our detection efficiency, we derived new constraints on the MACHOs presence in the Galactic Halo of 6% for $M=0.1-0.4 M_{\odot}$ and below 4% for masses in range $0.01-0.1 M_{\odot}$ (Fig. 1). For MACHOs with mass of $1 M_{\odot}$ the upper limit is $f < 9\%$ and $f < 20\%$ for $M < 6M_{\odot}$.

Our result indicates that baryonic DM in the form of relics of stars and very faint objects in the sub-solar-mass range are unlikely to inhabit the Milky Way's dark matter halo in any significant numbers. Presence of a black-hole lens candidate towards the SMC agrees with expected no more than 2% contribution of black-holes to the mass of the Galactic halo.

References

- [1] Dong S., Udalski A., Gould A., Reach W. T., et al. 2007, ApJ, **664**, 862
- [2] Wyrzykowski Ł., Kozłowski S., Skowron J., et al. 2009, MNRAS, **397**, 1228
- [3] Wyrzykowski Ł., Kozłowski S., Skowron J., et al., 2010, MNRAS, **407**, 189
- [4] Wyrzykowski Ł., Kozłowski S., Skowron J., et al. 2011, MNRAS, in press, arXiv: 1012.1154

Analysis of microlensing events towards the LMC

Luigi Mancini & Sebastiano Calchi Novati

Department of Physics, University of Salerno, Italy

IIASS, Vietri Sul Mare

Italy

The nature of the observed microlensing events towards the Magellanic Clouds is still an open issue. Indeed, in order to draw meaningful insights into the contribution of dark matter objects in form of MACHOs, it is essential first to estimate accurately all the possible contributions due to (luminous) lenses belonging to known populations located along the line of sight (to which we refer too as “self lensing”). A possibly non exhaustive list includes lenses belonging to the luminous components of the LMC (the disc and the bar) that can act as sources, the disc of the Milky Way and the somewhat elusive stellar halo for both the Milky Way and the LMC.

The results reported so far by the collaborations who carried out observational campaigns towards the LMC as for the MACHO contribution to the Galactic halo are in agreement to exclude MACHOs as a viable dark matter candidate for masses below $(10^{-1} - 10^{-2}) M_{\odot}$. However, a relevant discrepancy still exists as for compact halo object in the mass range $(0.1 - 1) M_{\odot}$. The MACHO collaboration claimed for an mass halo fraction in form of MACHOs of about $f \sim 20\%$ out of observations towards the LMC (Alcock et al., 2000), a result more recently confirmed by Bennett (2005). On the other hand, the EROS (Tisserand et al., 2007) and the OGLE (Wyrzykowski et al., 2009, 2010) collaborations, out of observations towards both the LMC and SMC, concluded that the expected self-lensing rate is sufficient to explain the observed rate also in this mass range. It is therefore important to address the issue of the nature of the observed events, either to be attributed to MACHO lensing or to self lensing.

In previous analyses we have considered the set of events reported by the MACHO collaboration and shown that, on the basis of both their number number and their characteristics (event duration and spatial distribution), they cannot all be attributed to self lensing (Mancini et al., 2004). In Calchi Novati et al. (2006) we have considered the possible role played by the LMC dark matter halo, in particular suggested that the halo fraction in form of MACHOs for the Milky Way and the LMC might not be equal. Finally, in Calchi Novati et al. (2009) we have discussed the results of the OGLE-II campaigns towards the LMC.

Here we report on a detailed analysis of the recent results of the OGLE-III campaign towards the LMC (Wyrzykowski et al, 2010). For all the possible lens populations (both luminous and dark), we present maps of the optical depth and a study of the

expected characteristics (duration, spatial distribution and number), to be compared with the observed events. This is done through an evaluation of the microlensing rate towards all the observed fields. Finally, we evaluate the probability distribution for the mass halo fraction in form of MACHO via a likelihood analysis. Overall, we find the observed rate to be compatible with the expected lensing signal by known luminous populations.

References

- [1] Alcock, A. et al. (MACHO) 2000. The MACHO Project: Microlensing Results from 5.7 Years of Large Magellanic Cloud Observations. *Astrophysical Journal* 542, 281-307
- [2] Bennett, D. 2005. Large Magellanic Cloud Microlensing Optical Depth with Imperfect Event Selection. *Astrophysical Journal* 633, 906-913
- [3] Tisserand, P. et al. (EROS) 2007. Limits on the Macho content of the Galactic Halo from the EROS-2 Survey of the Magellanic Clouds. *Astronomy and Astrophysics* 469, 387-404
- [4] Wyrzykowski, L. et al. (OGLE) 2009. The OGLE view of microlensing towards the Magellanic Clouds - I. A trickle of events in the OGLE-II LMC data. *Monthly Notices of the Royal Astronomical Society* 397, 1228-1242
- [5] Wyrzykowski, L. et al. (OGLE) 2010. The OGLE view of microlensing towards the Magellanic Clouds - II. OGLE-II Small Magellanic Cloud data. *Monthly Notices of the Royal Astronomical Society* 407, 189-200
- [6] Mancini, L., Calchi Novati, S., Jetzer, Ph., Scarpetta, G. 2004. LMC self-lensing from a new perspective. *Astronomy and Astrophysics* 427, 61-77
- [7] Calchi Novati, S., De Luca, F., Jetzer, Ph. Scarpetta, G. 2006. Microlensing towards LMC: a study of the LMC halo contribution. *Astronomy and Astrophysics* 459, 407-414
- [8] Calchi Novati, S., Mancini, L., Scarpetta, G. Wyrzykowski, L. 2009. LMC self lensing for OGLE-II microlensing observations. *Monthly Notices of the Royal Astronomical Society* 400, 1625-1631
- [9] Wyrzykowski, L. et al. (OGLE) 2010. The OGLE View of Microlensing towards the Magellanic Clouds. III. Ruling out sub-solar MACHOs with the OGLE-III LMC data. *Monthly Notices of the Royal Astronomical Society*, *accepted*. arXiv:1012.1154

Simulation of pixel lensing of M87 by HST

Sedighe Sajadian & Sohrab Rahvar

*Department of Physics, Sharif University of Technology, Tehran
Iran*

In this work we propose a new strategy of pixel lensing observation of the unresolved stars of M87 in the Virgo cluster by HST. We show that in contrast to the previous observational strategy in Baltz et al. (2004) with one observation per night for the duration of one month, a few days intensive observation with taking one image per one HST orbit, we can substantially increase the number of events more than one order of magnitude. In this observational strategy, high magnification microlensing events is predicted to be observed with the rate of ~ 4 event per day with a typical transit time scale of ~ 19 hours. We examine the possible detection of dark matter mini-halos with this observational strategy.

References

- [1] Baltz E. A., et. al., ApJ **610**, 691 (2004)
- [2] Crotts A. P. S., ApJ **399**, 43 (1992)
- [3] Baillon, P., et. al., A&A **277**, 1 (1993)
- [4] Gould, A., ApJ **470**, 201 (1996)
- [5] Gould, A., ApJ **455**, 44 (1995)
- [6] McLaughlin, D. E., ApJ **512**, 9 (1999)

M31 pixel lensing and the PLAN project

Sebastiano Calchi Novati

Department of Physics, University of Salerno Italy

IIASS, Vietri Sul Mare

Italy

1 Introduction: M31 Pixel Lensing and the issue of MACHO versus self lensing

Pixel lensing is a unique tool for the study of dark matter objects in form of MACHOs up to distant galaxies as M31. More than 20 pixel lensing events towards M31 have been reported so far from several different campaigns, but no firm conclusions on the MACHO issue have been reached yet (Calchi Novati, 2010). A fundamental problem in the analysis is the difficulty to disentangle microlensing signal due to dark matter MACHOs from “self lensing”, microlensing signal due to lenses belonging to known luminous populations. This is complicated first by the additional degeneracy in the microlensing event parameter space characteristics of *pixel* lensing, where one studies flux variations of *unresolved* objects. Second, by the rather large expected self-lensing signal, as compared to the MACHO lensing one, at least in the inner M31 region, where in any case most of the events, either MACHO or self lensing, are expected. In this respect, as for many others, M31 pixel lensing is peculiar with respect to microlensing towards the Magellanic Clouds, LMC and SMC (Moniez, 2010). Still, besides the underlying technique, also the fundamental physical issue one addresses to, that of MACHOs, is the same. The recent analyses of OGLE-II/SMC (Wyrzykowski et al., 2010) and OGLE-III/LMC (Wyrzykowski et al., 2010) both indicates that the observed rate of events is compatible with the expected self-lensing signal. This is in agreement with the previous OGLE-II/LMC (Wyrzykowski et al., 2009) and the EROS results (Tisserand et al. 2007). On the other hand, the MACHO collaboration claimed for a MACHO signal of about $0.5 M_{\odot}$ for a mass halo fraction in form of MACHO $f \sim 20\%$ (Alcock et al., 2000), a result more recently confirmed by the further analyses of Bennett (2005). To address the issue of MACHOs along a different line of sight is therefore important. Besides, looking towards M31 one can map its own full dark matter halo, which is not possible for the Galaxy one.

To explore the MACHO versus self-lensing issue, and more in general to address the problem of the nature of the observed events, the careful and through analysis

of *single events* have shown to be a very efficient tool even if it can only give partial indications. Relevant results have been reported for the M31 microlensing event PA-N1 (Aurière et al., 2001), PA-S3/GL1 (Riffeser et al., 2008), and by the more recent analysis of OAB-N2 by the PLAN collaboration (Calchi Novati et al., 2010). Remarkably, though with different level of confidence, all these analyses conclude that MACHO lensing is to be preferred to self lensing for the events studied. This approach runs in parallel with the analysis of full data set completed by a careful comparison of the observed and the expected rate (an approach which still has to deal with the limitation given by the rather small statistics involved). The more relevant results have been reported by the POINT-AGAPE (Calchi Novati et al., 2005) and the MEGA (de Jong et al., 2006) collaborations, working on the same data set. POINT-AGAPE claimed for an evidence of a MACHO signal, in the same mass range indicated by the MACHO LMC analysis, whereas MEGA concluded that self lensing was sufficient to explain the detected rate. An extremely promising new project for M31 pixel lensing observation is that of PAndromeda (Riffeser et al., 2011).

2 The PLAN project: an update

Within this still open framework we discuss some of the results we have obtained with the PLAN collaboration which is carrying out a long term monitoring project of M31 (with observational campaigns at the 1.5m OAB telescope from 2006 to 2010 and a pilot campaign at the 2m HCT telescope in October 2010). In Calchi Novati et al. (2009) as a result of a fully automated pipeline we have reported 2 microlensing candidate events out of the 2007 campaign (OAB-N1 and OAB-N2). The observed rate turned out to be relatively large, still, compatible with the expected self-lensing one. The available statistics was however too small to allow us to draw stringent conclusions on the MACHO issue. Since then we have followed both the indicated approaches to address the MACHO versus self-lensing issue.

First, some additional data made available by the WeCAPP collaboration along the OAB-N2 light curve and a more thorough analysis of KPNO and HST archive images used to better constrain the possible event source characteristics, have allowed us a much more detailed analysis of OAB-N2 (Calchi Novati et al., 2010). In particular, through a study of the lens proper motion, we have shown that this event is more likely to be attributed to MACHO lensing than to self lensing.

As for our full data set, more statistics is badly needed. Here we report some preliminary results of the 2008 and 2009 campaigns. As an output, no new microlensing candidate events have been detected. In particular we discuss the crucial role played by the selected bump unicity analysis we carry out on archive POINT-AGAPE light curves. We compare the observed rate to the expected one evaluated through a Monte Carlo simulation completed by an analysis of the efficiency of the

pipeline. The observed rate is compatible with the expected self-lensing one but still does not allow us to constrain MACHO lensing (Calchi Novati et al, 2011).

References

- [1] Calchi Novati, S. 2010. Pixel lensing. Microlensing towards M31. *General Relativity and Gravitation* 42, 2101-2126. *Invited Review*
- [2] Moniez, M. 2010. Microlensing as a probe of the Galactic structure: 20 years of microlensing optical depth studies. *General Relativity and Gravitation* 42, 2047-2074. *Invited Review*
- [3] Wyrzykowski, L. et al. (OGLE) 2010. The OGLE View of Microlensing towards the Magellanic Clouds. III. Ruling out sub-solar MACHOs with the OGLE-III LMC data. *Monthly Notices of the Royal Astronomical Society*, *accepted*. arXiv:1012.1154
- [4] Wyrzykowski, L. et al. (OGLE) 2010. The OGLE view of microlensing towards the Magellanic Clouds - II. OGLE-II Small Magellanic Cloud data. *Monthly Notices of the Royal Astronomical Society* 407, 189-200
- [5] Wyrzykowski, L. et al. (OGLE) 2009. The OGLE view of microlensing towards the Magellanic Clouds - I. A trickle of events in the OGLE-II LMC data. *Monthly Notices of the Royal Astronomical Society* 397, 1228-1242
- [6] Tisserand, P. et al. (EROS) 2007. Limits on the Macho content of the Galactic Halo from the EROS-2 Survey of the Magellanic Clouds. *Astronomy and Astrophysics* 469, 387-404
- [7] Alcock, A. et al. (MACHO) 2000. The MACHO Project: Microlensing Results from 5.7 Years of Large Magellanic Cloud Observations. *Astrophysical Journal* 542, 281-307
- [8] Bennett, D. 2005. Large Magellanic Cloud Microlensing Optical Depth with Imperfect Event Selection. *Astrophysical Journal* 633, 906-913
- [9] Aurière, M. et al. 2001. A Short-Timescale Candidate Microlensing Event in the POINT-AGAPE Pixel Lensing Survey of M31. *Astrophysical Journal Letter* 553, 137-140
- [10] Riffeser, A. et al. 2008. The M31 Microlensing Event WeCAPP-GL1/POINT-AGAPE-S3: Evidence for a MACHO Component in the Dark Halo of M31? *Astrophysical Journal* 684, 1093-1109

- [11] Calchi Novati, S. et al. (PLAN) 2010. M31 Pixel Lensing Event OAB-N2: A Study of the Lens Proper Motion. *Astrophysical Journal* 717, 987-994
- [12] Calchi Novati, S. et al. (POINT-AGAPE) 2005. POINT-AGAPE pixel lensing survey of M 31. Evidence for a MACHO contribution to galactic halos. *Astronomy and Astrophysics* 443, 911-928
- [13] de Jong, J. et al. (MEGA) 2006. MACHOs in M 31? Absence of evidence but not evidence of absence. *Astronomy and Astrophysics* 446, 855-875
- [14] Riffeser, A., Seitz, S., Bender, R., Chien-Hsiu Lee, C.-H., Koppenhoefer, J. 2011. PAndromeda - A Dedicated Deep Survey of M31 with Pan-STARRS 1. *this volume*
- [15] Calchi Novati, S. et al. (PLAN) 2009. Candidate Microlensing Events from M31 Observations with the Loiano Telescope. *Astrophysical Journal* 695, 442-454
- [16] Calchi Novati, S. et al. (PLAN) 2011. *in preparation*

Planetary events

OA-2009-BLG-266LB: the first cold Neptune with a measured mass

David Bennett

Increasing the detection rate of low-mass planets in high-magnification events and MOA-2006-BLG-130

Julie Baudry & Philip Yock

The complete orbital solution for OGLE-2008-BLG-513

Jennifer Yee

Planetary microlensing event MOA-2010-BLG-328

Kei Furusawa

Binary microlensing event OGLE-2009-BLG-020 gives orbit predictions verifiable by follow-up observations

Jan Skowron

MOA-2009-BLG-266LB: The First Cold Neptune with a Measured Mass

David P. Bennett

*University of Notre Dame, Notre Dame, IN
USA*

for the MOA, μ FUN, RoboNet, PLANET, MiNDSTEp, and OGLE Collaborations

The MOA-II survey detected beginning of the planetary signal in microlensing event MOA-2009-BLG-266, so MOA's prompt anomaly alert led to nearly complete sampling of the planetary anomaly. Good light curve coverage from MOA and a number of the follow-up telescopes after the anomaly enabled the measurement of a strong microlensing parallax signal that allows the mass to be measured.

MOA-2009-BLG-266 is also the first planetary microlensing event to be observed from a telescope in Heliocentric orbit, as it was observed for ~ 2 days by the High Resolution Instrument (HRI) of the Deep Impact (DI) spacecraft. The short duration and unfortunate timing of the space-based observations imply that these observations have only a weak constraint on the microlensing parallax measurement. But this data also indicates that future observations with the DI/HRI instrument in 2011-2014 will allow mass measurements of many microlens planets and their host stars, including the first mass measurements of planets in the Galactic bulge.

Increasing the detection rate of low-mass planets and MOA–2006-BLG-130

Julie Baudry
University of Orsay, Paris Sud XI
France

Philip Yock
Department of Physics, University of Auckland
New Zealand

1 Introduction

Extra-solar planets detection is one of the applications of the gravitational microlensing phenomenon: a perturbation on the light curve can betray the presence of a planet orbiting the lens star [1, 2]. Most microlensing planets have been found in events of high magnification. Events of highest magnification occur when the lens star transits the source star, but these events provide relatively poor sensitivity to planets. Previous research concentrated on highest magnification events, but, on purely geometrical grounds, near-perfect alignment is relatively rare and there must be more events at low magnification than at high magnification. It will be presented in a first part the interest of monitoring events of lower magnification, in order to increase the detection rate of low-mass planets.

MOA-2006-BLG-130 (OGLE-2006-BLG-437) is a microlensing event that occurred in August 2006 which exhibited a slight perturbation on the light curve. In a second part, we will present the analysis of this event, in order to see whether or not it is a binary lens.

2 Planetary perturbation detectability and magnification

Events of lower magnification may be subdivided into two classes : those in which the planet lies closer to the Einstein ring than the length of either Einstein arc (type I), and those in which the planet lies further away (type II), Figure 1. Both type I and type II events enjoy good sensitivity to planets. In type II events, the planet is closer

to the lens, and the planetary perturbation is greater when the magnification is higher. In type I events, the Einstein arc is affected by the proximity of the planet, and it will be shown that the sensitivity of these events to low-mass planets is almost independent of magnification. Using simulation programs of the MOA@UoA project [3], producing theoretical light curves, it will be demonstrated that the planetary perturbation is reasonably detectable in type I events, even at low magnification. It follows that monitoring further events of this type could increase the detection rate of low-mass planets.

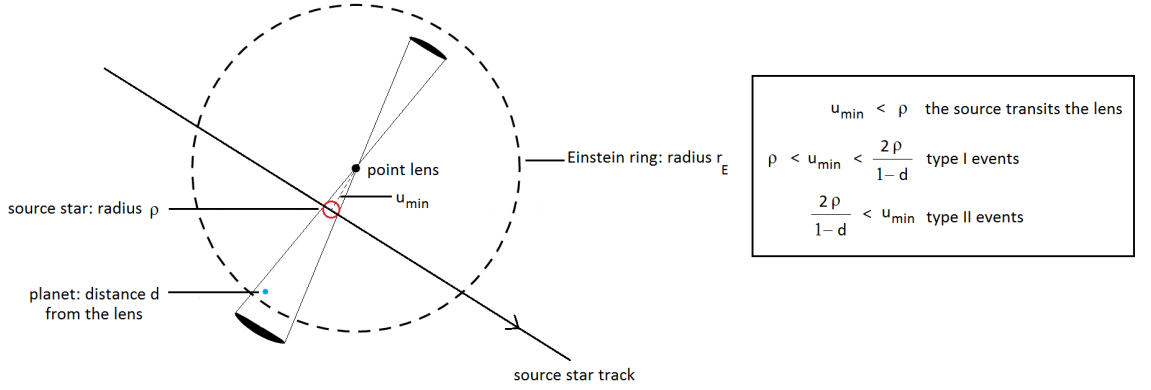


Figure 1: Different types of events, depending on the geometrical construction of the lens.

3 MOA-2006-BLG-130

This event, for which the data light curve is given in Figure 2, was tested with the MOA@UoA simulation code. We used a χ^2 marginalisation method, to test 27 binary lens, operation being repeated for each for 17 values of the source track angle. Results and analysis method will be presented. However, the coverage of this event was really sparse, so other phenomena were considered as possible cause of the perturbation.

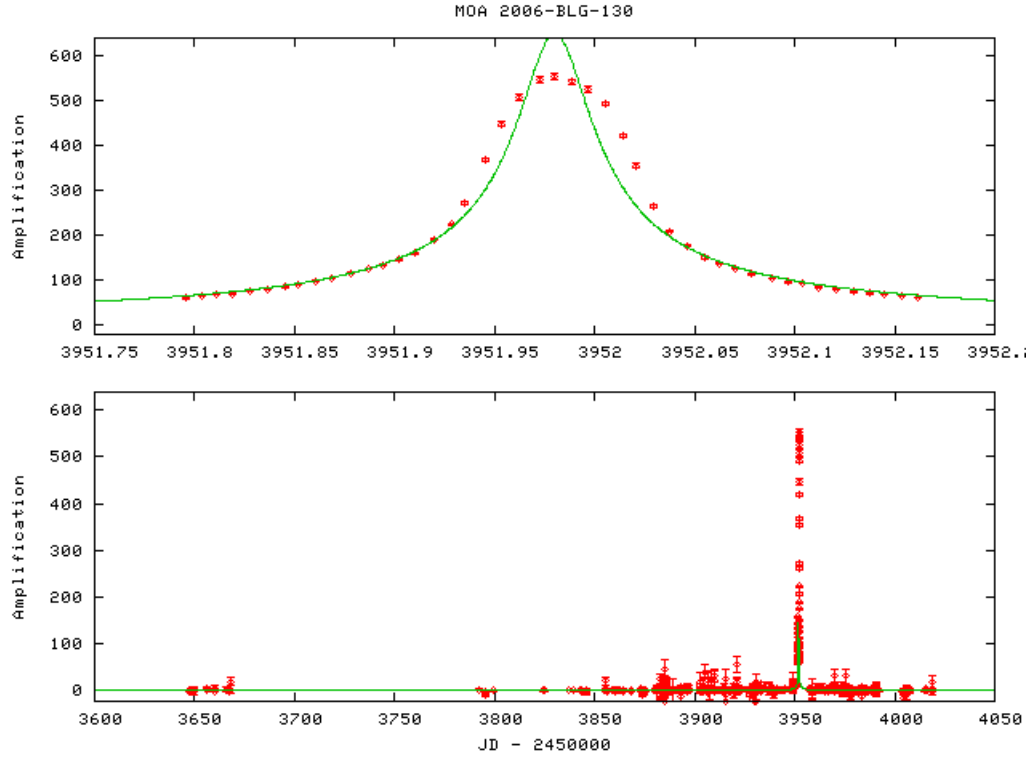


Figure 2: Data light curve for MOA-2006-BLG-130, from the MOA microlensing alerts [4].

References

- [1] Gould, A., & Loeb, A., ApJ 396, 104 (1992)
- [2] Bennett, D. R., & Rhie, S.H, ApJ 472, 660 (1996)
- [3] C. S. Botzler, 2006; S. Holderness, 2008; Y. Perrott, 2009; L. Philpott, 2005
- [4] <http://www.phys.canterbury.ac.nz/moa/>

The Keplerian Orbit of OGLE-2008-BLG-513/MOA-2008-BLG-401

Jennifer Yee
Ohio State University
USA

The light curve of OGLE-2008-BLG-513/MOA-2008-BLG-401 is characterized by two strong peaks due to companion to the lens with a mass ratio of $q = 0.027$. The timescale of this event is fairly long ($t_E = 32$ days) and the span of the 2-body perturbation is > 12 days because the caustic is resonant (the separation between the lens star and its companion in Einstein radii is ~ 1). Because of the timescales involved we were able to measure both the parallax effect and the orbital motion of the lens. Using information from the parallax and orbital motion effects, we find that the companion is a $7.8 M_{\text{Jup}}$ giant planet orbiting an $0.3 M_{\odot}$ host with a semi-major axis of 2.2 AU.

We initially fit the data with a static, 2-body lens model including parallax effects but were unable to find a model that satisfactorily data. We are able to fit the data successfully by allowing orbital motion in the 2-body lens. We use two different models: the first uses only the lens velocity projected onto the plane of the sky and the second uses a full Keplerian description for the lens motion. We find that the full Keplerian model is slightly preferred (χ^2 improvement of 10). This preference for full Keplerian motion indicates that we are measuring the curvature of the orbit during the event and allows us to place constraints on most of the orbital parameters.

The source star in this event is unusually blue compared to the other stars in the field: it is 0.95 mag bluer than the red clump. Given its blue color, one possibility for the source is that it is an A dwarf in the bulge or behind the the bulge in the far disk. An alternative hypothesis is that the source is well in the foreground, in front of most of the dust. In this case, it would be a low mass dwarf that appears blue because it experiences much less reddening than the other stars in the field. Various inconclusive arguments can be made supporting each hypothesis, drawing on the observed relative proper motion, astrometry, source limb-darkening, and arguments about the observed color and magnitude of the source. However, in our analysis of the light curve, we find that in order for the orbit of the lens planet to be bound, the source must be a nearby M dwarf. If the source star is a nearby, metal-poor thick disk star, this explanation accounts for almost all of the information we have on the source. In order to clarify the nature of the source, we have applied for and been granted time on the VLT to

get a spectrum of the source. Given our orbital motion observations, we predict that the source will be a low-mass star.

Regardless of the nature of the source, the mass ratio between the companion and the lens star is robust. A mass ratio of 0.027 is very rare among binary/brown dwarf/planetary systems regardless of the specific nature of the companion. If the spectrum confirms our interpretation of the event, this will be yet another example of a massive planet orbiting an M dwarf. Such planets are extremely difficult to form using present theories of planet formation. The core accretion theory predicts that such planets should be extremely rare because M dwarfs have less massive disks and short orbital timescales at the snow line where giant planets should form. The gravitational instability theory is able to form giant planets around M dwarfs but only at much larger distances than we observe in this system. This planet, and others like it, increasingly form a challenge to the accepted theories of planet formation.

Planetary microlensing event MOA-2010-BLG-328

*Kei Furusawa
Nagoya University
Japan*

1 Observation

Microlensing Observations in Astrophysics (MOA) monitors ~ 40 degree² of the Galactic bulge to find Microlensing events by 1.8m MOA-II telescope in New Zealand. Our real-time anomaly alert system checks new data points of each of microlensing events after five minutes of observation to find deviations due to planets. MOA has discovered 607 microlensing events and some anomaly events by the real-time anomaly alert system toward the Galactic bulge in 2010.

The microlensing event MOA-2010-BLG-328 was detected and alerted by MOA on 16 June 2010. Around UT 12:30 27 July, we found the deviations from single lens light curve of the event by anomaly alert system and issued the anomaly alert. Two days after the anomaly alert was issued, the deviations could be seen more clearly and David Bennett sent his preliminary planetary model. Following his e-mail, follow-up groups, μ FUN: CTIO (Chile), Farm Cove Observatory (New Zealand), Palomar Observatory (CA, USA), PLANET: Canopus (Australia), RoboNet: Faulkes Telescope North (Hawaii, USA), Faulkes Telescope South (Australia), Liverpool Telescope (Spain), MiNDSTeP: SAAO (South Africa), Danish (Chile) conducted intensive observation. Fortunately, the event occurred in OGLE-IV monitored fields so we got also OGLE data.

2 Analysis

The light curve is fitted by Markov Chain Monte Carlo (MCMC). Initial parameters for best fit model search are used over the range of the planet-star mass ratio (q) $-5 \leq \log q \leq 0$ and planet-star separation (s) $-1 \leq \log s \leq 1$, the total number of initial parameters is 858.

We estimate the dereddened source color and magnitude from fitting and color magnitude diagram (CMD). Then the estimated source star is G type star and we adopt Limb Darkening parameter of G type star.

Currently, as the result of the detail analysis of the light curve, the mass ratio q and the separation s are yielded 9.7×10^{-4} , 1.3 respectively. It remains possible that the light curve also shows the microlensing parallax which is caused by the orbital motion of the Earth around the Sun during the event. The parallax effect enables us to estimate the physical parameters of the planet.

3 Conclusion

We analyzed planetary microlensing event MOA-2010-BLG-328. As the result of this analysis, the lens has a companion with planet mass ratio. This result is preliminary because the parallax signal is very sensitive to systematic errors of data. The data are gradually improving, so we continue evaluating parallax in detail

Binary microlensing event OGLE-2009-BLG-020 gives orbit predictions verifiable by follow-up observations

Jan Skowron

*Department of Astronomy, Ohio State University
USA*

1 Introduction

We present the first example of binary microlensing for which the parameter measurements can be verified (or contradicted) by future Doppler observations. This test is made possible by a confluence of two relatively unusual circumstances. First, the binary lens is bright enough ($I = 15.6$) to permit Doppler measurements. Second, we measure not only the usual 7 binary-lens parameters, but also the “microlens parallax” (which yields the binary mass) and two components of the instantaneous orbital velocity. Thus we measure, effectively, 6 ‘Kepler+1’ parameters (two instantaneous positions, two instantaneous velocities, the binary total mass, and the mass ratio). Since Doppler observations of the brighter binary component determine 5 Kepler parameters (period, velocity amplitude, eccentricity, phase, and position of periastron), while the same spectroscopy yields the mass of the primary, the combined Doppler + microlensing observations would be overconstrained by $6 + (5 + 1) - (7 + 1) = 4$ degrees of freedom. This makes possible an extremely strong test of the microlensing solution.

We also introduce the uniform microlensing notation for single and binary lenses, define conventions, summarize all known microlensing degeneracies and extend set of parameters to describe full Keplerian motion of the binary lenses (see Appendix A in the main paper Skowron et al. 2011, in prep.).

2 Observational data

On 15 February 2009, heliocentric Julian Date (HJD) ~ 2454878 , the Optical Gravitational Lensing Experiment (OGLE) team announced ongoing microlensing event OGLE-2009-BLG-020 detected by Early Warning System (EWS) and observed on the 1.3m Warsaw Telescope in Las Campanas Observatory in Chile. The event was

also monitored by the Microlensing Observations in Astrophysics (MOA) 1.8m telescope on Mt. John in New Zealand. On $HJD' \sim 4915$ ($HJD' = HJD - 2450000$) it could be seen that light curve was deviating from the standard Paczyński model, and follow-up observations by other telescopes began. Intense monitoring of the event was performed until $HJD' \sim 4920$. During this period source crossed caustic twice and both crossings were observed.

In this work, beside the data obtained by survey telescopes, we use follow-up data from 8 additional observatories: the 2.0m Faulkes South (FTN), the 2.0m Faulkes North (FTN), the 36cm telescope at Kumeu Observatory, the 36cm telescope at Bronberg Observatory, the 1m telescope on Mt. Canopus (Utas), the 36cm telescope in Farm Cove Observatory (FCO), the SMARTS 1.3m Cerro Tololo Inter-American Observatory (CTIO), and the 40cm telescope in Campo Catino Austral Observatory (CAO). Light curve of the event is shown on Figure 1.

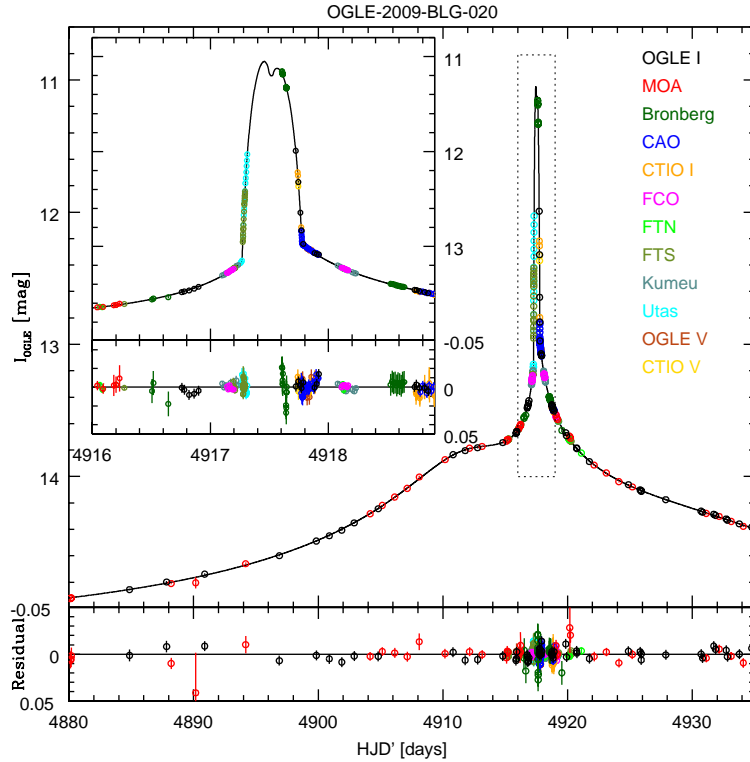


Figure 1: Light curve and best-fit model of OGLE-2009-BLG-020.

The whole light curve consists of 9 years of data with 121 days during the course of the visible magnification, of which 5 days constitute intense follow-up observations. The OGLE telescope performed observations in V and I bands, and CTIO telescope in V , I and H bands, which permit measurements of the color of the magnified source

star. Together we have 5333 data points in the light curve with 2247 during the course of the magnification event.

3 Microlensing fit with full Keplerian orbit

To find a microlensing model we use the method developed by S. Dong and described in Dong et al. (2006) and its modification in Dong et al. (2009, Section 3). Although we introduce a few changes in parametrization of the model. In order to allow comparison with the radial velocity (RV) measurements it is profitable to use the full Keplerian orbit parametrization. In addition to being more accurate, the additional advantage of this approach is to avoid all unbound orbital solutions (with eccentricity ≥ 1) and to enable introduction of priors on the values of orbital parameters directly into MCMC calculations, if one decides to adopt that approach.

We describe the orbit of the secondary component relative to the primary by giving 3 cartesian positions and 3 velocities at one arbitrarily chosen time ($t_{0,kep}$). See Figure 2. Our extended microlensing model (with parallax parameters) carries information about the mass ratio, the total mass of the lens, and the physical scale in the lens plane, so together with the six instantaneous phase-space coordinates it comprises a complete set of system parameters (except systemic radial velocity). This, for example, allows us to calculate the relative RV at any given time. We can use this for comparison with the RV curve from follow-up observations.

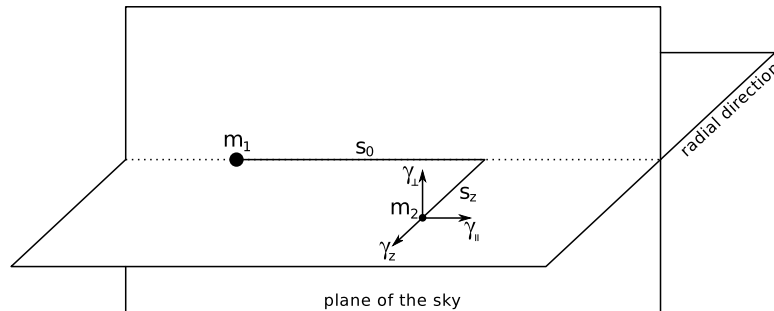


Figure 2: Definition of the phase-space parameters ($s_0, 0, s_z, \gamma_{\parallel}, \gamma_{\perp}, \gamma_z$) at $t_{0,kep}$, describing motion of the secondary binary lens component (m_2) relative to the primary (m_1). Vertical plane is the plane of the sky.

It is possible to calculate all properties in physical units as well as standard Kepler parameters of the orbit – i.e., eccentricity (e), time of periastron (t_{peri}), semi-major axis (a) and 3 Euler angles: longitude of ascending node (Ω_{node}), inclination (i) and argument of periapsis (ω_{peri}). (See Figure 3 for illustration of the orbital parameters and they relation to the phase-space parameters specified at the fixed time $t_{0,kep}$.)

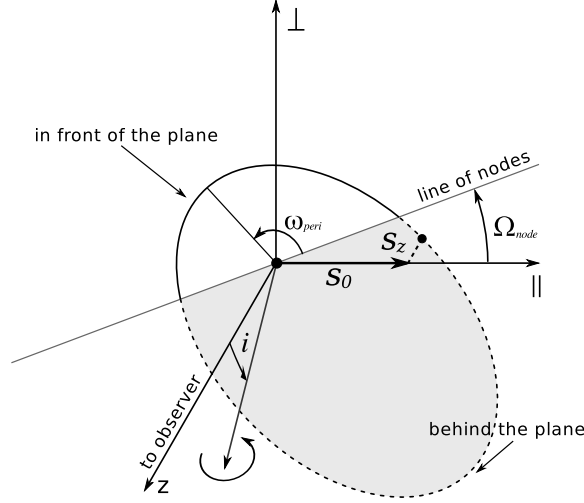


Figure 3: Figure shows an example of the relative binary orbit which is rotated by three Euler angles. The binary components at the time $t_{0,kep}$ are marked with 2 dots. The axis z points toward the observer; axes marked with symbols \parallel and \perp define the plane that is parallel to the plane of the sky and crosses the primary component of the binary. The portions of the line that lie behind the plane are dashed. The base coordinate system is related to the microlensing event such that at the time $t_{0,kep}$ the first axis coincides with the binary axis projected onto plane of the sky.

Likelihoods obtained from MCMC procedure suffer from degeneracy between one of the parallax parameters ($\pi_{E,\perp}$ – perpendicular to the Earth acceleration) and angular velocity of the lens in the plane of the sky. We break this degeneracy by choosing subset of solutions which yields observed brightness of the lens consistent with the theoretical main-sequence isochrone (we assume that all blended light is coming from the lens, and, with mass ratio $q = 0.27$, we expect that the secondary component of the lens does not contribute to the light). This leads to estimations of the lens distance and the mass of its primary component:

$$D_l = 1.1 \pm 0.1 \text{ kpc} \quad M_1 = 0.84 \pm 0.03 M_\odot \quad (1)$$

The observed magnitudes of the blend and the source are:

$$((V - I), I, (I - H))_b = (1.316 \pm 0.01, 15.680 \pm 0.01, 1.409 \pm 0.05) \quad (2)$$

$$((V - I), I)_s = (1.929 \pm 0.002, 16.43 \pm 0.04) \quad (3)$$

4 Test with radial velocity

Every link in the MCMC chain consist a complete set of parameters of the binary lens. It yields not only the mass, distance and separation in physical units, but also all Keplerian parameters of the orbit. Thus we can calculate the RV curve for any period of the binary.

Assuming the observations of the RV curve of the primary are taken, we can assign to every link the likelihood that it is consistent with those data. We derive the radial velocity for any time the data were taken and, allowing for systemic velocity of the center of mass of the binary to vary, we calculate the likelihoods for every point. In this way we construct new set of links weighted by, both, the microlensing light curve and radial velocity curve. This new set of solutions yields new, most probable, values of all lens parameters, which may or may not coincide with the values derived from the microlensing only solution. This would be a test of microlensing solution.

If new values of parameters will lie outside $3\text{-}\sigma$ limits of microlensing solution we can say that our method failed. By contrast, if solutions, which are consistent with the RV curve, lie near the best-fit values we obtained from microlensing we can not only believe our solution, but we can also read all parameters of the binary, which are not given by one or the other method alone. For example, radial velocity curve will give us period and systemic radial velocity, which we cannot read from the microlensing light curve alone. However, microlensing will yield the inclination, orientation on the sky and the 2-d velocity of the binary projected on the plane of the sky.

4.1 Useful information for RV observations

The selective power of the RV curve holds when the observation are taken through at least one period of the binary. We propose a 2 year span of observations since the period we derive is between 200 and 700 days ($2\text{-}\sigma$ limit).

The binary coordinates are ($18^h04^m20^s.99$, $-29^\circ31'08''.6$, $J2000.0$). The finding chart can be found on the OGLE EWS webpage¹.

The binary is blended with the “microlensing source” which, as its position on the CMD suggests, is a Galactic bulge giant. The binary has a mass ratio of 0.272, so assuming both components are the main-sequence stars, majority of the light is coming from the primary. The binary is 1.3 magnitude brighter in V and 0.8 mag brighter in I than the giant, however they are of similar brightness in H .

Since the binary is located in the Galactic disk, we anticipate it will be clearly separated in the velocity space from the blended Bulge giant. The radial velocity amplitude of the primary is expected to be of order of a few km s^{-1} .

¹<http://ogle.astrouw.edu.pl/ogle3/ews/2009/blg-020.html>

5 Conclusions

The binary star that manifested itself in the microlensing event OGLE-2009-BLG-020 is the first case of a lens that is close enough and bright enough to allow ground-based spectroscopic follow-up observations. This makes it a unique tool to test the microlensing solution.

We derive lens parameters using the same method by which majority of planetary candidates discovered by microlensing are analyzed. We detect a signal from the orbital motion of the lens in the microlensing light curve. This signal, as well as our measurements of the orbital parameters of the binary lens, can be confirmed or contradicted by the future observations.

Combining the microlensing solution with the radial velocity curve will yield a complete set of system parameters including 3-d Galactic velocity of the binary and all Kelperian orbit elements.

This work undertakes an effort to establish a uniform microlensing notation, extending work of Gould (2000) by including full set of orbital elements of the binary lens (see Appendix A in the paper). We also summarize all known microlensing degeneracies.

The method of deriving orbital elements from the 6 phase-space coordinates, used to parametrize microlensing event, is described in Appendix B in the paper.

References

- [1] Dong, S., et al. 2006, ApJ, 642, 842
- [2] Dong, S., et al. 2009, ApJ, 698, 1826
- [3] Gould, A. 2000, ApJ, 542, 785
- [4] Skowron, et al. 2011, in prep.

Theoretical investigations

Microlensing and planet populations - What do we know, and how could we learn more

Martin Dominik

The frequency of extrasolar planet detections with microlensing simulations

Rieul Gendron & Shude Mao

A semi-analytical model for gravitational microlensing events

Denis Sullivan, Paul Chote, Michael Miller

GPU-assisted contouring for modeling binary microlensing events

Markus Hundertmark, Frederic V. Hessman, Stefan Dreizler

Red noise effect in space-based microlensing observations

*Achille Nucita, Daniele Vetrugno, Francesco De Paolis, Gabriele Ingrosso,
Berlinda M. T. Maiolo, Stefania Carpano*

Light curve errors introduced by limb-darkening models

David Heyrovsky

Isolated, stellar-mass black holes through microlensing

*Kailash Sahu, Howard E. Bond, Jay Anderson, Martin Dominik,
Andrzej Udalski, Philip Yock*

The observability of isolated compact remnants with microlensing

Nicola Sartore & Aldo Treves

Gravitational microlensing by the Ellis wormhole

Fumio Abe

The deflection of light ray in strong field: a material medium approach

Asoke Kumar Sen

Rapidly rotating lenses - repeating orbital motion features in close binary microlensing

Matthew Penny, Eamonn Kerins, Shude Mao

Microensing and planet populations - What do we know, and how could we learn more?

Martin Dominik

*SUPA, University of St Andrews, School of Physics & Astronomy
United Kingdom*

1 Gravitational microlensing campaigns

Following a concrete suggestion brought up by Bohdan Paczyński [1], the first dedicated gravitational microlensing surveys [2, 3] were designed to measure a potential clumpy dark matter content in the galactic halo by means of observations towards the Magellanic Clouds. Observations towards the Galactic bulge have then been proposed for robustly testing whether the experimental set-ups are able to detect signals [4, 5], given that a possible negative result towards the Magellanic Clouds would remain ambiguous. Wider-reaching astrophysical applications of gravitational microlensing simply became add-ons to existing opportunities, and have subsequently shaped the evolutionary process of experiments. Exploiting the discovery potential of planets orbiting stars other than the Sun [6] by means of follow-up observations on ongoing microlensing surveys [7] became possible with real-time processing and public dissemination of data [8, 9]. The explicit goal to detect planets by microlensing was in particular engraved in the acronym of the Probing Lensing Anomalies NETwork (PLANET) [10].

2 Efficiency and planet population statistics

Planetary abundance statistics cannot be extracted simply from counting claimed detections. We need to understand what the characteristics of the monitoring campaigns are, which might have changed over time. In fact, the observed sample is a probabilistic realisation of the product of the underlying planet population and the detection efficiency of the experiment(s). This however means that the considered sample and the detection efficiency need to refer to the same detection criterion and monitoring strategy. Not only does the detection efficiency need to be evaluated in a statistical meaningful way, but also do the "detections" need to be counted accordingly [11].

Moreover, not surprisingly, with different approaches being followed by the various surveys and follow-up monitoring campaigns, their detection efficiencies are substantially different functions of the planet mass m_p and orbital separation r_p . For the most massive planets, there is not much gain with less than daily sampling, so that survey experiments with their larger number of observed events have the largest sensitivity [12, 13], whereas less massive planets with their shorter signals become undetectable by falling into the data gaps. With regular quasi-continuous high-precision round-the-clock monitoring, as carried out by PLANET [14], RoboNet [15, 16], or MiNDSTeP [17], the planet detection efficiency drops roughly as $\sqrt{m_p}$, until the finite size of the source stars at a few Earth masses causes a faster drop-off and subsequently undetectability [18, 19]. If, like μ FUN, one focuses on highly-magnified peaks, probing the central caustic close to the lens star, the detection efficiency is close to 100 % for a wide range of planetary masses, with just the range of orbital separations shrinking towards lower masses, and it then falls to zero rather suddenly [20].

The history of claimed microlensing planet detections seems to follow a pattern that matches the characteristics of the different campaigns: A first super-Jupiter from the OGLE and MOA surveys [21], the 5-Earth-mass planet OGLE-2005-BLG-390Lb from PLANET observations [22], and planets from high-magnification peaks monitored by μ FUN [23, 24]. Moreover, a larger number of detections in the region between Neptune and Saturn [25, 26] arose in the more recent years due to increased survey cadence.

However, rough planet abundance estimates give rather puzzling results. A well-defined sample of events with peak magnifications $A_0 \geq 200$, densely covered mostly by μ FUN data [20] indicates an abundance for massive gas giants that is about 10 times larger than what one would estimate from PLANET observations and the corresponding detections [27]. Despite the fact that both estimates are statistically compatible within their large uncertainties, these findings are somewhat surprising given that the PLANET observations are *more* powerful in this mass range, but have provided less detections. In fact, the 4-year μ FUN sample contains just 13 events, which means that the adopted strategy is not powerful enough for providing a planetary mass function in foreseeable time; increased efforts of monitoring a larger number of events at more moderate magnifications, as follow-up efforts or high-cadence surveys, are required [27]. The detection of a planetary signal in event MOA-2009-BLG-266, resembling the path that led to OGLE-2005-BLG-390Lb, clearly demonstrates the power of the regular follow-up approach (which in fact is just copied by the MOA high-cadence monitoring).

With the current small number of planetary detections, microlensing observations are still in their very infancy on the path to determining planet abundances, and any kind of planetary mass function is a long way ahead. A particular complication arises from the fact that the planet abundances strongly depend on the properties of the parent star, and microlensing events come with a probabilistic mixture of host

stars. Should more massive stars come with more or less planets of a certain kind, what planetary mass function are we talking about? Distinguishing between masses of planet host stars requires a much larger sample for drawing meaningful conclusions. Stellar metallicity is a further relevant parameter that is difficult to control, and the fact that microlensing probes both Galactic disk and bulge stars is a challenge as well as an opportunity.

While planetary microlensing naturally depends on the dimensionless separation parameter d and the planet-to-star mass ratio q , planet formation does not obey such a scaling law, regardless of whether planet formation theories give us good guidance or not. Moreover, the adoption of any specific functional form, just for its simplicity, that is not clearly supported by the data, may not be adequate to probe certain features. In particular, smooth monotonic functions are ill-suited to describe planetary deserts or cut-offs.

3 Moving forward

Maximizing the number of detections without adopting well-defined monitoring procedures might lead to further spectacular findings, but will be useless for studying planet populations. High-cadence surveys have already proven their extended sensitivity to planets with smaller masses. In order to obtain meaningful results on planet population statistics, deviations from a deterministic survey programme must be made in a deterministic way only as well. Otherwise, claimed detections cannot be used to gather statistical information. It has also been demonstrated that the automated detection of anomalies [28] increases the detection efficiency, and in particular allows for the realistic detection of planets of Earth mass and below, while keeping the deterministic process chain intact. The real-time identification of potential deviations from ordinary light curves is essential for the current ability to push further down in mass, but if we want to determine the abundance of such planets as well, this identification must not be left to human judgement. If planets of Earth mass and below are common, recent survey data give rise to speculating that opportunities have been missed for claiming such a detection. If we want to make an impact *now*, the real-time provision of photometric data within minutes (not within hours) is likely to make the crucial difference. Beyond that, and in the longer term, precision photometry on fainter stars would allow for far better statistics on low-mass planets.

References

- [1] B. Paczyński, *Astrophys. J.* **304**, 1 (1986)
- [2] É. Aubourg et al., *Nature* **365**, 623 (1993)

- [3] C. Alcock et al., *Nature* **365**, 621 (1993)
- [4] B. Paczyński, *Astrophys. J.* **371**, L63 (1991)
- [5] M. Kiraga, B. Paczyński, *Astrophys. J.* **430**, L101 (1994)
- [6] S. Mao, B. Paczyński, *Astrophys. J.* **374**, L37 (1991)
- [7] A. Gould, A. Loeb, *Astrophys. J.* **396**, 104 (1992)
- [8] A. Udalski, M. Szymański, J. Kałużny, M. Kubiak, M. Mateo, W. Krzemiński, B. Paczyński, *Acta Astron.* **44**, 227 (1994)
- [9] C. Alcock et al., *Astrophys. J.* **463**, L67 (1996)
- [10] M. D. Albrow et al., *Astrophys. J.* **509**, 687 (1998)
- [11] M. Dominik, *Gen. Rel. Grav.* **42**, 2075 (2010)
- [12] Y. Tsapras, K. Horne, S. Kane, R. Carson, *Mon. Not. R. Astron. Soc.* **343**, 1131 (2003)
- [13] C. Snodgrass, K. Horne, Y. Tsapras, *Mon. Not. R. Astron. Soc.* **351**, 967 (2004)
- [14] M. Dominik et al., *Planet. Space Sci.* **50**, 299 (2002)
- [15] M. J. Burgdorf et al., *Planet. Space Sci.* **55**, 582 (2007)
- [16] Y. Tsapras et al., *Astron. Nachr.* **330**, 4 (2009)
- [17] M. Dominik et al., *Astron. Nachr.* **331**, 671 (2010)
- [18] M. D. Albrow et al., *Astrophys. J.* **556**, L113 (2001)
- [19] B. S. Gaudi et al., *Astrophys. J.* **566**, 463 (2002)
- [20] A. Gould et al., *Astrophys. J.* **720**, 1073 (2010)
- [21] I. A. Bond et al., *Astrophys. J.* **606**, L155 (2004)
- [22] J.-P. Beaulieu et al., *Nature* **439**, 437 (2006)
- [23] A. Gould et al., *Astrophys. J.* **644**, L37 (2006)
- [24] J. Janczak et al., *Astrophys. J.* **711**, 731 (2010)
- [25] T. Sumi et al., *Astrophys. J.* **710**, 1641 (2010)

- [26] N. Miyake et al., *Astrophys. J.*, accepted, preprint [arXiv.org:1010.1809](https://arxiv.org/abs/1010.1809)
- [27] M. Dominik, *Mon. Not. R. Astron. Soc.*, in print, DOI: 10.1111/j.1365-2966.2010.17655.x (2010)
- [28] M. Dominik et al., *Mon. Not. R. Astron. Soc.* **380**, 792 (2007)

The frequency of extrasolar planet detections with microlensing simulations

Rieul Gendron

*Jodrell Bank Centre for Astrophysics, University of Manchester
United Kingdom*

Shude Mao

*Jodrell Bank Centre for Astrophysics, University of Manchester, UK
National Astronomical Observatories, Chinese Academy of Sciences
China*

It was first proposed by [1] that gravitational microlensing could be used to detect extrasolar planets. To date, over 500 have been discovered, with microlensing planets, although relatively few in number, probing a region of the mass versus semi-major axis plane that is currently out of reach of the other methods, with the sensitivity peaking just beyond ~ 1 AU. Microlensing planets are therefore very useful for placing constraints on planet formation models.

We simulate light curves for 1000 extrasolar planet systems around host stars of mass $0.25M_{\odot}$ drawn from the Ida & Lin core accretion models of planet formation [2]. The simulated data is first fitted with a single-lens model. If the fit is poor, combinations of the planets most likely to be causing perturbations are placed around the star and new light curves are generated to attempt to reproduce the original light curve.

We found that the majority of the light curves were well-fitted by single-lens models. However, 26 were not and hence were determined to contain perturbations due to at least one planet. Of the 26 interesting light curves, it was found that 16 could be explained by single planets. A greater number of planets were necessary to explain the remaining 10 cases. These results place an upper limit on the number of planets that would be deduced by a fitting procedure since it might be possible to produce the original light curve with a fewer number of planets.

References

- [1] S. Mao and B. Paczynski, *The Astrophysical Journal* **374**, L37-L40 (1991)
- [2] See the Ida & Lin set of papers, for example: S. Ida and D. N. C. Lin, *The Astrophysical Journal* **604**, 388-413 (2004)

A Semi-Analytical Model for Gravitational Microlensing Events

Denis Sullivan & Paul Chote, Michael Miller

*School of Chemical & Physical Sciences, Victoria University of Wellington
New Zealand*

1 Introduction

This paper describes the latest version of the software we have developed for modelling gravitational microlensing events that involve multiple lensing masses. Of particular interest is the modelling of planetary microlensing events requiring two or more lensing masses.

The basic thin lens equation relating a point source image position, \mathbf{s} , to the positions, \mathbf{r} , of the multiple images created by the N lensing masses is simple enough,

$$\mathbf{s} = \mathbf{r} - \sum_{j=1}^N \epsilon_j \frac{\mathbf{r} - \mathbf{r}_j}{|\mathbf{r} - \mathbf{r}_j|^2} \quad , \text{ where } \mathbf{r}_j \text{ and } \epsilon_j \text{ are the lens positions and mass fractions,}$$

The positions in this expression are in units of the Einstein ring radius corresponding to the total lens mass. Except for the single lens case, inverting the equation in order to determine each image position directly is not a trivial exercise. In fact, the inversion procedure is relatively complicated for even the two-mass lens and it rapidly becomes unmanageable when the number of lensing masses increases much beyond two.

2 Inverse Ray-tracing

The above inversion difficulty has led to wide-spread use of the “brute force” approach called inverse ray tracing: “all” potential positions in the image plane are checked in order to determine which ones are consistent with a given source position. Each determination is straight forward since it is clear that a simple substitution of an image position in the above lens equation yields a unique source position origin.

Due to the potentially large number of calculations required, access to significant computing power makes this technique a practical proposition, but it can also be improved by use of efficient image plane search techniques or better still recording

all image plane, source plane correspondences in order to create a so-called *magnification map*. This map can be used to generate a microlensing light curve, since the source magnification at a given position can be directly estimated from the area density of points (inverse rays) in the source plane relative to the density in the image plane. A particular light curve can be rapidly computed by calculating the changing “ray” density ratio for any chosen source track. This method includes finite source size effects directly along with source limb darkening if required, by weighting ray densities in the source disk. Observer/source parallax effects can also be included via appropriately curved source tracks. However, internal lens configuration changes will alter the magnification map and accuracy depends directly on the density of rays covering the image plane, which of course has computational implications.

Modelling code using this methodology was developed as part of a PhD programme at VUW [1] and it has been used to model a range of planetary microlensing events. Recently, we decided to pursue the approach of directly inverting the lensing equation. One particular motivation for this work was to enable satisfactory modelling of lens motion effects, but the overall approach is also more efficient, at least for systems with no more than four lenses.

3 The Polynomial Method

The algebra is greatly simplified by representing the two dimensional plane positions using complex coordinates as first introduced by Witt [2]. The lens equation relating source position ($\mathbf{s} \rightarrow \omega = u + iv$) to image positions ($\mathbf{r} \rightarrow z = x + iy$) for N lenses ($\mathbf{r}_j \rightarrow z_j = x_j + iy_j$) then becomes:

$$\omega = z - \sum_{j=1}^N \frac{\epsilon_j}{\bar{z} - \bar{z}_j} \quad \text{or,} \quad \bar{\omega} = \bar{z} - \sum_{j=1}^N \frac{\epsilon_j}{z - z_j} \quad (\text{in complex conjugate form})$$

Combining both forms of this lensing equation into one equation for image position z for a two mass lens system produces a complex fifth order polynomial, whose five roots are potential image positions. Back substitution is required in order determine if a root corresponds to a real image position, as there can be three or five images depending on the geometry. In general, the complex fifth order polynomial can only be solved numerically but there are algorithms to accomplish this. We use the method of Jenkins and Traub [3] in combination with root polishing using the Laguerre method [4] to obtain accurate root values.

Given that the light bending in a gravitational field does not change the intrinsic source brightness, the point source magnification at each image position, $\mathbf{z} = x + iy$, is given by the ratio of the infinitesimal area element $\delta A_{xy} = dxdy$ in the image plane to the corresponding elemental area δA_{uv} in the source plane at the position $\mathbf{w} = u + iv$. This quantity is given by the determinant of the Jacobian for the

transformation of the point $\mathbf{z}(x, y)$ in the image plane to the point $\mathbf{w}(u, v)$ in the source plane, as governed by the above lensing equation. But, it is the ‘Jacobian’ (J) of the inverse transformation from the source position to the image position that is readily determined and, given the geometrical nature of the quantity, the absolute value of the inverse provides the value of interest. We have:

$$J = \frac{\partial u}{\partial x} \frac{\partial v}{\partial y} - \frac{\partial u}{\partial y} \frac{\partial v}{\partial x} \implies \frac{\partial \omega}{\partial z} \frac{\partial \bar{\omega}}{\partial \bar{z}} - \frac{\partial \omega}{\partial \bar{z}} \frac{\partial \bar{\omega}}{\partial z} = 1 - \left| \frac{\partial \bar{\omega}}{\partial z} \right|^2 = 1 - \left| \frac{\partial \omega}{\partial \bar{z}} \right|^2$$

The point source magnification of each image formed at the position \mathbf{z} is therefore $1/|J(\mathbf{z})|$ and the combined magnification for all unresolved images is simply the sum over these quantities.

The critical curves (and the corresponding caustics) are the locii of points where the point source magnification formally diverges and are thus determined from the requirement that this inverse Jacobian is zero; this leads to a set of fourth order complex polynomials for the two mass lens system.

Assembling the expressions that give the coefficients of the complex polynomials is rather tedious [5] and a symbolic algebra computer package such as Maple is of considerable assistance. However, we have found that (substantial) further manual manipulation can lead to more compact and efficient expressions. This is particularly the case for lensing systems with *three* and even *four* masses. And, we have included both these cases in our code. The three-mass case yields a complex 10th order polynomial [5], while the four-mass system leads to a 17th order polynomial requiring the determination of no less than 18 complex coefficients. The critical curve polynomials for these systems are of 6th and 8th order respectively.

Finite source effects become important when the source disk is near a caustic curve and are important in planetary events. We have included these in the software package by using a combination of two methods: a hexadecapole expansion and a numerical integration procedure we call the polygon method. The hexadecapole expansion method [6] employs multiple point source magnification values to estimate the magnification resulting from a finite source, including limb darkening effects if required. The polygon method is based on the work of Gould and Gauchere [7] and uses polygons to represent the source disk and image figures and thereby estimate the areas. Limb darkening effects are included in this method by using a network of “concentric” polygons.

A method promoted by Bennett [8] for finite source effects first employs the polynomial approach to locate the image centres and then adopts the inverse ray-tracing method in the vicinity of each image to estimate the limb-darkening integrals over the images. We are looking at implementing this approach as well.

4 Conclusion

In spite of the expression complexity in calculating the lensing polynomial coefficients, we have found our new code to be competitive speed-wise with the inverse ray-tracing approach. The rapidly rising level of complexity and the large numbers of terms in the coefficient expressions makes the polynomial method impractical for more than four lensing masses. For n lenses the order of the polynomial is n^2+1 , so for $n = 5$ lenses we have 27 coefficients to determine. Furthermore, we need to employ numerical methods to extract 26 complex root values from the 26th order polynomial and determine which ones correspond to real image positions. It is reasonably clear that the inverse ray-tracing approach will be more efficient for these cases, at least for examples with no lens motion.

When lens motion is involved, the polynomial method is both more efficient and faster than inverse ray tracing. A three-mass lensing system consisting of a star and two planets has already been discovered and successfully modelled [9], and it could be the case that a system of a star and three planets is found and usefully modelled. But it is probably the case that endeavouring to model a microlensing light curve with five lensing masses or more (and perhaps even four) is very unlikely to produce useful physical information.

References

- [1] A. Korpela, PhD Thesis, Victoria University of Wellington (2007)
- [2] H. J. Witt, *Astronomy & Astrophysics*, 236, 311 (1990)
- [3] M. A. Jenkins & J. Traub, *Commun. ACM*, 15, 97 (1972)
- [4] K. F. Riley, M. P. Hobson & S. J. Bence, *Mathematical Methods for Physics and Engineering*, Cambridge University Press (2006)
- [5] S. H. Rhie, *ArXiv:astro-ph/0202294* (2002)
- [6] A. Gould, *Astrophysical Journal*, 681, 1593 (2008)
- [7] A. Gould & C. Gauchere, *Astrophysical Journal*, 477, 580 (1997)
- [8] D. P. Bennett, *Astrophysical Journal*, 716, 1408 (2010)
- [9] B. S. Gaudi et al., *Science*, 319, 2008 (2008)

GPU-assisted contouring for modeling binary microlensing events

*Markus Hundertmark, Frederic V. Hessman, Stefan Dreizler
Institut für Astrophysik, Georg-August-Universität Göttingen
Germany*

1 Introduction

Due to the continuously improving computer power available in dedicated hardware, clusters and computing grids, real-time binary modeling is now being tested and used by different microlensing groups. In addition to CPU-based computing, one can exploit the possibility of speeding-up calculations using graphic cards which are available at reasonable prices and have a reduced carbon footprint. These Graphics Processing Units (GPUs) offer a increased capability concerning the number of floating point operations per second but at the cost of careful flow control management. Naturally, these GPUs are well suited for ray-tracing but in this work a pointwise approach for simulating lightcurves on the basis of contouring techniques is also possible, despite some system dependent drawbacks concerning the accuracy.

2 GPU-contouring

The use of GPUs for gravitational microlensing simulations seems natural as their design is driven by the needs of intensive ray-tracing computer games applications. The advantages and disadvantages when used for scientific ray-tracing have been shown, e.g. by [1],[2]. One bottle-neck for a fast fitting environment is the limited data transfer capacity between CPU and GPU. In order to ease the burden of transfer back and forth to the GPU a large fraction of the analysis must be executed on the GPU and needs to be optimized for these machines, since they offer the highest performance for standard single-precision floating point numbers.

As an alternative, we have implemented the contouring technique on GPUs aiming to preserve the pointwise calculation of lightcurves by parallelizing the root-finding and subsequent integration of the image contours as by [3].

Due to the technical limitations of a computing system with many processing units, the number of required computations and variables has to be kept low. This comes at the price of careful flow control management. For this purpose, the squared

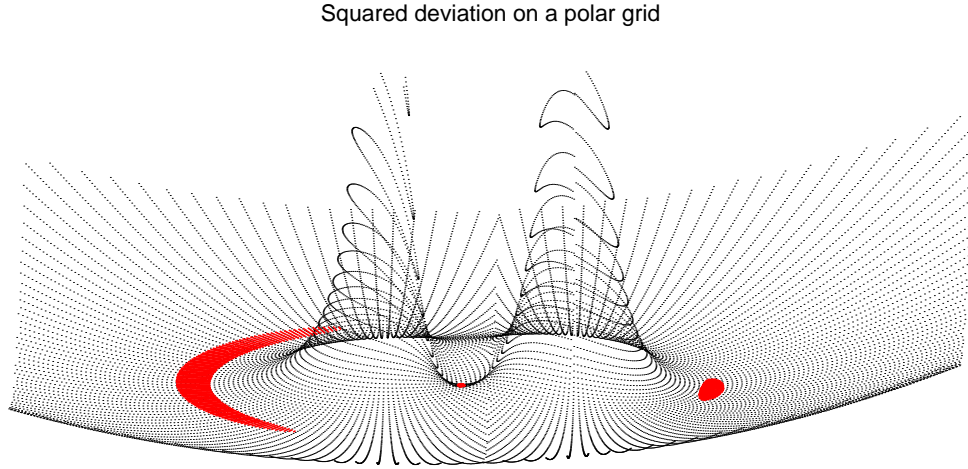


Figure 1: Two-grided polar parameterization of the lens plane for root-finding.

deviation between lens and source position as introduced by [4] has been used. A point-wise parallelisation of the root-finding was achieved by solving the lens equation on a polar grid (cf. [5]), where the radial search for potential roots was carried out as one thread, as illustrated in Fig. 1. Afterwards, the elements are integrated with a simple Gaussian quadrature. This approach is particularly efficient for planetary events with modest angular separations and source positions $|\beta| < 1.5 \theta_E$. A test implementation on a system with 240 streaming processors¹ is able to simulate a lightcurve consisting of 1000 points in one second. Root-finding threads cannot communicate in this approach and thus it would be more difficult to implement a hierarchical approach as by [6].

In contrast to existing CPU-based solutions, the demanded accuracy cannot always be achieved, as most commonly used GPUs exclusively compute with single-precision² floating numbers or require a substantial overhead for operating at double-precision. On single-precision machines the root-finding accuracy is limited by $5 \cdot 10^{-7} \theta_E$ in the radial direction, which directly affects the maximal achievable accuracy and accessible sources star radii r_* . Estimating the magnification as an integration of evenly sized squares in 128^2 search directions per grid gives at zeroth order an uncertainty of

$$\sigma_\mu \approx 10^{-6} r_*^{-1}. \quad (1)$$

¹NVIDIA® Tesla™ C1060

²IEEE 754 single-precision (32 bits)

Models for ground-based microlensing lightcurves require a model accuracy of better than 10^{-3} and thus the applicability of the model is limited to source star radii $\geq 10^{-3} \theta_E$. Beyond that limit, only relative precision can be guaranteed. The effect of missing solutions at the edges is $\propto 1/N$ and thus the aforementioned number of 128^2 elements is a compromise between runtime, single-precision round-off error, and numerical uncertainty of the integration. The benefits of refining the grids for keeping the requested accuracy is shown in Fig. 2. Comparing current simulations with magnification maps [7],[8], indicate that the numerical accuracy stays below 10^{-3} at one sigma level as demanded.

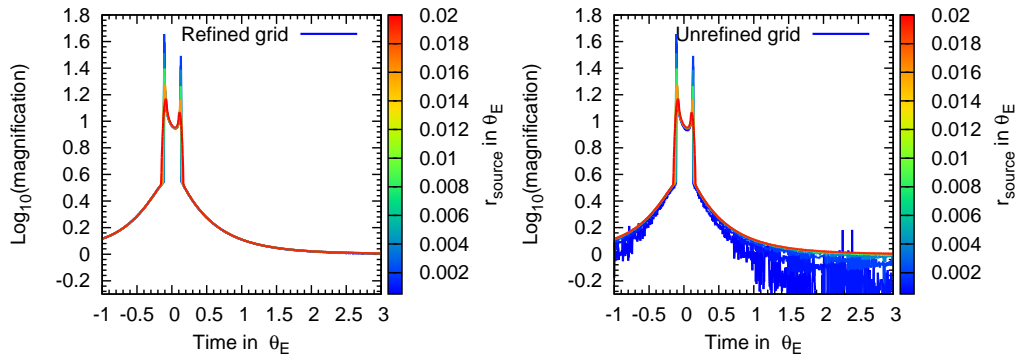


Figure 2: Lightcurves simulated with GPU-assisted contouring are shown for different source star radii with a constant number of integration elements and for a number of integration elements adapted to a predefined accuracy limit.

3 Summary and further work

A first point-wise implementation of the contouring technique on GPUs has been achieved. The rapidly increasing number of streaming processors and the recently introduced double-precision capability³ supports the development of these systems as the existing software can be scaled to a new state-of-the-art equipment just by re-compiling. In addition, this approach can be used with existing sophisticated fitting codes and the simulation can even be mixed with other pointwise contouring techniques which are more suitable for highly accurate simulations, such as the system introduced by [9].

M.H. would like to acknowledge the support from the DFG and the DFG Research Training Group GrK - 1351 “Extrasolar Planets and their host stars”.

³NVIDIA® Fermi™

References

- [1] Bate, N. F., Fluke, C. J., Barsdell, B. R., Garsden, H., & Lewis, G. F. 2010, *New Astronomy*, 15, 726
- [2] Thompson, A. C., Fluke, C. J., Barnes, D. G., & Barsdell, B. R. 2010, *New Astronomy*, 15, 16
- [3] Gould, A., & Gaucherel, C. 1997, *ApJ*, 477, 580
- [4] Schramm, T., & Kayser, R. 1987, *A&A*, 174, 361
- [5] Bennett, D. P. 2010, *ApJ*, 716, 1408
- [6] Dominik, M. 2007, *MNRAS*, 377, 1679
- [7] Kayser, R., Refsdal, S., & Stabell, R. 1986, *A&A*, 166, 36
- [8] Wambsganss, J. 1997, *MNRAS*, 284, 172
- [9] Bozza, V. 2010, *MNRAS*, 408, 2188

Red noise effect in space-based microlensing observations

*Achille A. Nucita, Daniele Vetrugno, Francesco De Paolis, Gabriele Ingrosso,
Berlinda M. T. Maiolo*

*Department of Physics, University of Salento, Lecce, Italy
INFN, Sez. di Lecce, Lecce, Italy*

Stefania Carpano

*ESA, Research and Scientific Support Department, ESTEC, Noordwijk
The Netherlands*

1 Introduction

Gravitational microlensing, first developed to investigate the distribution of Galactic dark matter [1], represents now a powerful and important tool to explore many other astrophysical contexts. For example, in the last years, the possibility to investigate the distribution of exo-planetary systems by means of the microlensing has been pointed out to the scientific community. The advantages for using it are huge and span from the high sensitivity to relatively low mass planets and large observer-lens distances to the unique possibility of detecting free-floating planets. Gravitational microlensing surveys may also give the possibility of a planetary census throughout the Galaxy [2]. Another technique used to search for exo-planets is that of detecting transit events by means of the differential photometry analysis of the sources.

Both transits and microlensing techniques are very close from the observational point of view, since both are photometric-based and the observer has to search for deviations from the baseline flux. In the transit case one seeks for a decrease in the signal flux while for microlensing events an amplification is present. In both cases, the analysis is to be made on light curves.

To this aim, we decided to study and characterize the noise (typically red or pink noise which could mimic a microlensing feature) of a sample of light curves from a space-based experiment. In this perspective we have considered a sample of light curves taken from the CoRoT¹ satellite, a space-based experiment projected by the “Centre National d’Etudes Spatiales” (CNES) in collaboration with the French

¹More detailed information are available at the web site <http://smc.cnes.fr/COROT/>

laboratories and other international partners (Europe, Brasil) launched in December 2006.

D.Vetrugno acknowledges support from the Faculty of the European Space Astronomy Centre (ESAC) and for the kind hospitality. The CoRoT space mission, launched on 2006 December 27, was developed and is operated by the CNES, with participation of the Science Programs of ESA, ESA's RSSD, Austria, Belgium, Brazil, Germany and Spain.

References

- [1] Paczynski, B., ApJ **304**, 1 (1986)
- [2] Gould, A., New Astronomy Review **49**, 424 (2005)

Light curve errors introduced by limb-darkening models

David Heyrovský

Institute of Theoretical Physics, Charles University in Prague

Czech Republic

During the analysis of caustic-crossing microlensing events the source star is typically modeled by analytical limb-darkening laws - most often linear, in a few cases higher-order laws (square-root, quadratic). An alternative option is to use a non-analytical limb-darkening model based on principal component analysis of model atmospheres [1, 2], which gives a more accurate description of the source-star intensity profile [3]. To guide the choice of limb-darkening model during event analysis we need to know the photometric error introduced by assuming a particular model. In order to answer this question, we compute single-lens caustic-crossing light curves for stellar model atmospheres from Kurucz's ATLAS9 grid in a representative set of photometric bands, and compare them with light curves of sources with different approximations of the underlying limb darkening. We demonstrate both the amplitude of the introduced photometric error and the corresponding residual pattern. We discuss the implications of our results for the analysis of single and two-point-mass caustic-crossing events.

References

- [1] Heyrovský, D. 2008, in Proceedings of the Manchester Microlensing Conference, ed. E. Kerins, S. Mao, N. Rattenbury, & L. Wyrzykowski (Manchester, Univ. of Manchester), Proceedings of Science (GMC8) 028
- [2] Zub, M., et al. 2011, A&A, 525, 15
- [3] Heyrovský, D. 2003, ApJ, 594, 464

Detecting Isolated Stellar-Mass Black Holes through Astrometric Microlensing using HST

*Kailash C. Sahu, Howard E. Bond, Jay Anderson
Space Telescope Science Institute, Baltimore, USA*

*Martin Dominik
School of Physics & Astronomy, University of St. Andrews, St. Andrews, UK*

*Andrzej Udalski
Warsaw University Observatory, Warszawa, Poland*

*Philip Yock
Department of Physics, University of Auckland, Auckland, New Zealand*

1 Introduction

Stars with masses greater than $\sim 20 M_{\odot}$ are thought to end their lives as stellar-mass black holes (BHs) (e.g., Fryer & Kalogera 2001). Yet, there has never been an unambiguous detection of an isolated black hole, since they emit no radiation. The only detected BHs to date are through their X-ray emissions in binary systems, where their masses have been measured through radial velocity measurements. Solitary BHs are detectable with current microlensing searches like OGLE and MOA. These campaigns have already detected several BH candidates. Bennett et al. (2002) have described two events: MACHO 96-BLG-5 and MACHO 98-BLG-6, with mass estimates of > 6 solar mass. Mao et al. (2002) concluded that MACHO 99-BLG-22 is a BH candidate with a minimum mass of $10.5 M_{\odot}$. However, all these claims are statistical in nature, since determination of the lens mass from the microlensing light curve alone suffers from a degeneracy between the distance to the lens, the mass of the lens, and the source-lens relative proper motion.

2 Black Hole Detections through Microlensing

Microlensing survey programs typically detect > 1000 microlensing events towards the Galactic bulge per year. A few of them have long durations, and these long-duration events ($t_E > 150$ days) could potentially be arising from lenses with masses

larger than $10 M_{\odot}$. For most of them, the light from the lens itself is negligible. So it has been suggested that a majority of them are due to massive, non-luminous stellar remnants. However, a long-duration microlensing event can be also by a low-mass lens passing in front of the source with a small relative motion.

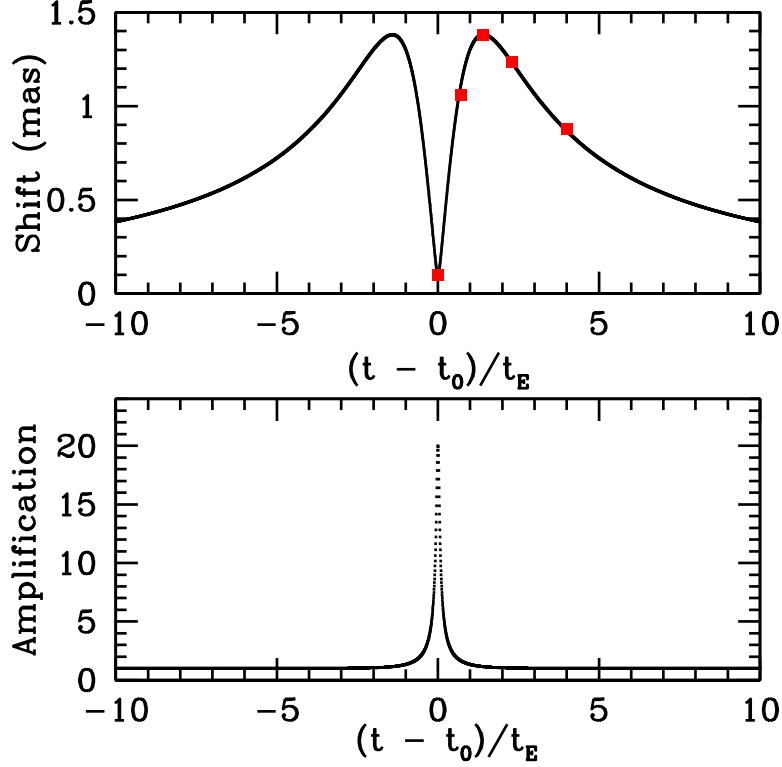


Figure 1: The lower panel shows a photometric microlensing light curve with minimum impact parameter $u=0.05$, and the upper panel shows the corresponding expected astrometric shifts. The astrometric shift peaks at $u \sim 1.4$, which is about 1.4 milliarcsec for a BH lens with a mass of $5 M_{\odot}$ in the Sagittarius arm. The timing of our 5 proposed observations is shown by red dots in the upper panel. These 5 measurements will unambiguously separate the shifts caused by microlensing from the shifts caused by blending and proper motion of the source.

3 Astrometry Resolves the Degeneracy

Microlensing not only causes a photometric amplification, but it also causes a small astrometric shift in the position of the source (see Fig. 1 for illustrations). This astrometric shift is generally undetectable from ground-based observations. But, for

lenses with masses of $\sim 5 M_{\odot}$, the astrometric shift is expected to be ~ 1.4 mas, which is easily detectable with HST. This astrometric shift, coupled with the parallax effect generally observed for the long-duration events, allows a determination of the mass of the lens unambiguously, thus resolving the degeneracy between the low-mass and the high-mass lenses (Sahu & Dominik 2001).

4 Mass Determinations of the BH Candidates and Implications

We expect to achieve an astrometric precision of ~ 0.2 mas at each epoch of HST observations. Thus a shift of 1.4 mas as expected from a $5 M_{\odot}$ BH would be detected at 7 sigma. The 0.2 mas error translates to an error of about $0.75 M_{\odot}$ in mass measurement. Thus we can determine masses with about 15% precision at $5 M_{\odot}$ or 8% at $10 M_{\odot}$.

Thus our program has the potential of making the first unequivocal detections of isolated black holes, and the first direct mass measurements for isolated stellar-mass BHs through any technique. We expect to observe 5 promising long-duration events with WFC3/HST, possibly leading to detection of some confirmed BHs. Detection of these BHs will provide the very first clues on the frequency of isolated BHs in the Galaxy, which have strong implications on the slope of the IMF at high masses.

This project uses the NASA/ESA Hubble Space Telescope, operated by AURA for NASA.

References

- [1] Bennett, D.P., et al. 2002, ApJ, 579, 639
- [2] Dominik, M., & Sahu, K. C. 2000, ApJ, 534, 213
- [3] Fryer, C. L., & Kalogera, V., 2001, ApJ, 554, 5.
- [4] Mao, S., et al. 2002, MNRAS, 329, 349
- [5] Paczynski, B. 1996, Ann. Rev. A&A, 34, 419

The observability of isolated compact remnants with microlensing

Nicola Sartore

*INAF - Istituto di Astrofisica Spaziale e Fisica Cosmica, Milano
Italy*

Aldo Treves

*Dipartimento di Fisica e Matematica, Università dell’Insubria, Como
Italy*

1 Introduction

The observability of old isolated compact remnants is a long standing problem. To date, blind searches for neutron stars and stellar-mass black holes (NSs and BHs hereafter) likely accreting from the interstellar medium (ISM) have failed to reveal any promising candidates.

Dark compact objects may still manifest themselves through the effect of their gravitational field on the light of background sources, i.e. as microlensing events, in particular towards the Galactic bulge, where the density sources is larger. The contribution of NSs and BHs to the microlensing rate towards the bulge has been estimated by e.g. [1], [2] and [3]. Here we present a quantitative analysis of this contribution, under the hypothesis that both NSs and BHs are born with large kick velocities (see e.g. [4]) and compare this contribution with that of “normal” stars, that is brown dwarfs, main sequence stars and white dwarfs.

2 Model and Results

We built a model of the distribution of normal stars in the bulge and disk of the Galaxy (see [5] for a detailed description of the model and procedure adopted) and followed the orbits of synthetic bulge-born and disk-born isolated compact objects in the Galactic potential. Following [1], the normalization of the phase space distribution of NSs and BHs was estimated from the stellar initial mass function assuming that all stars with initial mass greater than $1 M_{\odot}$ are in the remnant phase. In particular, stars with initial mass between 8 and 40 solar masses are now NSs with $M = 1.4 M_{\odot}$, while stars with mass $> 40 M_{\odot}$ are now BHs with $M = 10 M_{\odot}$.

Then, we calculated the optical depth and the distribution of event time scales for normal stars, NSs and BHs towards different lines of sight (l.o.s. hereafter). The optical depth obtained was lower than the case in which NSs and BHs are born without kicks. This can be easily explained since objects with large velocity have a larger scale height. Thus, the spatial density along the l.o.s. is lower. On the other hand, a fast moving object is expected to give a higher rate of events with respect to an object with lower velocity. In fact, we found that the fraction of microlensing events due to isolated NSs and BHs is larger than that expected in the case of non kicks. In particular, for events longer than 100 days, we estimated that about 50% of the events are likely due to NSs and BHs.

3 Conclusions and Future Prospects

Cosidering the large number of microlensing events observed by several microlensing surveys, our results suggest that a non-negligible fraction of these events is likely related to NSs and BHs, in particular among long duration events. Indeed, an excess of long duration events has been reported in the literature. Thus, microlensing surveys are a suitable tool to probe the statistical properties of old isolated compact remnants. However, the nature of single lenses has to be assessed as further confirmation. We are performing a cross-check of archival X-ray data to find counterparts of long duration events. The detection of X-ray emission would be a strong indication that the lens is a compact object.

References

- [1] A. Gould, 2000, ApJ, 535, 928
- [2] A. Wood and S. Mao, 2005, MNRAS, 362, 945
- [3] S. Calchi Novati et al., 2008, A&A, 480, 273
- [4] G. Hobbs et al., 2005, MNRAS, 360, 974
- [5] N. Sartore and A. Treves, 2010, A&A, 523, A33

Gravitational microlensing by the Ellis wormhole

Fumio Abe

Solar-Terrestrial Environment Laboratory

Nagoya University

Japan

1 abstract

A method to calculate light curves of the gravitational microlensing of the Ellis wormhole is derived in the weak-field limit. In this limit, lensing by the wormhole produces one image outside the Einstein ring and one other image inside. The weak-field hypothesis is a good approximation in Galactic lensing if the throat radius is less than 10^{11} km. The light curves calculated have gutters of approximately 4% immediately outside the Einstein ring crossing times. The magnification of the Ellis wormhole lensing is generally less than that of Schwarzschild lensing. The optical depths and event rates are calculated for the Galactic bulge and Large Magellanic Cloud fields according to bound and unbound hypotheses. If the wormholes have throat radii between 100 and 10^7 km, are bound to the galaxy, and have a number density that is approximately that of ordinary stars, detection can be achieved by reanalyzing past data. If the wormholes are unbound, detection using past data is impossible.

2 Introduction

A solution of the Einstein equation that connects distant points of space-time was introduced by [16]. This “Einstein–Rosen bridge” was the first solution to later be referred to as a wormhole. Initially, this type of solution was just a trivial or teaching example of mathematical physics. However, [24] proved that some wormholes are “traversable”; i.e., space and time travel can be achieved by passing through the wormholes. They also showed that the existence of a wormhole requires exotic matter that violates the null energy condition. Although they are very exotic, the existence of wormholes has not been ruled out in theory. Inspired by the Morris–Thorne paper, there have been a number of theoretical works (see [41, 22] and references therein) on wormholes. The curious natures of wormholes, such as time travel, energy conditions, space-time foams, and growth of a wormhole in an accelerating universe have been studied. Although there have been enthusiastic theoretical studies, studies searching

for real evidence of the existence of wormholes are scarce. Only a few attempts have been made to show the existence or nonexistence of wormholes.

A possible observational method that has been proposed to detect or exclude the existence of wormholes is the application of optical gravitational lensing. The gravitational lensing of wormholes was pioneered by [13], who inferred that some wormholes show “negative mass” lensing. They showed that the light curve of the negative-mass lensing event of a distant star has singular double peaks. Several authors subsequently conducted theoretical studies on detectability [32, 9]. Another gravitational lensing method employing gamma rays was proposed by [38], who postulated that the singular negative-mass lensing of distant active galactic nuclei causes a sharp spike of gamma rays and may be observed as double-peaked gamma-ray bursts. They analyzed BASTE data and set a limit for the density of the negative-mass objects.

There have been several recent works [34, 28, 26, 30, 15] on the gravitational lensing of wormholes as structures of space-time. Such studies are expected to unveil lensing properties directly from the space-time structure. One study [15] calculated the deflection angle of light due to the Ellis wormhole, whose asymptotic mass at infinity is zero. The massless wormhole is particularly interesting because it is expected to have unique gravitational lensing effects. The Ellis wormhole is expressed by the line element

$$ds^2 = dt^2 - dr^2 - (r^2 + a^2)(d\theta^2 + \sin^2(\theta)d\phi^2), \quad (1)$$

where a is the throat radius of the wormhole. This type of wormhole was first introduced by [18] as a massless scalar field. Later, [24] studied this wormhole and proved it to be traversable. The dynamical feature was studied by [35], who showed that Gaussian perturbation causes either explode to an inflationary universe or collapse to a black hole. [14] showed that the tachyon condensate can be a source for the Ellis geometry.

In this paper, we derive the light curve of lensing by the Ellis wormhole and discuss its detectability. In Section 2, we discuss gravitational lensing by the Ellis wormhole in the weak-field limit. The light curves of wormhole events are discussed in Section 3. The validity of the weak-field limit is discussed in Section 4. The optical depth and event rate are discussed in Section 5. The results are summarized in Section 6.

3 Gravitational lensing

Magnification of the apparent brightness of a distant star by the gravitational lensing effect of another star was predicted by [17]. This kind of lensing effect is called “microlensing” because the images produced by the gravitational lensing are very close to each other and are difficult for the observer to resolve. The observable effect is the changing apparent brightness of the source star only. This effect was discovered in 1993 [39, 1, 5] and has been used to detect astronomical objects that do not emit

observable signals (such as visible light, radio waves, and X rays) or are too faint to observe. Microlensing has successfully been applied to detect extrasolar planets [8] and brown dwarfs [10, 19]. Microlensing is also used to search for unseen black holes [4, 7, 29] and massive compact halo objects [3, 37, 42], a candidate for dark matter.

The gravity of a star is well expressed by the Schwarzschild metric. The gravitational microlensing of the Schwarzschild metric [31, 21, 27] has been studied in the weak-field limit. In this section, we simply follow the method used for Schwarzschild lensing. Figure 1 shows the relation between the source star, the lens (wormhole), and the observer. The Ellis wormhole is known to be a massless wormhole, which means that the asymptotic mass at infinity is zero. However, this wormhole deflects light by gravitational lensing [12, 11, 26, 15] because of its curved space-time structure. The deflection angle $\alpha(r)$ of the Ellis wormhole was derived by [15] to be

$$\alpha(r) = \pi \left\{ \sqrt{\frac{2(r^2 + a^2)}{2r^2 + a^2}} - 1 \right\}, \quad (2)$$

where r is the closest approach of the light. In the weak-field limit ($r \rightarrow \infty$), the deflection angle becomes

$$\alpha(r) \rightarrow \frac{\pi}{4} \frac{a^2}{r^2} - \frac{5\pi}{32} \frac{a^4}{r^4} + o\left(\frac{a}{r}\right)^6. \quad (3)$$

The angle between the lens (wormhole) and the source β can then be written as

$$\beta = \frac{1}{D_L} b - \frac{D_{LS}}{D_S} \alpha(r), \quad (4)$$

where D_L , D_S , D_{LS} , and b are the distances from the observer to the lens, from the observer to the source, and from the lens to the source, and the impact parameter of the light, respectively. In the asymptotic limit, Schwarzschild lensing and massive Janis–Newman–Winnicour (JNW) wormhole lensing [15] have the same leading term of $o(1/r)$. Therefore, the lensing property of the JNW wormhole is approximately the same as that of Schwarzschild lensing and is difficult to distinguish. As shown in Equation (3), the deflection angle of the Ellis wormhole does not have the term of $o(1/r)$ and starts from $o(1/r^2)$. This is due to the massless nature of the Ellis wormhole and indicates the possibility of observational discrimination from the ordinary gravitational lensing effect. In the weak-field limit, b is approximately equal to the closest approach r . For the Ellis wormhole, $b = \sqrt{r^2 + a^2} \rightarrow r (r \rightarrow \infty)$. We thus obtain

$$\beta = \frac{r}{D_L} - \frac{\pi}{4} \frac{D_{LS}}{D_S} \frac{a^2}{r^2} \quad (r > 0). \quad (5)$$

The light passing through the other side of the lens may also form images. However, Equation (5) represents deflection in the wrong direction at $r < 0$. Thus, we must

change the sign of the deflection angle:

$$\beta = \frac{r}{D_L} + \frac{\pi}{4} \frac{D_{LS}}{D_S} \frac{a^2}{r^2} \quad (r < 0). \quad (6)$$

It would be useful to note that a single equation is suitable both for $r > 0$ and $r < 0$ images in the Schwarzschild lensing. However, such treatment is applicable only when the deflection angle is an odd function of r .

If the source and lens are completely aligned along the line of sight, the image is expected to be circular (an Einstein ring). The Einstein radius R_E , which is defined as the radius of the circular image on the lens plane, is obtained from Equation (5) with $\beta = 0$ as

$$R_E = \sqrt[3]{\frac{\pi}{4} \frac{D_L D_{LS}}{D_S} a^2}. \quad (7)$$

The image positions can then be calculated from

$$\beta = \theta - \frac{\theta_E^3}{\theta^2} \quad (\theta > 0) \quad (8)$$

and

$$\beta = \theta + \frac{\theta_E^3}{\theta^2} \quad (\theta < 0), \quad (9)$$

where $\theta = b/D_L \approx r/D_L$ is the angle between the image and lens, and $\theta_E = R_E/D_L$ is the angular Einstein radius. Using reduced parameters $\hat{\beta} = \beta/\theta_E$ and $\hat{\theta} = \theta/\theta_E$, Equations (8) and (9) become simple cubic formulas:

$$\hat{\theta}^3 - \hat{\beta} \hat{\theta}^2 - 1 = 0 \quad (\hat{\theta} > 0) \quad (10)$$

and

$$\hat{\theta}^3 - \hat{\beta} \hat{\theta}^2 + 1 = 0 \quad (\hat{\theta} < 0). \quad (11)$$

As the discriminant of Equation (10) is $-4\hat{\beta}^3 - 27 < 0$, Equation (10) has two conjugate complex solutions and a real solution:

$$\hat{\theta} = \frac{\hat{\beta}}{3} + U_{1+} + U_{1-}, \quad (12)$$

with,

$$U_{1\pm} = \sqrt[3]{\frac{\hat{\beta}^3}{27} + \frac{1}{2} \pm \sqrt{\frac{1}{4} \left(1 + \frac{2\hat{\beta}^3}{27}\right)^2 - \frac{\hat{\beta}^6}{27^2}}}. \quad (13)$$

The real positive solution corresponds to the physical image.

The discriminant of Equation (11) is $4\hat{\beta}^3 - 27$. Thus it has a real solution if $\hat{\beta} < \sqrt[3]{27/4}$:

$$\hat{\theta} = \frac{\hat{\beta}}{3} + U_{2+} + U_{2-}, \quad (14)$$

where,

$$U_{2\pm} = \omega \sqrt[3]{\frac{\hat{\beta}^3}{27} - \frac{1}{2} \pm \sqrt{\frac{1}{4} \left(1 - \frac{2\hat{\beta}^3}{27}\right)^2 - \frac{\hat{\beta}^6}{27^2}}}, \quad (15)$$

with $\omega = e^{(2\pi/3)i}$. This solution corresponds to a physical image inside the Einstein ring. For $\hat{\beta} > \sqrt[3]{27/4}$, Equation (11) has three real solutions. However, two of them are not physical because they do not satisfy $\hat{\theta} < 0$. Only the solution

$$\hat{\theta} = \frac{\hat{\beta}}{3} + \omega U_{2+} + U_{2-} \quad (16)$$

corresponds to a physical image inside the Einstein ring.

Figure 2 shows the calculated images for source stars at various positions on a straight line (source trajectory). The motion of the images are similar to those of the Schwarzschild lensing. Table 1 shows the Einstein radii and angular Einstein radii for a bulge star ($D_S = 8$ kpc and $D_L = 4$ kpc are assumed) and a star in the Large Magellanic Cloud (LMC, $D_S = 50$ kpc and $D_L = 25$ kpc are assumed) for various throat radii. The detection of a lens for which the Einstein radius is smaller than the star radius ($\approx 10^6$ km) is very difficult because most of the features of the gravitational lensing are smeared out by the finite-source effect. Thus, detecting a wormhole with a throat radius less than 1 km from the Galactic gravitational lensing of a star is very difficult.

4 Light curves

The light curve of Schwarzschild lensing was derived by [27]. The same method of derivation can be used for wormholes. The magnification of the brightness A is

$$A = A_1 + A_2 = \left| \frac{\hat{\theta}_1}{\hat{\beta}} \frac{d\hat{\theta}_1}{d\hat{\beta}} \right| + \left| \frac{\hat{\theta}_2}{\hat{\beta}} \frac{d\hat{\theta}_2}{d\hat{\beta}} \right| = \left| \frac{\hat{\theta}_1}{\hat{\beta} \left(1 + \frac{2}{\hat{\theta}_1^3}\right)} \right| + \left| \frac{\hat{\theta}_2}{\hat{\beta} \left(1 - \frac{2}{\hat{\theta}_2^3}\right)} \right|, \quad (17)$$

$$= \left| \frac{1}{\left(1 - \frac{1}{\hat{\theta}_1^3}\right) \left(1 + \frac{2}{\hat{\theta}_1^3}\right)} \right| + \left| \frac{1}{\left(1 + \frac{1}{\hat{\theta}_2^3}\right) \left(1 - \frac{2}{\hat{\theta}_2^3}\right)} \right|, \quad (18)$$

where A_1 and A_2 are magnification of the outer and inner images, $\hat{\theta}_1$ and $\hat{\theta}_2$ correspond to outer and inner images, respectively. The relation between the lens and source trajectory in the sky is shown in Figure 3. The time dependence of $\hat{\beta}$ is

$$\hat{\beta}(t) = \sqrt{\hat{\beta}_0^2 + (t - t_0)^2/t_E^2}, \quad (19)$$

where $\hat{\beta}_0$ is the impact parameter of the source trajectory and t_0 is the time of closest approach. t_E is the Einstein radius crossing time given by

$$t_E = R_E/v_T, \quad (20)$$

where v_T is the transverse velocity of the lens relative to the source and observer. The light curves obtained from Equations (18) and (19) are shown as thick red lines in Figure 4. The light curves corresponding to Schwarzschild lensing are shown as thin green lines for comparison. The magnifications by the Ellis wormhole are generally less than those of Schwarzschild lensing. The light curve of the Ellis wormhole for $\hat{\beta}_0 < 1.0$ shows characteristic gutters on both sides of the peak immediately outside the Einstein ring crossing times ($t = t_0 \pm t_E$). The depth of the gutters is about 4% from the baseline. Amazingly, the star becomes fainter than normal in terms of apparent brightness in the gutters. This means that the Ellis wormhole lensing has off-center divergence. In conventional gravitational lensing theory [33], the convergence of light is expressed by a convolution of the surface mass density. Thus, we need to introduce negative mass to describe divergent lensing by the Ellis wormhole. However, negative mass is not a physical entity. As the lensing by the Ellis wormhole is convergent at the center, lensing at some other place must be divergent because the wormhole has zero asymptotic mass. For $\hat{\beta}_0 > 1.0$, the light curve of the wormhole has a basin at t_0 and no peak. Using these features, discrimination from Schwarzschild lensing can be achieved. Equations (7) and (20) indicate that physical parameters (D_L , a , and v_T) are degenerate in t_E and cannot be derived by fitting the light-curve data. This situation is the same as that for Schwarzschild lensing. To obtain or constrain these values, observations of the finite-source effect [25] or parallax [2] are necessary.

The detectability of the magnification of the star brightness depends on the timescale. The Einstein radius crossing time t_E depends on the transverse velocity v_T . There is no reliable estimate of v_T for wormholes. Here we assume that the velocity of the wormhole is approximately equal to the rotation velocity of stars ($v_T = 220$ km/s) if it is bound to the Galaxy. If the wormhole is not bound to our Galaxy, the transverse velocity would be much higher. We assume $v_T = 5000$ km/s [32] for the unbound wormhole. Table 2 shows the Einstein radius crossing times of the Ellis wormhole lensings for the Galactic bulge and LMC in both bound and unbound scenarios. As the frequencies of current microlensing observations are limited to once every few hours, an event for which the timescale is less than one day

is difficult to detect. To find very long timescale events ($t_E \geq 1000$ days), long-term monitoring of events is necessary. The realistic period of observation is ≤ 10 years. Thus, the realistic size of the throat that we can search for is limited to $100 \text{ km} \leq a \leq 10^7 \text{ km}$ both for the Galactic bulge and LMC if wormholes are bound to our Galaxy. If wormholes are unbound, the detection is limited to $10^5 \text{ km} \leq a \leq 10^9 \text{ km}$.

5 Validity of the weak-field hypothesis

First, we consider the outer image. In the previous section, we applied the weak-field approximation to the impact parameter b and the deflection angle $\alpha(r)$. As previously mentioned, the impact parameter b is written as

$$b = \sqrt{r^2 + b^2} \approx r(1 + \frac{1}{2} \frac{a^2}{r^2}). \quad (21)$$

The condition to neglect the second term is $a \ll \sqrt{2}r$. As the image is always outside the Einstein ring,

$$a \ll \sqrt{2}R_E. \quad (22)$$

From the deflection angle, we obtain a similar relation from Equation (3):

$$a \ll \sqrt{\frac{8}{5}}R_E. \quad (23)$$

The values of a and R_E in Table 1 show that the weak-field approximation is suitable for $a \ll 10^{11} \text{ km}$ in the Galactic microlensing. More generally, $R_E \approx D_S^{1/3} a^{2/3}$ is derived from Equation (7) for $D_L \approx D_S/2$. This means that R_E is much greater than a if $a \ll D_S$. Thus, the weak-field approximation is suitable if the throat radius is negligibly small compared with the source distance. For the inner image, the higher-order effect is expected to be greater than that for the outer image. However, the contribution of the inner image to the total brightness is small and decreases quickly with $\hat{\beta}$ ($A_2/A = 0.034$ for $\hat{\beta} = 2$ and 0.013 for $\hat{\beta} = 3$). On the other hand, the absolute value of the corresponding $\hat{\theta}$ does not decrease as quickly ($\hat{\theta} = -0.618$ for $\beta = 2$ and -0.532 for $\beta = 3$). Thus the contribution of the higher order effect of the second image to the total brightness is expected to be small.

Another possibility of deviation from the weak-field approximation is the contribution of relativistic images. Recently, gravitational lensing in the strong-field limit [40] has been studied for lensing by black holes. In this limit, light rays are strongly bent and wound close to the photon sphere. As a result, a number of relativistic images appear around the photon sphere. However, it has been shown that there is no photon sphere [15] in Ellis wormhole lensing. Therefore, there is no contribution of relativistic images to the magnification in Ellis wormhole lensing. We thus conclude that the weak-field hypothesis is a good approximation unless the throat radius is comparable to the galactic distance.

6 Optical depth and event rate

The probability of a microlensing event to occur for a star is expressed by the optical depth τ :

$$\tau = \pi \int_0^{D_S} n(D_L) R_E^2 dD_L, \quad (24)$$

where $n(D_L)$ is the number density of wormholes as a function of the line of sight. Here we simply assume that $n(D_L)$ is constant ($n(D_L) = n$):

$$\tau = \pi n \int_0^{D_S} \frac{\pi}{4} \left[\frac{D_L(D_S - D_L)}{D_S} a^2 \right]^{2/3} dD_L, \quad (25)$$

$$= \sqrt[3]{\frac{\pi^5}{2^4}} n a^{4/3} D_S^{5/3} \int_0^1 [x(1-x)]^{2/3} dx, \quad (26)$$

$$\approx 0.785 n a^{4/3} D_S^{5/3}. \quad (27)$$

The event rate expected for a source star Γ is calculated as

$$\Gamma = 2 \int_0^{D_S} n(D_L) R_E v_T dD_L, \quad (28)$$

$$= \sqrt[3]{2\pi} n v_T D_S^{4/3} a^{2/3} \int_0^1 \sqrt[3]{x(1-x)} dx, \quad (29)$$

$$\approx 0.978 n v_T a^{2/3} D_S^{4/3}. \quad (30)$$

There is no reliable prediction of the number density of wormholes. Several authors [20, 22] have speculated that wormholes are very common in the universe, at least as abundant as stars. Even if we accept such speculation, there are still large uncertainties in the value of n because the distribution of wormholes is not specified. Here, we introduce two possibilities. One is that wormholes are bound to the Galaxy and the number density is approximately equal to the local stellar density. The other possibility is that wormholes are not bound to the Galaxy and are approximately uniformly distributed throughout the universe. For the bound hypothesis, we use $n = \rho_{Ls} / \langle M_{star} \rangle = 0.147 \text{ pc}^{-3}$, where ρ_{Ls} is the local stellar density in the solar neighborhood, $\rho_{Ls} = 0.044 M_\odot \text{ pc}^{-3}$, and $\langle M_{star} \rangle$ is the average mass of stars. We use $\langle M_{star} \rangle = 0.3 M_\odot$, a typical mass of an M dwarf; *i.e.*, the dominant stellar component in the Galaxy. For the unbound hypothesis, we assumed that the number density of the wormholes is the same as the average stellar density of the universe. The stellar density of the universe is estimated assuming that the fraction of baryonic matter accounted for by star is the same as that of the solar neighborhood. Then we obtain $n = \rho_c \Omega_b \rho_{Ls} / (\rho_{Lb} \langle M_{star} \rangle) = 4.97 \times 10^{-9} \text{ pc}^{-3}$, where $\rho_c = 1.48 \times 10^{-7} M_\odot \text{ p}^{-3}$ is the critical density, $\Omega_b = 0.042$ is the baryon density of the universe divided by the critical density, and $\rho_{Ls} = 0.044 M_\odot \text{ pc}^{-3}$ and $\rho_{Lb} = 0.18 M_\odot \text{ pc}^{-3}$ are the local star and local baryon densities, respectively.

Using these values, we calculated the optical depths and event rates for bulge and LMC lensings. Table 3 presents the results for the bulge lensings. In an ordinary Schwarzschild microlensing survey, observations are made of more than 10 million stars. Thus, we can expect approximately $10^7\Gamma$ events in a year. However, the situation is different in a wormhole search. As mentioned previously, the magnification of wormhole lensing is less than that of Schwarzschild lensing, and a remarkable feature of wormhole lensing is the decreasing brightness around the Einstein radius crossing times. Past microlensing surveys have mainly searched for stars that increase in brightness. The stars monitored are those with magnitudes down to the limiting magnitude or less. However, we need to find stars that decrease in brightness in the wormhole search. To do so, we need to watch brighter stars. Therefore, far fewer stars can be monitored than in an ordinary microlensing survey. Furthermore, the detection efficiency of the wormhole is thought to be less than that for Schwarzschild lensing because of the low magnification. Here we assume that the effective number of stars monitored to find a wormhole is 10^6 . To expect more than one event in a survey of several years, Γ must be greater than $\sim 10^{-6}$. The values in Table 3 indicate that the detection of wormholes with $a > 10^4$ km is expected in the microlensing survey of the Galactic bulge in the case of the bound model. The results of the optical depths and the event rates for LMC lensing are presented in Table 4. On the basis of the same discussion for bulge lensing, we expect $\Gamma > 10^{-6}$ to find a wormhole. The event rates expected for LMC lensing are greater than those for bulge lensing. We expect detection of a wormhole event if $a > 10^2$ km for the bound model. If no candidate is found, we can set upper limits of Γ and/or τ as functions of t_E . To convert these values to physical parameters (n and a) requires the distribution of v_T . Right now, there is no reliable model of the distribution except for using the bound or unbound hypothesis. On the other hand, the event rates for the unbound model are too small for the events to be detected.

In past microlensing surveys [3, 37, 42, 36], large amounts of data have already been collected for both the bulge and LMC fields. Monitoring more than 10^6 stars for about 10 years can be achieved by simply reanalyzing the past data. Thus, discovery of wormholes can be expected if their population density is as high as the local stellar density and $10^2 \leq a \leq 10^7$ km. Such wormholes of astronomical size are large enough for humans to pass through. Thus, they would be of interest to people discussing the possibility of space-time travel. If no candidate is found, the possibility of a rich population of large-throat wormholes bound to the Galaxy can be ruled out. Such a limit, however, may not affect existing wormhole theories because there is no prediction of the abundance. However, theoretical studies on wormholes are still in progress. The limit imposed by observation is expected to affect future wormhole theories. On the other hand, the discovery of unbound wormholes is very difficult even if their population density is comparable to that of ordinary stars. To discover such wormholes, the monitoring of a much larger number of stars in distant galaxies

would be necessary. For example, $\Gamma = 1.7 \times 10^{-6}$ and $t_E \approx 380$ days for the M101 microlensing survey ($D_S = 7.4$ Mpc) if the throat radius is 10^7 km. To carry out such a microlensing survey, observation from space is necessary because the resolving of a large number of stars in a distant galaxy is impossible through ground observations.

Only the Ellis wormhole has been discussed in this paper. There are several other types of wormholes [34, 26, 30] for which deflection angles have been derived. These wormholes are expected to have different light curves. To detect those wormholes, calculations of their light curves are necessary. The method used in this paper can be employed only when we know the analytic solutions of the image positions. If no analytic solution is found, the calculation must be made numerically.

7 Summary

The gravitational lensing of the Ellis wormhole is solved in the weak-field limit. The image positions are calculated as real solutions of simple cubic formulas. One image appears on the source star side and outside the Einstein ring. The other image appears on the other side and inside the Einstein ring. A simple estimation shows that the weak-field hypothesis is a good approximation for Galactic microlensing if the throat radius is less than 10^{11} km. The light curve derived has characteristic gutters immediately outside the Einstein ring crossing times. Optical depths and event rates for bulge and LMC lensings are calculated for simple bound and unbound hypotheses. The results show that the bound wormholes can be detected by reanalyzing past data if the throat radius is between 10^2 and 10^7 km and the number density is approximately equal to the local stellar density. If the wormholes are unbound and approximately uniformly distributed in the universe with average stellar density, detection of the wormholes is impossible using past microlensing data. To detect unbound wormholes, a microlensing survey of distant galaxies from space is necessary.

We would like to thank Professor Hideki Asada of Hirosaki University, Professor Matt Visser of Victoria University, and Professor Tomohiro Harada of Rikkyo University for discussions and their suggestions concerning this study. We thank Professor Philip Yock of Auckland University for polishing our manuscript. Finally, we would like to thank an anonymous referee who pointed out the existence of a second image.

References

- [1] Alcock, C., et al. 1993, *Nat.*, 365, 621
- [2] Alcock, C., et al. 1995, *ApJ*, 454, L125

- [3] Alcock, C., et al. 2000, *ApJ*, 542, 281
- [4] Alcock, C., et al. 2001, *ApJ*, 550, L169
- [5] Aubourg, E. et al. 1993, *Nat.*, 365, 623
- [6] Beaulieu J.-P., et al. 2006, *Nat.*, 439, 437
- [7] Bennett, D. P. et al. 2002, *ApJ*, 579, 639
- [8] Bond, I. A. 2004, *ApJ*, 606, L155
- [9] Bogdanov, M. B. & Cherepashchuk, A. M. 2008, *Ap&SS* 317, 181
- [10] Calchi Novati, S., Mancini, L., Scarpetta, G., & Wyrzykowski, L. 2009, *MNRAS*, 400, 1625
- [11] Chetouani, L. & Clément, G. 1984, *Gen. Relativ. Gravit.* 16, 111
- [12] Clément, G. 1984, *J. Theor. Phys.* 23, 335
- [13] Cramer, J. G., Forward, R. L., Morris, M. S., Visser, M., Benford, G., & Landis, G. A. 1995, *PRD*, 51, 3317
- [14] Das, A., & Kar, S. 2005, *Class. Quan. Grav.*, 22, 3045
- [15] Dey, T. K. & Sen, S. 2008, *Mod. Phys. Lett. A* 23, 953
- [16] Einstein, A., & Rosen, N. 1935, *Phys. Rev.* 48, 73
- [17] Einstein, A. 1936, *Science* 84, 506
- [18] Ellis, H. G. 1973, *J. Math. Phys.*, 14, 104
- [19] Gould, A. et al. 2009, *ApJ*, 698, L147
- [20] Krasnikov, S. 2000, *PRD*, 62, 084028
- [21] Liebes, S. 1964, *Phys. Rev.*, 133, 835
- [22] Lobo F. S. N. 2007, arXiv:0710.4474v1 [gr-qc]
- [23] Mao, S. et al. 2002, *MNRAS*, 329, 349
- [24] Morris, M. S., & Thorne, K. S. 1988, *Am. J. Ph.*, 56, 395
- [25] Nemiroff, R. J. & Wickramasinghe, W. A. D. T. 1994, *ApJ*, 424, L21

- [26] Nandi, K. K., Zhang, Y.-Z., & Zakharov, A. V. 2006, PRD, 74, 024020
- [27] Paczyński, B. 1986, ApJ, 304, 1
- [28] Perlick, V. 2004, PRD, 69, 064017
- [29] Poindexter, S., et al., 2005, ApJ, 633, 914
- [30] Rahaman, F., Kalam, M., & Chakraborty, S. 2007, Chin. J. Phys. 45, 518
- [31] Refsdal, S. 1964, MNRAS, 128, 295
- [32] Safonova, M., Diego, F. T., & Romero, G. E. 2002, PRD, 65, 023001
- [33] Schneider, P., Ehlers, J., & Falco, E. E., 1992, Gravitational Lenses, Springer-Verlag New York, ISBN 0-387-97097-3, p. 175
- [34] Shatsukiĭ, A. A. 2004, Astr. Rep. 48, 525
- [35] Shinkai, H. & Hayward, S. A. 2002, PRD, 66, 044005
- [36] Sumi, T., et al., 2003 ApJ, 591, 204
- [37] Tisserand, P., et al. 2007, A & A, 469 387
- [38] Torres, D. F., Romero, G. E., & Anchordoqui, L. A. 1998, PRD, 58, 123001
- [39] Udalski A., et al., 1993, AcA 43, 289
- [40] Virbhadra, K. S. & Ellis, G. F. R. 2000, PRD 62, 084003
- [41] Visser, M. "Lorentzuan Wormholes: From Einstein to Hawking", American Institute of Physics, New York, 1995
- [42] Wyrzykowski, Ł. et al. 2009, MNRAS, 397, 1228

Table 1: Einstein radii for bulge and LMC lensings

a (km)	Bulge		LMC	
	R_E (km)	θ_E (mas)	R_E (km)	θ_E (mas)
1	3.64×10^5	0.001	6.71×10^5	< 0.001
10	1.69×10^6	0.003	3.12×10^6	0.001
10^2	7.85×10^6	0.013	1.45×10^7	0.004
10^3	3.64×10^7	0.061	6.71×10^7	0.018
10^4	1.69×10^8	0.283	3.12×10^8	0.083
10^5	7.85×10^8	1.31	1.45×10^9	0.387
10^6	3.64×10^9	6.10	6.71×10^9	1.80
10^7	1.69×10^{10}	28.3	3.12×10^{10}	8.35
10^8	7.85×10^{10}	131	1.45×10^{11}	38.7
10^9	3.64×10^{11}	610	6.71×10^{11}	180
10^{10}	1.69×10^{12}	2 832	3.12×10^{12}	835
10^{11}	7.85×10^{12}	13 143	1.45×10^{13}	3 874

Table 2: Einstein radius crossing times for bulge and LMC lensings

a (km)	Bulge		LMC	
	t_E (day)		t_E (day)	
	Bound	Unbound	Bound	Unbound
1	0.019	0.001	0.035	0.002
10	0.089	0.004	0.164	0.007
10^2	0.413	0.018	0.761	0.033
10^3	1.92	0.084	3.53	0.155
10^4	8.90	0.392	16.4	0.721
10^5	41.3	1.82	76.1	3.35
10^6	192	8.44	353	15.5
10^7	890	39.2	1 639	72.1
10^8	4 130	182	7 608	335
10^9	$> 10^4$	843	$> 10^4$	1 553
10^{10}	$> 10^4$	3915	$> 10^4$	7 212

Table 3: Optical depths and event rates for bulge lensing

a (km)	Bound		Unbound	
	τ	Γ (1/year)	τ	Γ (1/year)
10	8.24×10^{-12}	2.45×10^{-8}	2.78×10^{-19}	1.88×10^{-14}
10^2	1.77×10^{-10}	1.14×10^{-7}	6.00×10^{-18}	8.73×10^{-14}
10^3	3.82×10^{-9}	5.27×10^{-7}	1.29×10^{-16}	4.05×10^{-13}
10^4	8.24×10^{-8}	2.45×10^{-6}	2.78×10^{-15}	1.88×10^{-12}
10^5	1.77×10^{-6}	1.14×10^{-5}	6.00×10^{-14}	8.73×10^{-12}
10^6	3.82×10^{-5}	5.27×10^{-5}	1.29×10^{-12}	4.05×10^{-11}
10^7	8.24×10^{-4}	2.45×10^{-4}	2.78×10^{-11}	1.88×10^{-10}
10^8	1.77×10^{-2}	1.14×10^{-3}	6.00×10^{-10}	8.73×10^{-10}
10^9	3.82×10^{-1}	5.27×10^{-3}	1.29×10^{-8}	4.05×10^{-9}
10^{10}	8.24	2.45×10^{-2}	2.78×10^{-7}	1.88×10^{-8}

Table 4: Optical depths and event rates for LMC lensing

a (km)	Bound		Unbound	
	τ	Γ (1/year)	τ	Γ (1/year)
10	1.75×10^{-10}	2.82×10^{-7}	5.90×10^{-18}	2.17×10^{-13}
10^2	3.76×10^{-9}	1.31×10^{-6}	1.27×10^{-16}	1.01×10^{-12}
10^3	8.11×10^{-8}	6.07×10^{-6}	2.74×10^{-15}	4.67×10^{-12}
10^4	1.75×10^{-6}	2.82×10^{-5}	5.90×10^{-14}	2.17×10^{-11}
10^5	3.76×10^{-5}	1.31×10^{-4}	1.27×10^{-12}	1.01×10^{-10}
10^6	8.11×10^{-4}	6.07×10^{-4}	2.74×10^{-11}	4.67×10^{-10}
10^7	1.75×10^{-2}	2.82×10^{-3}	5.90×10^{-10}	2.17×10^{-9}
10^8	3.76×10^{-1}	1.31×10^{-2}	1.27×10^{-8}	1.01×10^{-8}
10^9	8.11	6.07×10^{-2}	2.74×10^{-7}	4.67×10^{-8}
10^{10}	175	2.82×10^{-1}	5.90×10^{-6}	2.17×10^{-7}

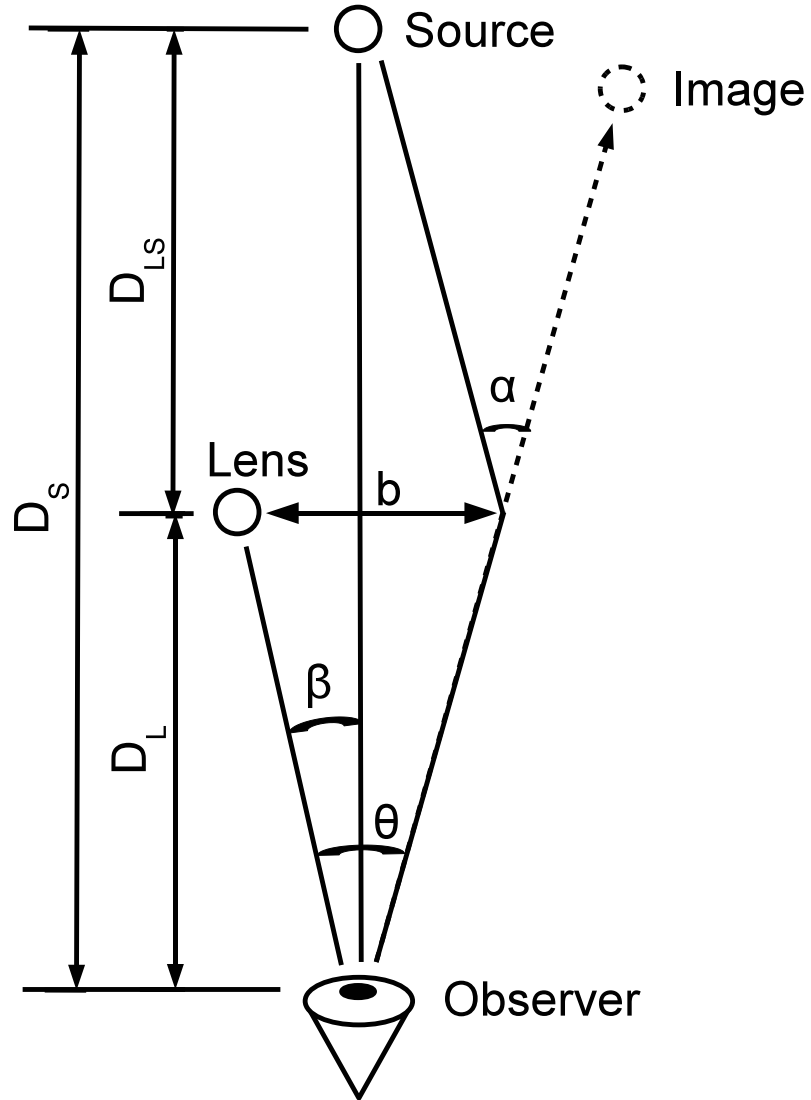


Figure 1: Sketch of the relation between the source star, lens (wormhole), and observer.

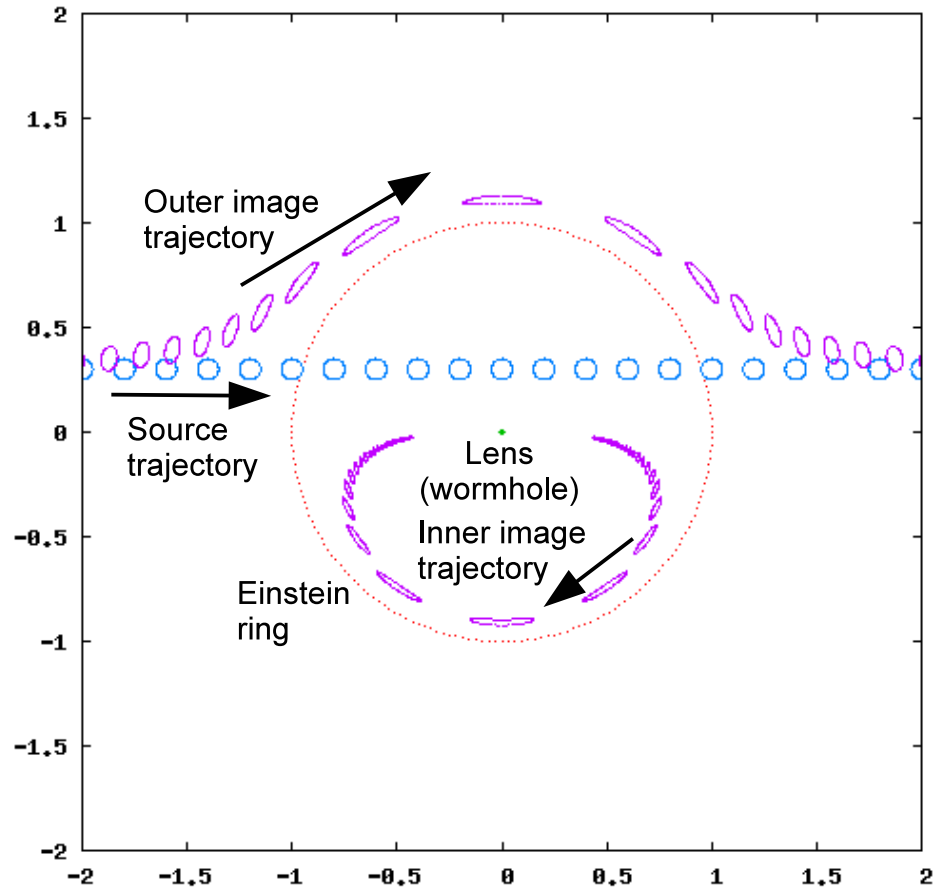


Figure 2: Source and image trajectories in the sky from the position of the observer.

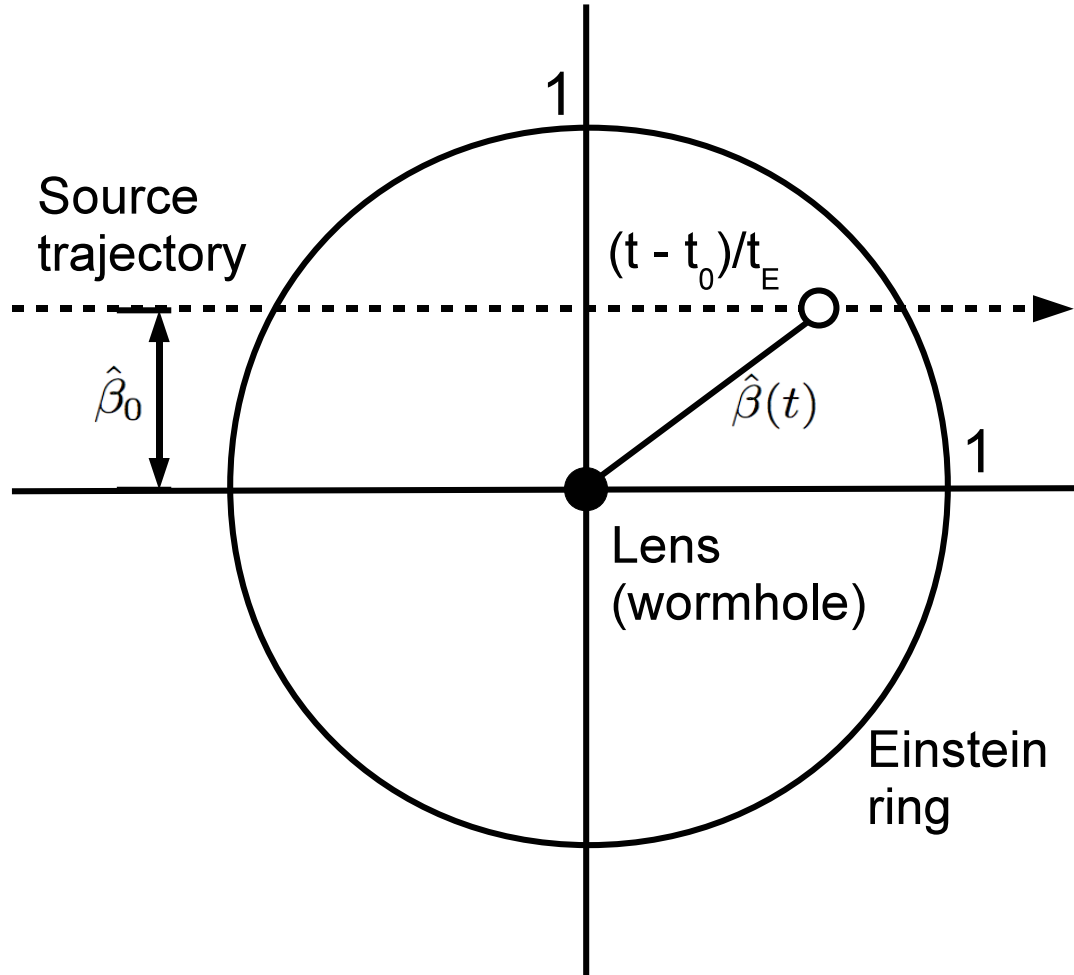


Figure 3: Sketch of the relation between the source trajectory and the lens (wormhole) in the sky. All quantities are normalized by the angular Einstein radius θ_E .

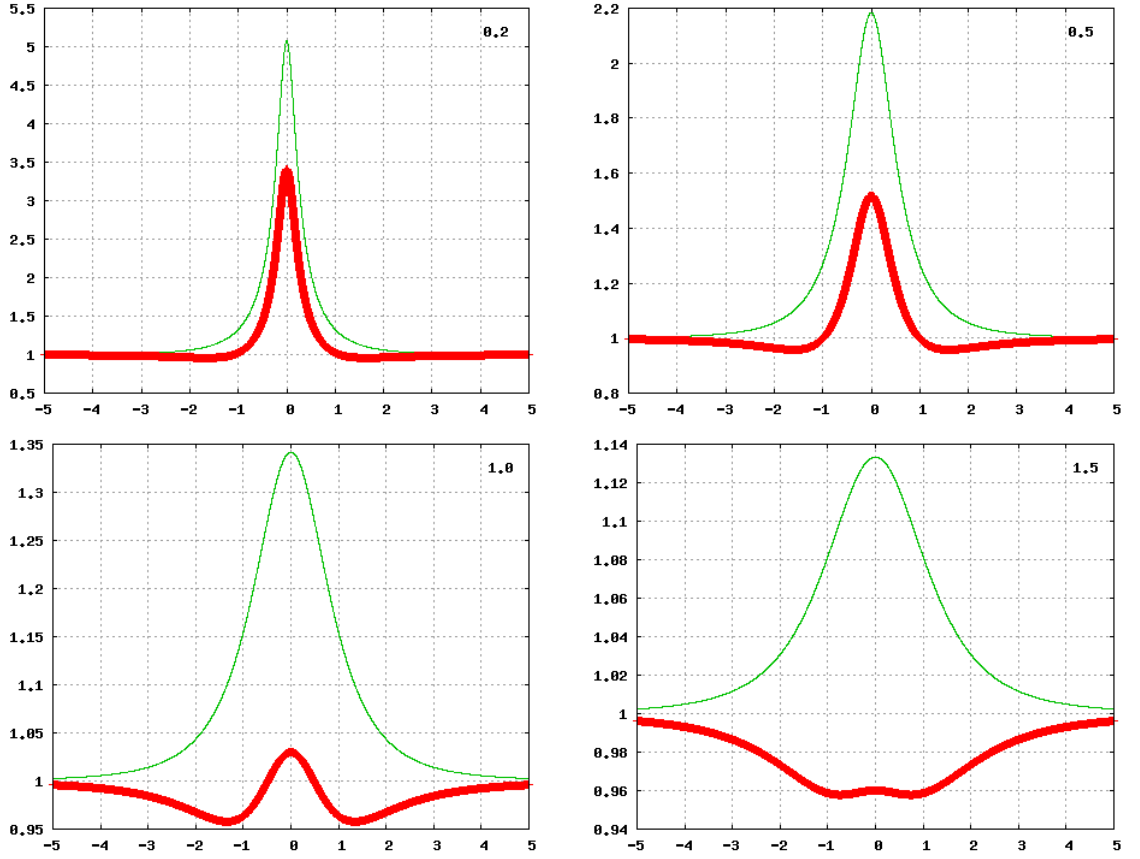


Figure 4: Light curves for $\hat{\beta}_0 = 0.2$ (top left), $\hat{\beta}_0 = 0.5$ (top right), $\hat{\beta}_0 = 1.0$ (bottom left), and $\hat{\beta}_0 = 1.5$ (bottom right). Thick red lines are the light curves for wormholes. Thin green lines are corresponding light curves for Schwarzschild lenses.

The deflection of light ray in strong field: *a material medium approach*

Asoke Kumar Sen
Department of Physics
Assam University
India

1 Introduction

The first correct expression for gravitational deflection of light due to a gravitational mass (M) was derived by Einstein in 1915, with an expression for bending given by $4GM/(c^2 r_{\odot})$, where r_{\odot} is the closet distance of approach, which is approximately the solar radius. The exact amount of deflection for a ray of light can be worked out from the null geodesic, which a ray of light follows [1,2,3,4]. The deflection of a light ray passing close to a gravitational mass can be alternately calculated by following an approach, where the effect of gravitation on the light ray is estimated by considering the light ray to be passing through a *material medium*[5-9]. The value of the refractive index of that medium in this case is decided by the strength of gravitational field [10].

Fischbach and Freeman [7], derived the effective refractive index of the material medium and calculated the second order contribution to the gravitational deflection. Sereno [8] had also used the material medium approach for gravitational lensing calculations by drawing trajectory of light ray by Fermat's principle. More recently Ye and Lin [9], using similar approach calculated the gravitational time delay and the effect of lensing. On the other hand, the calculation of higher order deflection terms, due to Schwarzschild Black hole, from the null geodesic, have been performed by various authors [11-14].

With the above background, in the present work, the *material medium* approach is followed, to calculate a more exact expression for the deflection term due to a non-rotating sphere (Schwarzschild geometry), without any weak field approximation.

2 The trajectory of a light ray described by material medium

The Schwarzschild equation expressed in isotropic form is given by[10]

$$ds^2 = \left(\frac{1 - r_g/(4\rho)}{1 + r_g/(4\rho)}\right)^2 c^2 dt^2 - \left(1 + \frac{r_g}{4\rho}\right)^4 (d\rho^2 + \rho^2 (\sin^2 \theta d\phi^2 + d\theta^2)) \quad (1)$$

By setting $ds = 0$, the velocity of light from above can be identified as :

$$v(\rho) = \frac{(1 - \frac{r_g}{4\rho})c}{(1 + \frac{r_g}{4\rho})^3} \quad (2)$$

and this results in an effective value of refractive index $n(r) = \frac{c}{v(r)} = \frac{r}{r - r_g}$, where $r_g = 2GM/c^2$ is Schwarzschild radius. Here the trajectory of the light ray and gravitational mass together define a plane and the equation of light ray in polar co-ordinate system can be written as[15]:

$$\theta = A. \int_{r_\odot}^{\infty} \frac{dr}{r \sqrt{n^2 r^2 - A^2}} \quad (3)$$

The trajectory is such that $n(r).d$ always remains a *constant*, where d is the perpendicular distance between the trajectory of the light ray from the origin and the *constant* is taken here as A [15]. From geometry we identify $A = n(r_\odot)r_\odot$ and the value of deflection $(\Delta\phi)$, can be accordingly written as :

$$\Delta\phi = 2 \int_{r_\odot}^{\infty} \frac{dr}{r \sqrt{\left(\frac{n(r).r}{n(r_\odot).r_\odot}\right)^2 - 1}} - \pi \quad (4)$$

After certain mathematical steps we can write:

$$\Delta\phi = 2D \int_0^a \frac{xdx}{\sqrt{1 - D^2 x^2 (1 - x)^2}} \quad (5)$$

where $D = \frac{r_\odot^2}{r_g(r_\odot - r_g)}$ and $a = r_g/r_\odot$.

Using Mathematica to perform integration, we can write the final expression for gravitational deflection as :

$$\Delta\phi = 4 \left\{ \frac{(\sqrt{D} + \sqrt{D - 4})E - (2\sqrt{D - 4})F}{(\sqrt{D + 4} - \sqrt{D - 4})} \right\}_{x=0}^{x=a} \quad (6)$$

where $E \equiv E(p, q^2)$ is the Elliptic Integral of first kind and $F \equiv F(-q, p, q^2)$ is Incomplete Elliptic Integral of Third kind. The arguments $p, q^2, -q, p, q^2$ are expressed by the following mathematical relations:

$$p = \arcsin \sqrt{\frac{(\sqrt{D-4} - \sqrt{D+4})(\sqrt{D-4} + (2x-1)\sqrt{D})}{(\sqrt{D-4} + \sqrt{D+4})(\sqrt{D-4} - (2x-1)\sqrt{D})}} \quad (7)$$

$$q = \frac{(\sqrt{D-4} + \sqrt{D+4})}{(\sqrt{D-4} - \sqrt{D+4})} \quad (8)$$

This mathematical expression for deflection, in strong field is claimed to be more exact than all other expressions derived so far using *material medium* approach. It has been tested under various boundary conditions.

References

- [1] C. W. Misner, K. S. Thorne and J. A. Wheeler, **Gravitation**, (W. H. Freeman and Company, Newyork 1972)
- [2] S. Weinberg, *Principles and Applications of the General Theory of Relativity*, (John Wiley & Sons Inc. 1972)
- [3] P. Schneider, P. Ehlers, E. E. Falco, *Gravitational Lenses*, (Springer, Berlin 1999)
- [4] C. Darwin, *Proceedings of the Royal Society of London, Series A, Mathematical and Physical Sciences* 249 No. 1257, 180 (1959).
- [5] R. D'E Atkinson, *AJ*, 70 No 8, 517 (1965)
- [6] F. de Felice, *Gen. Relativ. Gravit.* **2**, No. 4, 347 (1971)
- [7] E. Fischbach and B. S. Freeman, *Phys. Rev. D* **67**, 2950, (1980)
- [8] M. Sereno, *Phys. Rev. D* **67**, 064007 (2003)
- [9] X-H. Ye and Q. Lin , *Journal Mod. Opt.* **55**, Issue 7, 1119 (2008)
- [10] *The Classical Theory of Fields volume 2*; J. L. D. Landau and E. M. Lifshitz (1st edition Pergamon Press, 1951; 4 th edition' Butterworth-Heinemann 1980)
- [11] S. V. Iyer and A. O. Petters, *Gen. Relativ. Gravit.* **39**, 1563 (2007)
- [12] K. S. Virbhadra and George F. R. Ellis, *Phys. Rev. D* **62**, 084003 (2000)

- [13] S. Frittelli, T. P. Kiling, and E.T. Newman, Phys. Rev. D. **62**, 064021 (2000)
- [14] G. S. Bisnovatyi-Kogan and O. Yu. Tsupko Astrophysics, **51**, No 1, 99 (2008)
- [15] M. Born and E. Wolf 1947, *Principles of Optics* (7th Edition, Cambridge University Press, Cambridge,1999) p121

Rapidly Rotating Lenses: Repeating orbital motion features in close binary microlenses

Matthew T. Penny, Eamonn Kerins

Jodrell Bank Centre for Astrophysics, University of Manchester, UK

Shude Mao

Jodrell Bank Centre for Astrophysics, University of Manchester, UK

National Astronomical Observatories, Chinese Academy of Sciences

China

Most binary lenses detected in microlensing events complete only a small fraction of their orbits during the event, as binaries with shorter period orbits tend not to show detectable binary signatures. However, we show that there exist some lenses (rapidly rotating lenses or RRLs) with detectable binary signatures that can complete several orbits while their binary lens features are detectable, and hence the same features can be seen to repeat in a lightcurve. Using simple analytical constraints we show there exist regions of the total lens mass-semimajor axis plane where repeating features are detectable, and confirm this with numerical calculations and example lightcurves. With a photometric precision of 1 percent, the region of detectability covers total masses $\sim 0.1M_{\odot}$ and above, and semimajor axes $\sim 0.2\text{--}2$ AU for typical stellar binary lenses. The detectability increases with decreasing lens-source velocities and increasing lens distances. We also present a method of modelling microlensing events with repeating features, by timing the occurrence of lightcurve features, which reduces the need for computationally expensive lightcurve fitting. If fitted successfully, the combination of finite source effects, and the orbital motion of the lens can lead to a mass measurement [1], and possibly a determination of orbital parameters such as inclination and eccentricity.

References

- [1] Dominik M., 1998, A&A, 329, 361

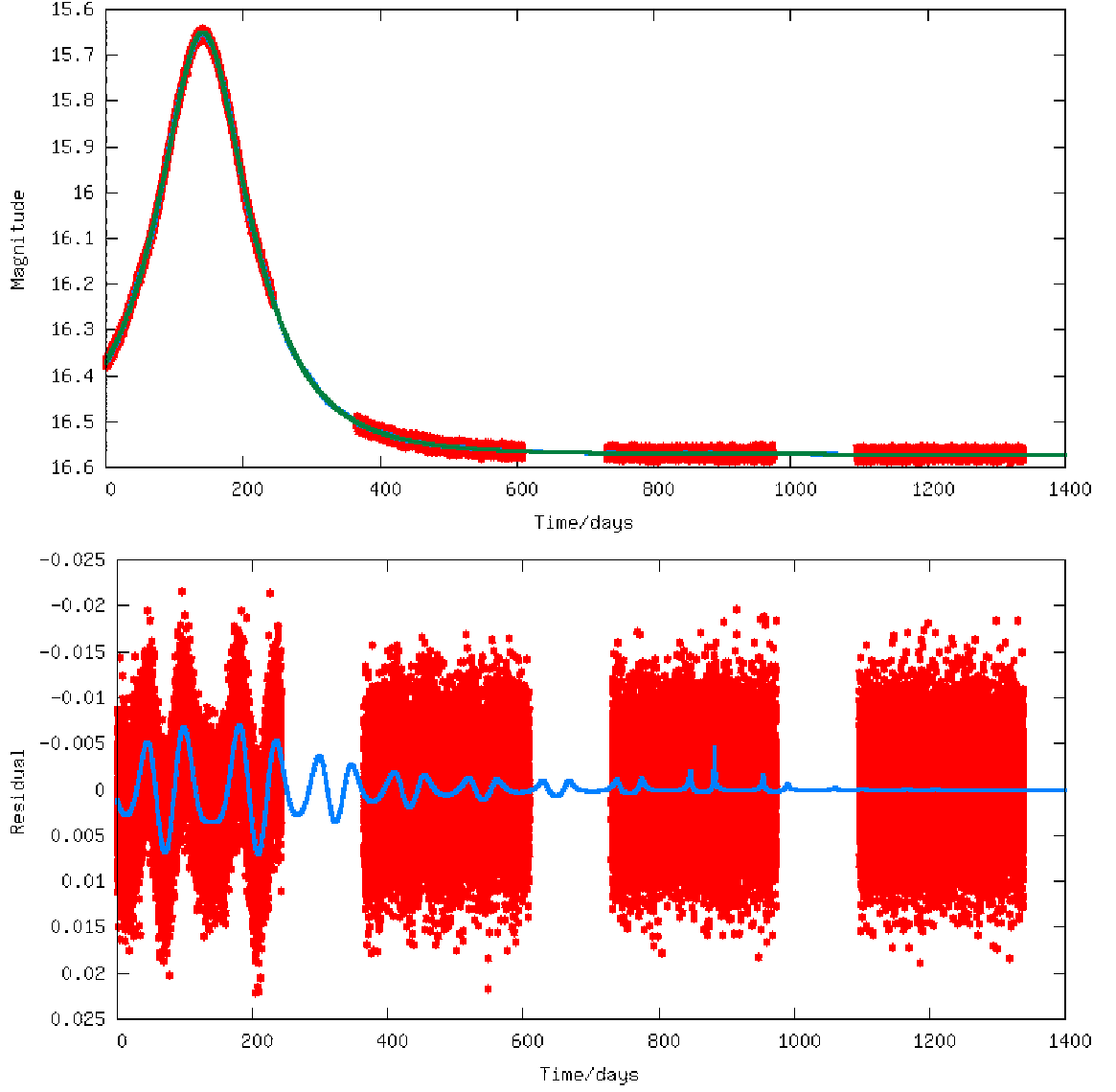


Figure 1: An example of an RRL. The lightcurve is plotted above, and its residual to a single lens lightcurve below. Red points show simulated data that would be typical for a space based microlensing survey, while the blue line shows the model RRL lightcurve and the green line shows the single lens model.

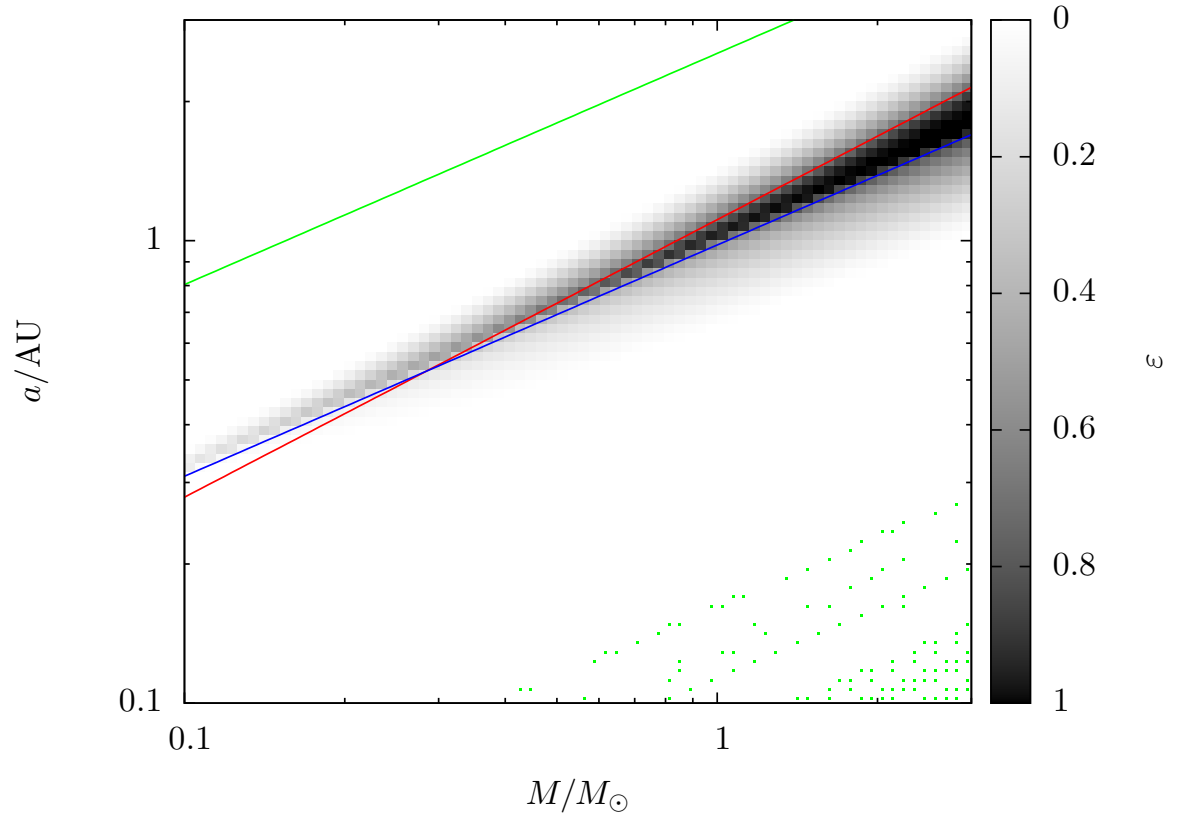


Figure 2: The region of the total mass – semimajor axis plane where RRLs are detectable, for a typical set of lensing parameters. The red and blue lines show the analytically derived region of detectability, which agrees well with the region of numerical determined region of guaranteed detectability (where $\varepsilon = 1$).

Towards the future: new facilities/instrumentation/procedures

Microensing with the SONG global network

Uffe G. Jørgensen, Kennet B. W. Harpsøe, Per K. Rasmussen, Michael I. Andersen, Anton N. Sørensen, Jørgen Christensen-Dalsgaard, Søren Frandsen, Frank Grundahl, Hans Kjeldsen

Next-generation microensing pilot planet search and the frequency of planetary systems

Dan Maoz & Yossi Shvartzvald

Kohyama Astronomical Observatory: current status

Atsunori Yonehara, Mizuki Isogai, Akira Arai, Hiroki Tohyama

Optimal imaging for gravitational microensing

Kennet B. W. Harpsøe, Uffe G. Jørgensen, Per K. Rasmussen, Michael I. Andersen, Anton N. Sørensen, Jørgen Christensen-Dalsgaard, Søren Frandsen, Frank Grundahl, Hans Kjeldsen

IPACs role as the science center for NASAs WFIRST mission

Kaspar von Braun

EUCLID microensing planet hunt

Jean-Philippe Beaulieu & Matthew Penny

Space-based microensing exoplanet survey: WFIRST and/or Euclid

David Bennett

Microensing with Gaia satellite

Lukasz Wyrzykowski

Microlensing with the SONG global network

*Uffe Gråe Jørgensen, Kennet B. W. Harpsøe, Per Kjærgaard, Michael I. Andersen,
Anton Norup Sørensen*

*Niels Bohr Institute and Centre for Star and Planet Formation
University of Copenhagen
Denmark*

*Jørgen Christensen-Dalsgaard, Søren Frandsen, Frank Grundahl, Hans Kjeldsen
Dep. Phys. Astronomy, Aarhus University, Aarhus
Denmark*

1 Introduction

SONG (Stellar Observations Network Group) is a network of 1m robotic telescopes, designed for microlensing exoplanet follow-up observations and long time-series of high-precision radial velocity observations of bright stars for asteroseismology and exoplanet research. The prototype of the telescope is under installation at Teide observatory and will have first light mid-2011. Two more nodes are under construction in China and Argentina, and several national applications are in the process for further nodes around the globe. The telescope design has been described in detail recently by Grundahl et al. 2009 [1]. Here we will describe the design and organization of the network with emphasis on the microlensing aspects.

2 The telescope, dome and network construction

All nodes in the network will have a 1m telescope with two lucky imaging cameras at the Nasmyth and a spectrograph at the Coudé focus. The telescope is produced by Astelco in Germany, the cameras by Andor in UK, and the spectrograph for the prototype is build in our workshop at Aarhus University in Denmark. A movable mirror will direct the light either to the cameras at the Nasmyth platform or pass it through a vacuum tube into the Coudé room in a temperature stabilized adherent shipping container. In the end of the container facing away from the telescope, and separated from the Coudé room, is a small control room with the connecting computers. The data from each telescope will be uploaded on-line to a central data centre which is under construction. All data will be stored at the data centre at least for the lifetime of the project, and all participants in the project can access and download all data.

A group or an individual becomes a member of the project by supplying a substantial contribution to the network, typically a node or the operation of a node, and is then automatically member of the steering committee, whose role is to coordinate the scientific and operational decisions.

3 The microlensing observations

Follow-up microlensing exoplanet observations have until today been performed by networks of existing all-purpose and amateur telescopes. This situation will change in the near future with 3 modern network coming on-line, the Las Cumbres Observatory Global Telescope Network, LCOGT (<http://lcogt.net/>), the Korean Microlensing Telescope Network, KMT-Net, and SONG (<http://song.phys.au.dk/>). While LCOGT has a broad scientific and educational goal, KMT-Net is focused on microlensing, and has with its 20Kx20K 0.36'' pixel size a large survey capacity together with a high cadence. SONG differs from the two other networks by being designed for high-spatial-resolution dedicated high-cadence follow-up microlensing observations. For this purpose, each of the SONG telescopes have two lucky imaging cameras at the Nasmyth focus, with a pixel size of only 0.09'' in order to sample diffraction limited images with two pixels. Experiments with high frame rate techniques (also called frame selection, and including the lucky imaging technique) have demonstrated the ability to obtain near-diffraction limited images from the ground (e.g. Baldwin et al. 2001 [2] 2008 [3] Smith et al. 2009 [4] Tokovinin et al. 2010 [5]). The advantage of the obtainable high spatial resolution is in being able to resolve dimmer source stars in crowded fields. This is the same advantage which has been pointed out in connection with possible space born microlensing missions, but here at a few per cent of the cost of a space mission.

Our present network, MiNDSTeP (<http://www.mindstep-science.org/>), was during 2008-2010 operated from the Danish 1.54m telescope (build in 1975) at ESO's La Sila Observatory, and will from 2011 include also the MONET 1.2m telescope in South Africa (<http://monet.uni-goettingen.de/foswiki>) with further support from the MONET McDonald telescope, the SONG prototype at Tenerife, a Chinese 1.5m telescope and two survey telescopes (VYSOS, <http://vysos.ifa.hawaii.edu/>) in Chile and at Hawaii. The 1.54m telescope CCD has a pixel size of 0.4'', and experience with microlensing research near the Galactic centre has shown us that the corresponding resolution of 0.8'' determines a de facto limiting source star magnitude of $I \sim 18$. This corresponds to a limiting stellar radius of a typical K-giant source star of $10 R_{\odot}$ at the distance of the Galactic centre. Experiments with a lucky imaging camera mounted at the 1.54m telescope has resulted in 0.35'' resolution. This limit is set by the optics of the telescope, and we expect to routinely reach 0.25'' with the SONG telescopes, which are designed for the higher spatial resolution. This corresponds to collecting

10 times more photons per area of sky per time unit with SONG than with the 1.54m telescope with a conventional CCD, since the higher throughput will compensate for the smaller mirror size. On top of this, the 4 times broader filters, the faster slew time, and the more efficient robotic observing schedule are expected to give us a gain of additional a factor 10 in number of collected photons per time unit, so efficiently 100 times more photons per sky area per time unit. This gain will be divided into observing more targets at lower exposure times. Allowing to go 2.5 magnitudes deeper in the field (a factor 10 in number of collected photons) corresponds to a factor 10 smaller $(\Theta_s)^2$ (with Θ_s the angular source radius), and hence a factor 10 smaller reachable $(\Theta_E)^2$ (with Θ_E the exoplanetary Einstein radius) from identical photometric accuracy, corresponding to a factor 10 smaller reachable exoplanetary mass. Present surveys with conventional CCDs, like the one at the Danish 1.54m telescope, have allowed detections of exoplanets typically in the mass range 100 to 5 Earth masses, which makes us expect a similar detection efficiency with SONG for 10 Earth masses to planets smaller than Earth. Theoretical models predict 50 times higher abundance for planets in this latter mass range (in the terrestrial zone) than in the mass range which has been accessible with the present microlensing surveys, making the coming years a very promising time for microlensing exoplanetary research.

The present microlensing campaigns have high sensitivity to Jupiter-Saturn like exoplanets in Jupiter-Saturn like orbits. With the high sensitivity to low-mass exoplanets in terrestrial like orbits expected from coming surveys, and an increasing sensitivity to giant planets in larger orbits, microlensing campaigns in the coming decade will be able to answer the question of how abundant solar system analogues are among the planetary systems in our galaxy. Also the question about the abundance of exoplanets in orbits where life as we know it could exist at the planetary surface is expected to be answered by microlensing in the coming decade(s), and here we expect SONG to play a central role, due to its high sensitivity to low-mass planets in the terrestrial zone (see also Jørgensen 2008 [6]). In this connection it is important to stress that the habitable zone most often is described as the orbital distances where liquid water can exist at the planetary surface, even when people actually think of the distances where liquid water could exist at the surface if the planet was the size of the Earth, had an Earth-like atmosphere, and rotated as the Earth. In particular the latter point is important, because it implies that a truly habitable zone might only exist around solar type stars. Planets orbiting stars with less than half a solar mass will be tidally locked if they are in the habitable zone distance, and stars above 2 solar masses have a main sequence lifetime short compared to biological timescales. Radial velocity and transit studies are, for technical reasons, biased toward finding small-mass planets around M-dwarfs. Microlensing, on the other hand is not biased toward any particular stellar lens-mass range, and statistically one fourth of the lensing stars will be solar like (i.e. between half and two solar masses). SONG will therefore be highly sensitive toward detecting Earth-mass exoplanets in the (truly) habitable zone

around such lensing stars.

References

- [1] F. Grundahl, J. Christensen-Dalsgaard, H. Kjeldsen, U. G. Jørgensen, T. Arntoft, S. Frandsen, P. Kjærgaard, in: ASP Conf. Ser. **416**, 579 (2009)
- [2] J. E. Baldwin, R. N. Tubbs, G. C. Cox, C. D. Mackay, R. W. Wilson, M. I. Andersen, Astron. Astrophys. 368, L1-L4 (2001)
- [3] J. E. Baldwin, P. J. Warner, C. D. Mackay, Astron. Astrophys. 480, 589 (2008)
- [4] A. Smith, J. Bailey, J. H. Hough, S. Lee, MNRAS 398, 2069 (2009)
- [5] A. Tokovinin, R. Cantarutti, R. Tighe, P. Schurter, N. van der Bliet, M. Martinez, E. Mondaca, arXiv1010.4176 (2010)
- [6] U. G. Jørgensen, Physica Scripta, **T130**, 014008 (2008)

Next Generation Microlensing and the Frequency of Planetary Systems: Preliminary Results from a Pilot Experiment

*Dan Maoz & Yossi Shvartzvald
Tel-Aviv University
Israel*

1 Introduction

Current microlensing planet surveys have been based on wide-field, low-cadence, searches for microlensing events toward the bulge of the Galaxy by two main surveys: OGLE (Udalski et al. 2008) and MOA (Sako et al. 2008). These surveys send out public “alerts” when they detect lensing events in which fits to the initial light curve suggest high peak magnifications, of order 100 or more. The high-magnification events constitute about 1 per cent of all lensing events. Events that appear promising to be of high magnification trigger intensive photometric followup efforts by networks of small telescopes (including dedicated amateurs) to obtain coverage, over the peak of the event, that is as continuous as possible. The motivation for this observing strategy has been that, near the peak of a high magnification event, the source star is distorted into a nearly complete Einstein ring that covers a large area in the lens plane. The snow lines of typical lens stars happen to roughly coincide with their Einstein radii. Thus, planets, if they exist around a lens, and if projected in the vicinity of the snow line, will always produce significant perturbations to the light curves of high-magnification lensing events. There are about 700 lensing events per yearly bulge season, and of order 10 are of high magnification. Fair coverage of these events over their peaks by the current generation of followup observations has yielded 2-3 planets per year, suggesting that a fraction of roughly 1/10 to 1/3 of lens stars have planets near their snow lines (Gould et al. 2010; Sumi et al. 2010). But, this low detection rate also explains why the current strategy has, over the past 5 years, produced only about a dozen microlensing planet discoveries, a tiny fraction of the 500 known extrasolar planets.

As opposed to the current microlensing surveys, which have focused on the rare high-magnification lensing events that probe the “central” caustics of host+planet lenses, “Generation-2” surveys will go after the much more common, low-magnification, events and the perturbations caused by their “planetary” caustics. To harvest this

potential new crop of microlensing-discovered planets requires the combination of a wide survey area with dense temporal sampling. This has now become possible with the availability of degree-scale CCD imaging mosaics on several 1m- to 2m-class telescopes. In Generation-2 microlensing, such telescope-camera combinations, situated around the globe, continuously monitor about 10 deg^2 of the Galactic bulge with cadences of less than one hour. A large fraction of the 700 or so lensing events that occur per bulge season are monitored. Among those lenses that host planets, a perturbation, which can last as little as several hours, is detected in the light curve in those events where a lensed image happens to pass close to the planet. Simulations by us (see below) and by others (e.g. Penny et al. 2010) show that this observing approach should produce dozens of planet discoveries per year. Over several years, the sample of microlensing-discovered planets could then start to be comparable to those from other planet-detection methods, but would probe very different regions of planetary parameter space than those probed by the other methods.

2 A Generation-2 Pilot Survey

In the summer of 2010, we launched the pilot stage of a Generation-2 microlensing planet survey. During two 3-week periods, we observed the bulge fields having the highest past lensing event rates using a network of four telescopes. Up to the unavoidable but moderate weather gaps, we obtained continuous coverage for 81 microlensing events, with full coverage of the event for about 15. We plan to continue and expand this survey in the coming years and to address the following questions: What is the frequency of occurrence of planets and planetary systems around disk and bulge stars in the Milky Way? Are most of the systems Solar analogs, or are they clearly distinct, and in what ways? What is the emerging picture regarding planetary formation and evolution, when combining these results with those from the complementary, ongoing, radial-velocity and transit surveys (e.g. Howard et al. 2010)?

The pilot phase took place in June-July 2010 during two 3-week periods (separated by a one-week break around the full moon), when we monitored the 8 deg^2 of the Galactic bulge that have the highest microlensing event rates. We used the 1m-telescope at Wise Observatory in Israel with the LAIWO camera (1 deg^2 field of view). Our observations were coordinated with those of the 1.3m Warsaw University telescope in Chile with the OGLE-IV camera (1.4 deg^2 field of view); the 1.8m MOA-II telescope in New Zealand with the MOA-cam3 camera (2.2 deg^2 field of view); and the Palomar Observatory 1.2m Oschin telescope in California with the PTF camera (7.8 deg^2 ; Law et al. 2009; this telescope participated only in the second 3-week run). Observing cadence at each telescope was between 20 and 40 minutes. During each of the 3 weeks, coverage was about 90% of fully continuous. During our pilot, 81 lensing events (identified as such by MOA) were covered or partly covered by

our observations. We are performing difference-image analysis (DIA) on the data for these events, to obtain the most accurate photometry for each event. We will show some of the emerging light curves, based on preliminary analysis of the data from Wise, MOA, and PTF (data obtained by OGLE are still being reduced).

3 Numerical Simulations and Future Prospects

In parallel, we have carried out numerical ray-tracing simulations, both for planning the experiment and with a view toward analysing the results, whether statistically or in terms of modeling individual events. We begin by producing large numbers of simulated light curves. The physical parameters – lens mass, distance, and the effective lens-source velocities – are drawn from the distributions of those parameters that, when combined with Galactic structure models, reproduce the lens-crossing timescale distributions observed in real lensing events of the past years (Dominik 2006). Impact parameters and the magnitudes of the source stars (and hence the photometric errors, see below) are also chosen to reproduce the observed distributions. The interesting but unknown physical parameters – number, orbital separation, and masses of the planets, are input according to various possible prescriptions. For example, one possibility is that some fraction f of all stars hosts planetary systems that mimic the Solar System, but the planets are scaled in mass and orbital radius with the host mass M , according to the snow-line radius, with some power-law of index s , $R_{\text{snow}} \propto M^s$. Thus, for a choice of s and f , we can produce many systems with random orbital phases of their planets and random line-of-sight inclinations of their orbital planes. We then ray trace through them to obtain simulated light curves. The light curves from a particular choice of model parameters are then “observed”, in terms of including all the observational effects: we temporally sample the light curves with observing sequences drawn from the real existing observations, and scatter the photometry based on a realistic measurement error distribution, as observed in the real data (and thus including all error types – Poisson, backgrounds from bright stars, outliers due to improperly subtracted DIA residuals). We then search these simulated light curves for planetary deviations. For a given combination of physical parameters, the simulations can give us the probability of the observed lensing statistics, such as number and type of perturbations, and will thus permit to constrain the interesting physical parameter space.

We will show predictions from our Monte Carlo simulations, in which, for various combinations of planetary population parameters and experiment parameters, a Generation-2 survey is repeated many times. This gives the Monte-Carlo distribution of the number of detected planetary events per season, for a combination of seasonal experiment duration, observing cadence, fraction f of stars hosting Solar-like planetary systems, and power-law index s relating system size to host-star mass. The

results of the real experiment, when compared with the distributions from such mock experiments, will permit constraining the physical parameter space. Our current calculations indicate that we can realistically expect to discover up to a few dozen planets per bulge season, and up to the order of 100 planets in the course of several years.

References

- [1] Dominik, M. 2006, *Stochastic distributions of lens and source properties for observed galactic microlensing events*, Monthly Notices of the Royal Astronomical Society, 367, 669
- [2] Gould, A., et al. 2010, *Frequency of Solar-like Systems and of Ice and Gas Giants Beyond the Snow Line from High-magnification Microlensing Events in 2005-2008*, Astrophysical Journal, 720, 1073
- [3] Howard, A. W., Marcy, G. W., Johnson, J. A., Fischer, D. A., Wright, J. T., Isaacson, H., Valenti, J. A., Anderson, J., Lin, D. N. C., & Ida, S. 2010, *The Occurrence and Mass Distribution of Close-in Super-Earths, Neptunes, and Jupiters*, Science, 330, 653
- [4] Law, N. M., et al. 2009, *The Palomar Transient Factory: System Overview, Performance, and First Results*, Publications of the Astronomical Society of the Pacific, 121, 1395
- [5] Penny, M. T., Mao, S., & Kerins, E. 2010, *Detectability of Orbital Motion in Stellar Binary and Planetary Microlenses*, arXiv:1010.5940
- [6] Sako, T., et al. 2008, *MOA-cam3: a wide-field mosaic CCD camera for a gravitational microlensing survey in New Zealand*, Experimental Astronomy, 22, 51
- [7] Sumi, T., et al. 2010, *A Cold Neptune-Mass Planet OGLE-2007-BLG-368Lb: Cold Neptunes Are Common*, Astrophysical Journal, 710, 1641
- [8] Udalski, A., Szymanski, M. K., Soszynski, I., & Poleski, R. 2008, *The Optical Gravitational Lensing Experiment. Final Reductions of the OGLE-III Data*, Acta Astronomica, 58, 69

Kohyama Astronomical Observatory: Current Status

*Atsunori Yonehara, Mizuki Isogai, Akira Arai, Hiroki Tohyama
Department of Physics, Faculty of Science, Kyoto Sangyo University, JAPAN*

1 Introduction

Kohyama Astronomical Observatory locates at north rim of Kyoto city. The location is not so ideal for astronomical observation, especially for observing southern sky, but quite convenient for any urgent observation program such as follow-up observations of galactic microlensing. Construction of our observatory has been finished on 22nd December 2009, and we have 1.3-meter, optical and near-infrared, telescope (we call it Araki Telescope) in our observatory.

2 Dual Band Imager, ADLER

After the construction has been finished, we equipped several observational instruments to our telescope. The most important instrument for microlensing observation is a dual band imager, ADLER (Araki telescope DuaL band imagER). ADLER is equipped at Cassegrain focus of our telescope, and the wavelength covergae is from 380nm to 900nm. Photons are divided in two wavelength regime, from 380nm to 670nm and from 670nm to 900nm by dichroic mirror. Gunn-g' filter is available at shorter wavelength regime, and Gunn-i' and -z' filters are available at longer wavelength regime currently. The field of view is $12' \times 12'$ which is covered by $2k \times 2k$ CCD camrea, Spectral Instruments 850 series. Recently, regular observations by using ADLER starts from this October, and now we have several scientific targets for observations with ADLER.

For microlensing community, it should be mentioned that galactic and quasar microlensing observations are one of the most important targets in our observatory, since other targets are cataclysmic variables, comets, and transits. Thanks to the dual band imaging and wide field of view, we are able to perform DIA photometry for galactic microlensing with two waveband at the same time. Dual band imaging is not so essential for planet microlensing huntings, but chromaticity during quasar microlensings provides us important information for quasar central engine.

3 Current Status

We have already made several photometries for cataclysmic variables and transits, and we are able to achieve less than 1 percent accuracy for relative photometry with ADLER in both wavelength regime. Sky brightness strongly depends on wavelength regime and sky direction. Shorter wavelength regime and southern sky is worse due to Kyoto city lights, and some quantitative studies for such dependence will be presented. Now we are accumulating various targets for scientific purpose and for checking capabilities of our telescope/instruments.

Further, some observational data (transits, quasars), weather conditions (typically 30 percent fine weather) and seeing (typically a few arcsec) in a half year or so will be shown in presentation.

I am grateful to other members in Kohyama Astronomical Observatory.

Optimal Imaging for Gravitational Microlensing

*Kennet B.W. Harpsøe, Uffe G. Jørgensen, Per K. Rasmussen, Michael I. Andersen,
Anton N. Sørensen*

*The Niels Bohr Institute, University of Copenhagen
Denmark*

*Jøgen Christensen-Dalsgaard, Søren Frandsen, Frank Grundahl, Hans Kjeldsen
Dep.Phys.Astronomy, Aarhus University
Denmark*

1 Introduction

High framerate imaging of astronomical sources offers new possibilities for improved resolution and short timescale photometry. Image motion due to turbulence is the most important contribution to atmospheric seeing. By taking images at a framerate comparable to the dynamic timescale of the atmosphere (10-100Hz), it is possible to “freeze” the motion and correct for it, thereby improving the image quality significantly. One well known variations of this is the lucky imaging method, where only nearly diffraction limited frames are kept and co added. The main obstacle for pursuing this path in astronomy has been read out noise in CCD’s. The large number of frames needed to collect appreciable amounts of photons from faint astronomical sources at the required framerates implies that the signal is completely overwhelmed by the read out noise typical of CCD’s.

2 The EMCCD

The invention of the EMCCD (Electron Multiplying CCD) has made read out noise on the sub electron level possible. The read out register of an EMCCD has been extended into a solid state version of a photomultiplier. This makes it possible to amplify a single photoelectron into hundreds of electrons, thereby overcoming the read out noise. But the electron cascades resulting from the amplification are stochastic, and new methods must be employed to reduce the images for extracting photometric information. It is reasonable to assume that the distribution of the final size of the cascades is exponential, with some decay constant called the EM gain. For instance, spurious charge is present but undetectable in all conventional CCDs. It is visible in

an EMCCD, making it impossible to estimate the bias from a simple average of bias frames.

EMCCD's can be operated in two distinct ways: a photon counting mode with only shot noise, but with coincidence losses at high flux levels; or a linear mode with shot noise inflated by a factor of two. At present, we are employing the linear mode. But real photon counting optimal imaging is theoretically possible and a very interesting concept.

3 Optimal Imaging Methods

If a standard Kolmogorov model for atmospheric turbulence is assumed, the six most dominant Zernike terms aberrating an image will be piston, tip and tilt, focus and the two astigmatism terms, listed in descending order of power [3]. Piston is unimportant for imaging, and tip and tilt result in an overall solid-body translation of the image that can be corrected simply by shifting the images and co-add. This methods colloquially know as shift and add.

Focus, astigmatism, and higher order terms will blur the images. The amount of blurring in the individual frames will be random; sometimes one will be lucky and obtain an image near the diffraction limit. By collecting only these images, then shifting and co-adding them, nearly diffraction limited images with useful signal to noise ratios can be obtained, hence this method is known as lucky imaging [1].

All of the images obtained in a high framerate sequence will contain information, though, and for every combination of target and desired measurement there must exist an optimal weighting scheme for combining the images.

4 Optimal Imaging in Microlensing

The optimal imaging techniques are highly interesting for gravitational microlensing as it can resolve much of the flux blending in the dense fields where microlenses are most often observed. Furthermore the technique works best on the small size telescopes often used for microlensing followups, and it is relatively inexpensive and straightforward to implement on telescopes.

From experience we know that with the DFOSC conventional CCD camera, at the Danish 1.54m telescope at the ESO La Silla observatory, we can get useful photometry from stars down to $I=18$, but not fainter due to crowding. With the improved resolution from the Lucky Imaging we expect to be able to do photometry on stars down to about $I=21$ [2]. Assuming a constant distance and surface temperature of the source stars, this allows us to track microlensing event in stars with ten times smaller Θ_s^2 , where Θ_s is the angular source size. Which means that planets with squared Einstein radii ten times smaller will be detectable without being washed out

by finite source effects; this corresponds to being able to detect planets with one tenth of the mass. [4].

References

- [1] R. N. Tubbs, Ph.D. Thesis Dissertation. Cambridge Uni. (2003)
- [2] J. A. Holtzman, A.J., **115**, 1946 (1998)
- [3] V. I. Tartarski, McGraw-Hill (1961)
- [4] U. G. Jørgensen, Physica Scripta, **T130**, 014008 (2008)

IPAC's Role as the Science Center for NASA's WFIRST Mission

*Kaspar von Braun
NASA Exoplanet Science Institute
California Institute of Technology
USA*

I will discuss the roles NASA's Infrared Processing and Analysis Center (IPAC) and the NASA ExoPlanet Science Institute (NExScI) will play in the WFIRST mission. As the Science Center for WFIRST, IPAC will work with the project, the Science Definition Team, and scientific community to develop all three of WFIRST's scientific themes in preparation for a new star later in the decade: Dark Energy, a near-IR survey, and a microlensing survey to conduct a census of planets covering a wide range of masses and orbital periods. In the near-term, NExScI will continue to develop its archive of microlensing events and lightcurves analogous to its archives of transit datasets. In addition, the topic of NExScI's next Sagan Exoplanet Summer Workshop will be planet searches using microlensing (<http://nexsci.caltech.edu/workshop/2011/>). IPAC will be working with the microlensing community as their science advocate within the WFIRST project, developing relevant archives and tools in the decade leading up to the launch of WFIRST, and ultimately in developing mission products that will take full advantage of WFIRST's remarkable capabilities.

EUCLID: From frozen Mars to habitable Earth via microlensing

Jean-Philippe Beaulieu
Institut d'Astrophysique de Paris
France

Matthew Penny
Manchester University
UK

In the last fifteen years, astronomers have found over 500 exoplanets including some in systems that resemble our very own solar system. These discoveries have already challenged and revolutionized our theories of planet formation and dynamical evolution. Several different methods have been used to discover exoplanets, including radial velocity, stellar transits, direct imaging, pulsar timing, astrometry, and gravitational microlensing which is based on Einstein's theory of general relativity. So far 10 exoplanets have been published with this method. While this number is relatively modest compared with that discovered by the radial velocity method, microlensing probes a part of the parameter space (host separation vs. planet mass) not accessible in the medium term to other methods. The mass distribution of microlensing exoplanets has already revealed that cold super-Earths (at or beyond the "snow line" and with a mass of around 5 to 15 Earth mass appear to be common (Beaulieu et al., 2006, Gould et al., 2006, Sumi et al. 2010) . We detected a scale 1/2 model of our solar system (Gaudi et al., 2008), several hot Neptunes/Super Earth, shown that our detection efficiencies extends to 1 Earth mass planets (Batista et al., 2009). We have made the first measurement of the frequency of ice and gas giants beyond the snow line, and have shown that this is about 7 times higher than closer-in systems probed by the Doppler method. This comparison provides strong evidence that most giant planets do not migrate very far (Gould et al. 2010).

Microlensing is currently capable of detecting cool planets of super-Earth mass from the ground (and on favourable circumstances down to 1 Earth), with a network of wide-field telescopes strategically located around the world, could routinely detect planets with mass as low as the Earth. Old, free-floating planets can also be detected; a significant population of such planets are expected to be ejected during the formation of planetary systems. Microlensing is roughly uniformly sensitive to planets orbiting all types of stars, as well as white dwarfs, neutron stars, and black holes, while other method are most sensitive to FGK dwarfs and are now extending

to M dwarfs. It is therefore an independent and complementary detection method for aiding a comprehensive understanding of the planet formation process. Ground-based microlensing mostly probes exoplanets outside the snow line, where the favoured core-accretion theory of planet formation predicts a larger number of low-mass exoplanets (Ida & Lin 2005). The statistics provided by microlensing will enable a critical test of the core accretion model. Exoplanets probed by microlensing are much further away than those probed with other methods. They provide an interesting comparison sample with nearby exoplanets, and allow us to study the extrasolar population throughout the Galaxy.

Ultimately, a comprehensive census of cold planets below Earth masses, and habitable Earth mass planets requires a space-based microlensing survey. The remarkable synergy between Dark Energy probes by Cosmic shear has been realized and implemented in Europe since 2006 with the DUNE proposal, and has been developed in EUCLID. A 3 month microlensing program is part of the additional science of EUCLID aiming at low mass telluric planets down to the mass of Mars at the snow line and first hint on habitable super Earth (described in the yellow book and in Beaulieu et al. 2010). There is a proposition for an extension of the initial 3 month “additional science” program by a 9 months “legacy program” with the objective of measuring the abundance of habitable Earth around solar like stars. This legacy program could take place once the Dark Energy objective will have been reached, at the end of the mission. We suggest to have a first survey of 2 months shortly after the launch to guaranty high profiles results (detection of planets down to the mass of Mars) early in the mission. Results with high visibility would be valuable for EUCLID within the first year of operation. It is important to have observations early in the mission life time and after few years to maximize the baseline in order to be able to have better constraints on host masses.

With the 9 month legacy program in addition to the 3 month that are currently in the additional science of EUCLID we will provide: a) a complete census of planets down to Earth mass with separations exceeding 1 AU b) complementary coverage to Kepler of the planet discovery space c) sensitivity to planets down to $0.1 M_{\odot}$, including all Solar System analogues except for Mercury d) complete lens solutions for most planet events, allowing direct measurements of the planet and host masses, and distance from the observer.

Space-Based Microlensing Exoplanet Survey: WFIRST and/or Euclid

David P. Bennett
University of Notre Dame, Notre Dame, IN
USA

The US Astro2010 Decadal Survey report, “New Worlds, New Horizons in Astronomy and Astrophysics” recommended a new mission called WFIRST as its top ranked large space mission for the next decade. The WFIRST mission is to have two major science programs that will drive the design requirements: a dark energy program and a microlensing planet search program, based on the Microlensing Planet Finder (MPF) concept. ESA is considering a similar mission, known as Euclid, which addresses dark energy, but also has a modest microlensing program that could be expanded. Both NASA and ESA have expressed interest in a possible joint program to address both the WFIRST and Euclid science goals, assuming that Euclid is selected. However, there are a number of political and technical issues that would complicate such a joint program.

I discuss the science justification for the WFIRST microlensing program, and consider a variety of mission designs that might be considered by the WFIRST Science Definition Team.

Microensing with Gaia satellite

Lukasz Wyrzykowski, Vasily Belokurov
Institute of Astronomy, University of Cambridge
UK

Gaia is an ambitious astrometric survey satellite that will be launched by ESA in 2012/2013. Its unique combination of precise astrometry, photometry and spectroscopy will have a tremendous impact on many fields of astrophysics, from Galaxy structure, stellar models, variable stars to asteroids and extra-solar planets [1].

Gaia offers a unique contribution to the field of microensing with its uniform continuous all-sky coverage over 5 years and a superb astrometry as its primary goal. When employed in the microensing studies it would provide an one-off opportunity for studying microensing events. Sole ground-based photometric observations only in very special cases allow for solving and working out the combination of parameters of the microensing event participating objects.

The astrometric accuracy of a single 1 dimensional measurement in Gaia is about $50 \mu\text{as}$ at 14 mag and $400 \mu\text{as}$ at 18 mag. It is enough to detect typical displacement of the centroid of the images of 1 mas. About 15,000 astrometric events are expected to occur over the whole sky during the 5 year of the mission, however only in few percent of them the mass of the lens can be recovered with a reasonable accuracy [2].

Gaia sparse sampling prevents from obtaining detailed light curves of the events, see example in Fig. 1, hence the characterisation of the events is difficult. Photometric and astrometric microensing deviations will be detected by the Gaia Science Alerts system, currently being developed and installed in Cambridge. The system will operate in near-real-time, analysing all data incoming from the satellite as soon as they are arrive and are preliminarily processed, usually between couple and 24 hours after observation. It will utilise all Gaia data available at these time-scales, including low-resolution spectroscopy. Thanks to that the classification of the observed deviations will be less affected by false-positives.

Gaia Science Alerts will therefore release alerts to the community about plausible microensing photometric and astrometric deviations. However, without well-organized ground-based all-sky follow-up of the events detected by Gaia it will not be possible to fully exploit the scientific potential of these microensing events. When Gaia data are supplemented by ground-based observations the number of measured masses increases by several factors.

Due to characteristic sampling of Gaia vast majority of alerted events will usually have long time-scales. The detection efficiency reaches 100% for events with time-scales of around 100 days. These will be mainly caused by relatively nearby disk

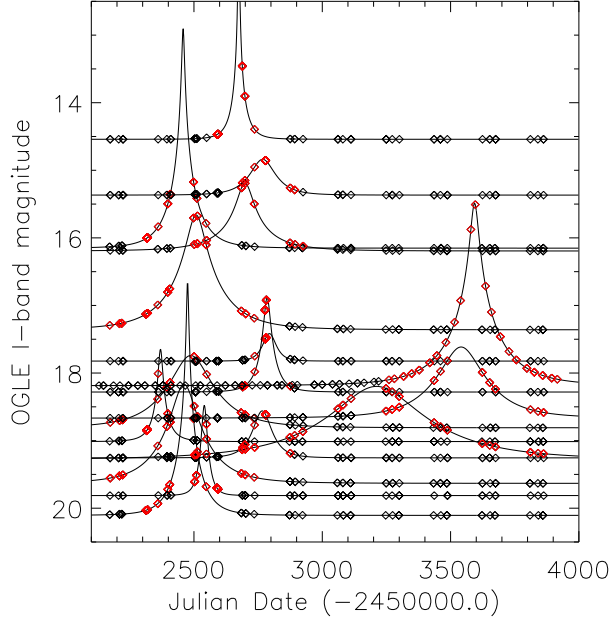


Figure 1: Selected OGLE microlensing events as would have been observed by Gaia. Red indicate data points taken during the actual event. Only shown are events with the number of data points during the event more than 20.

lenses, exhibiting a parallax effect and allowing for probing the local mass function. Moreover, Gaia will create an opportunity to detect massive stellar remnants, like neutron stars or black-holes, acting as lenses in the detected events.

Gaia Science Alerts Working Group wiki is available at this address:

<http://www.ast.cam.ac.uk/research/gsaawg>.

This is a platform containing important information about the design and operation of the alerting system. It is also a site where we gather all relevant information about possible triggers of alerts. One can also find there archived talks and presentation from the first Science Alerts workshop held in June 2010 in Cambridge.

The website also provides information about the forthcoming workshop in June 2011, dedicated to the follow-up and verification of the Gaia Science Alerts.

References

- [1] Perryman M.A.C. et al. 2001, *A&A*, **369**, 339
- [2] Belokurov V., Evans N.W., 2002, *MNRAS*, **331**, 649

Poster session

Critical curve topology in special triple lens configurations

Kamil Danek

PAndromeda - A Dedicated Deep Survey of M31 with Pan-STARRS 1

Chien-Hsiu Lee, Arno Riffeser, Stella Seitz, Ralf Bender, Johannes Koppenhoefer

Critical curve topology in special triple lens configurations

Kamil Daněk, & David Heyrovsky
Institute of Theoretical Physics, Charles University in Prague
Czech Republic

Inspired by the Erdl & Schneider [1] analysis of the parameter dependence of binary lensing topologies, we extend their approach to special cases of the triple lens. While the binary lens is characterised by two parameters, three more parameters are needed to describe the triple lens. We analysed several two-dimensional cuts through the five-dimensional parameter space, identifying the boundaries of regions with different critical curve topology. For each region we present corresponding critical curves and caustics.

References

- [1] Erdl, H., Schneider, P., 1993, A&A, 268, 453

PAndromeda - A Dedicated Deep Survey of M31 with Pan-STARRS 1

*Chien-Hsiu Lee, Arno Riffeser, Stella Seitz, Ralf Bender, Johannes Koppenhoefer
Max Planck Institute for Extraterrestrial Physics, Garching
Germany*

Pan-STARRS 1 Science Consortium University of Hawaii, Pan-STARRS Project Office, Max Planck Institute for Astronomy, Max Planck Institute for Extraterrestrial Physics, Johns Hopkins University, University of Durham, University of Edinburgh, Queens University of Belfast, Harvard-Smithsonian Center for Astrophysics, Los Cumbres Observatory Global Telescope Network, National Central University of Taiwan

The Pan-STARRS 1 (PS1) survey of M31 (PAndromeda) is designed to identify gravitational microlensing events, caused by bulge and disk stars (self-lensing) and by compact matter in the halos of M31 and the MW (halo lensing, or lensing by MACHOs). PAndromeda will improve our understanding of the M31 distance, the mix of stellar ages and metallicities of the M31 disk, bulge, halo, stellar streams & dwarfs, it will constrain the extinction within M31 and will provide insight into stellar population properties based on the color profiles, SFB-fluctuations, resolved stars and variables. These results are required for an accurate interpretation of the microlensing events. Here we present photometric observations of gravitational microlensing candidates discovered during the first season in 2010.